ISSN : 1411-1098
Akreditasi Nomor : 263/AU1/P2MBI/05/2010

Jurnal
Sains Materi Indonesia
Indonesian Journal of Materials Science

Vol. 12, No. 2, Februari 2011

Pusat Teknologi Bahan Industri Nuklir
Badan Tenaga Nuklir Nasional
INDONESIA

ISSN 1411-1098
Akreditasi Nomor : 263/AU1/P2MBI/05/2010

JURNAL SAINS MATERI INDONESIA

Indonesian Journal of Materials Science

Vol. 12, No. 2, Februari 2011
Terbit empat bulanan : Oktober, Februari, Juni

Penerbit : Pusat Teknologi Bahan Industri Nuklir, BATAN
Terbit Pertama Kali : Oktober 1999
Alamat Redaksi/Editorial Address : PTBIN - BATAN, Gedung 43, Kawasan Puspiptek Serpong 15314, Tangerang
Telepon : (021) 75874261, 7562860 Ext. 4009 - 4010, *Fax :* (021) 7560926
E-mail : jusami@batan.go.id, *Website :* http://jusami.batan.go.id

ISSN 1411-1098
Akreditasi LIPI Nomor : 263/AU1/P2MBI/05/2010

JURNAL SAINS MATERI INDONESIA
Indonesian Journal of Materials Science
Vol. 12, No. 2, Februari 2011

KATA PENGANTAR

Dewan redaksi Jurnal Sains Materi Indonesia (JUSAMI) mengucapkan terimakasih atas naskah yang diterima baik dari kalangan lembaga penelitian maupun universitas. Untuk lebih meningkatkan kualitas komunikasi antar pemangku kepentingan, secara bertahap JUSAMI akan tampil secara *online*. Semua bentuk komunikasi dengan dewan redaksi dapat dilakukan melalui e-mail:jusami@batan.go.id, sedangkan untuk *website* JUSAMI dapat diakses melalui: http://jusami.batan.go.id.

Jurnal Sains Materi Indonesia Vol. 12 No. 2, Februari 2011 ini adalah edisi regular tetapi memiliki kekhususan, dimana semua makalah terbit dalam bahasa Inggris. Dari hasil seleksi Dewan Redaksi, 15 makalah dinyatakan layak untuk diterbitkan dalam edisi regular ini. Isi dari ke 15 makalah tersebut terdistribusi atas 5 makalah tentang pengembangan bahan alam seperti karet alam, minyak sawit dan selulosa, 3 makalah tentang peningkatan kinerja bahan polimer komersial seperti polivinil klorida dan polipropilen, 3 makalah terkait dengan pengembangan nanomaterial dan 4 makalah tentang material untuk aplikasi kedokteran.

Abu Hasan dkk, melaporkan tentang karakteristik proses *curing* dari karet alam hasil vulkanisasi sedangkan Indra Gunawan dkk, melaporkan hasil upaya pengembahan karet alam hasil proses iradiasi dengan penambahan partikel silika. Tutun Nugraha dkk melaporkan hasil upayanya memanfaatkan bahan alam bentonit untuk pengolahan minyak sawit untuk digunakan sebagai minyak goreng. Sedangkan pemanfaatan poliol dari minyak sawit sebagai bahan dasar poliuretan dilaporkan oleh Evi Triwulandari dkk. Asep Riswoko dkk telah mengupayakan modifikasi selulosa dengan teknik *grafting* menggunakan iradiasi berkas elektron. Laporan-laporan tersebut akan memberikan kontribusi dalam upaya peningkatan pendayagunaan bahan alam khsususnya di Indonesia.

Peningkatan kinerja seperti kemudahan proses, keuletan, kelenturan dan kekuatan bahan polimer komersil masih merupakan tantangan sesuai dengan bidang aplikasinya. Nutt Lumpikanond dkk telah mencoba menjawab kemudahan proses polivinil klorida sebagai bahan profil pintu dan jendela, dengan penambahan bahan pengisi. Ariadne L. Juwono dkk telah berupaya meningkatkan kelenturan dan kekuatan polipropilen dengan penambahan bentonit dalam bentuk nanokomposit. A. Zainal Abidin dkk juga telah melakukan *grafting* bentonit ke dalam polimer akrilat untuk membuat bahan superabsorben dengan daya serap dan daya simpan air yang tinggi.

Pengembangan teknologi pembuatan dan perlakukan nanomaterial untuk memenuhi tuntutan aplikasi masih menarik perhatian peneliti. Akhmad Hermawan Yuwono dkk telah mengkaji faktor utama yang mempengaruhi rendahnya nanokristalinitas partikel TiO_2 hasil derivasi sol gel yang diikuti dengan perlakukan *annealing* dan hidrotermal. Sedangkan Yuni K. Krisnandi dkk serta Muhammad Ghufron dkk menaruh perhatian pada nanomaterial berbasis besi masing-masing untuk bahan elektroda dan bahan magnet.

Bahan untuk aplikasi kedokteran dalam edisi ini ditampilkan dalam 4 makalah. Irna Farikhah dkk melaporkan studi tentang kristal cair dari elastomer yang berpotensi untuk aplikasi otot buatan. Decky J. Indrani dkk melaporkan hasil sintesis hidroksiapatit sebagai bahan rekayasa jaringan tulang. Yoga W. Wardhana dkk mengungkapkan meningkatkan stabilitas obat terhadap kelembaban, dengan mengambil contoh *theophylline* yang dikenal sebagai obat asma. Diky Mudhakir dkk melaporkan tentang peningkatan efisiensi pengobatan kanker paru-paru dengan pengembangan vektor yang mendorong pencapaian ke organ target.

Luasnya tema pembahasan dalam edisi ini diharapkan dapat menjadi sarana komunikasi lintas disiplin ilmu dari para pemangku kepentingan penelitian dan pengembangan material baik yang berada di institusi penelitian, universitas, lembaga pemerintahan maupun di industri.

Editor

ISSN 1411-1098
Akreditasi LIPI Nomor : 263/AU1/P2MBI/05/2010

JURNAL SAINS MATERI INDONESIA
Indonesian Journal of Materials Science
Vol. 12, No. 2, February 2011

EDITORIAL PREFACE

The editorial board of Indonesian Journal of Materials Science (JUSAMI) is very grateful to receive many articles from research institutes and universities. In order to improve the communication quality between the stake holders, step by step JUSAMI will appear online. Communications with editorial board will be done by e-mail, jusami@batan.go.id, while the website can be accessed in http://jusami.batan.go.id.

This Indonesian Journal of Material Science, Vol. 12, No. 2, February 2011, is the regular edition, but it is special since all of the articles are written in English. After considering the contents accompanied by further selection process, the editorial board accepted 15 articles to be published in this regular edition. Contents of the 15 articles are distributed in 5 articles covering natural based materials such as natural rubber, palm oil and celluloses, 3 articles are talking about properties improvement of commercial polymer such as poly(vinyl chloride) and polypropylene, 3 articles are concerned with the development of nanomaterials, and 4 articles are covering materials for medical application.

Abu Hasan et. al. reported about curing characteristics of vulcanized natural rubber, while Indra Gunawan et. al. reported their attempts to improve the properties of irradiated natural rubber by adding silica particles. Tutun Nugraha et. al. reported results of their attempt to modify and utilize bentonite for the bleaching of crude palm oil to be utilized as vegetable oil, while the utilization of polyol from palm oil as raw material of polyurethane was reported by Evi Triwulandari et. al. Asep Riswoko et. al. has modified cellulose by grafting technique using electron beam irradiation method. These reports will contribute in the development of natural based materials especially in Indonesia.

Properties improvement such as processability, toughness, flexural modulus and tensile strength of commercial polymer materials are still presenting challenges in their application. Nutt Lumpikanond et. al. have attempted to answer the problems of poly(vinyl chloride) processability for doors and windows profiles by adding fillers. Ariadne L. Juwono et. al. have tried to improve the flexural modulus of polypropylene by adding bentonite in the form of nanocomposite while A. Zainal Abidin et. al. have grafted bentonite into acrylic polymer to make superabsorbent with high water absorbing and water storing characteristics.

Technology development for the synthesis and the treatment of nanomaterials to fulfill their applications are still becoming the point of interest. Akhmad Hermawan Yuwono et. al. studied the major factor causing the low nanocrystalinity of TiO_2 obtained from Sol Gel process, followed by annealing and hydrothermal treatment, while Yuni K. Krisnandi et.al. and Muhammad Ghufron et.al. focused their attention to iron based nanomaterials to be used as electrodes and magnetic materials.

Articles about material for medical application in this edition are represented by 4 articles. Irna Farikhah et. al. reported their studies on liquid crystal elastomers which have potential applications for artificial muscles. Decky J. Indrani et. al. reported their results of the study on hydroxy-apatite for bone tissue engineering. Yoga W. Wardhana et. al. described their attempts to improve drugs stability due to humidity, utilizing theophylline, known as medication for the asthmatics, as the example. Finally, Diky Mudhakir et. al. reported their attempts to improve the efficiency of lung cancer therapy by designing a vector to help the drug to reach the target tissue most efficiently.

It is hoped that the wide scope of theme being discussed in this edition can commence an interdisciplinary communication between the various stakeholders of material research and development whether they within research institution, university, government or the industries.

Editor

Akreditasi LIPI Nomor : 452/D/2010
Tanggal 6 Mei 2010

THE INFLUENCE OF MASTICATION TO CURING CHARACTERISTIC OF NATURAL RUBBER AND PHYSICAL PROPERTIES OF ITS VULCANIZATES

Abu Hasan[1], Rochmadi[2], Hary Sulistyo[2] and Suharto Honggokusumo[3]
[1]Chemical Engineering Department-State Polytechnic of Sriwijaya
Jl. Srijaya Negara Bukit Besar, Palembang 30139, Indonesia
[2]Chemical Engineering Department, Faculty of Engineering-Gadjah Mada University
Jl. Grafika No. 2, Yogyakarta 55281, Indonesia
[3]The Indonesian Rubber Association (Gapkindo)
Jl. Cideng Barat No. 62A, Jakarta 10150, Indonesia
e-mail : abu_hasan@polisriwijaya.ac.id

ABSTRACT

THE INFLUENCE OF MASTICATION TO CURING CHARACTERISTIC OF NATURAL RUBBER AND PHYSICAL PROPERTIES OF ITS VULCANIZATES. The research on the mastication that influences the curing characteristic of natural rubber and physical properties of its vulcanizates has been conducted. The research started from rubber mastication with variation of carbon black filler addition into rubber compound. Rubber compound was then measured to identify its curing characteristic using rheometer and tested its viscosity using Mooney viscosity tester. Physical properties of rubber vulcanizates such as abrasion resistance, tear strength, and elongation at break were also measured. The results indicated that curing characteristic tended to decrease, while only scorch time tended to increase from B1, B2, B3 and B4. Elongation at break tended to decrease, while tear resistance and abrasion resistance tended to increase from B1, B2, B3 and B4. Mooney viscosity of the compound also tended to decrease. It can be concluded that B1 is better than B2, B3 and B4. However, if rubber vulcanizates require high tear resistance and abrasion resistance, such as for shoes sole and tread of tire, then B4 is the most appropriate vulcanizate.

Key words : Carbon black, Curing characteristic, Mastication, Natural rubber

ABSTRAK

PENGARUH MASTIKASI TERHADAP KARAKTERISTIK PROSES *CURING* DARI KARET ALAM DAN SIFAT FISIK DARI HASIL VULKANISASINYA. Studi ini mempelajari pengaruh dari proses mastikasi terhadap karakteristik proses *curing* dari karet alam dan sifat fisis dari hasil vulkanisasinya. Percobaan diawali dengan proses mastikasi dari karet alam dengan memvariasikan *carbon black* sebagai material pengisi (*filler*). Material yang dihasilkan kemudian dianalisis untuk mengukur karakteristik dari proses *curing* dengan menggunakan *rheometer* serta diuji dengan *Mooney Viscosity tester*. Sifat fisis dari hasil vulkanisasi yang diuji termasuk ketahanan abrasi, ketahanan sobek, serta perpanjangan putus. Hasil uji menunjukkan bahwa *curing characteristic* cenderung menurun, sementara waktu pemanasan cenderung naik dari B1, B2, B3 dan B4. Perpanjangan putus cenderung menurun, sementara ketahanan sobek dan abrasi cenderung naik dari B1, B2, B3 dan B4. Viskositas *Mooney* dari campuran juga cenderung menurun. Dapat disimpulkan bahwa B1 lebih baik dari B2, B3, dan B4. Meskipun demikian, untuk hasil vulkanisasi yang memerlukan ketahanan sobek dan ketahanan abrasi yang tinggi, seperti untuk alas sepatu atau ban, maka B4 merupakan produk yang paling tepat.

Kata kunci : *Carbon black*, *Curing characteristic*, Mastikasi, Karet alam

INTRODUCTION

The use of filler on rubber compound is very important in determining the physical properties of vulcanizates and economical consideration of the products. In terms of economical aspect, filler reduces the price of rubber compound without decreasing the physical characteristics, and even there are synergies of reinforcement of certain physical properties of rubber vulcanizates. Particle size and structure of carbon black filler determine the physical properties of rubber vulcanizates. To function carbon black as reinforcing filler, it requires its total area and specific surface activity [1]. Filler addition into rubber compound in the

Vol. 12, No. 2, Februari 2011, hal : 81 - 85
ISSN : 1411-1098

form of carbon black, silica, and carbon-silica influenced dynamical properties of rubber vulcanizates [2,3], as well as rubber mastication procedure, i.e. the way to add carbon black filler into rubber. For filler added first to the rubber and oil was added after carbon black had been incorporated, the abrasion resistance was higher than that of carbon black and rubber mixed by oil and carbon black addition together [4].

Mixing sequence of ingredients and mixing sequence of coupling agent influencing the dynamical properties have been also studied [5]. The effort to know good filler dispersion was conducted by measuring carbon black flocculation. Flocculation was evaluated by the variation of the electrical resistivity of rubber samples aged under different conditions. There was a correlation between flocculation and bound rubber. Bound rubber influenced curing characteristic [6]. The filler dispersion of carbon black obtained by electrical measurement was found to be more dependent on the particle size [7, 8].

Here, carbon black type was used which had different structure N 326, N 330, and N 351 [9]. Carbon black type N 220 and N 550 was used to study curing characteristic of rubber. Types of carbon black influenced to the curing rate and curing time [10]. The existence of carbon black filler decreased the scorch time and functioned as a catalyst of the crosslink formation [11]. From this point of view, carbon black filler addition into rubber, type and structure of filler, and sequence of rubber mixing (mastication) were the most important factors to make the expected curing characteristic and physical and dynamical properties of rubber vulcanizates. However there are no thorough consideration concerning the method of carbon black addition into rubber.

Rubber mastication was the main purpose in this research, with the aim to study the filler addition into rubber and variation of mastication procedure. The filler used is carbon black type N 330.

EXPERIMENTAL METHOD

Materials

The main raw materials used in the experiment were natural rubber Ribbed Smoked Sheet (RRS-1) and carbon black filler type N 330. The chemical ingredients were sulfur, Tert Butyl Benzothiazole Sulfenamide (TBBS), Tetra Methyl Quinone (TMQ), ZnO, stearic acid and oil.

Equipment

The equipment used in the experiment are open roll mill, rheometer MDR 2000, temperature thermocouple, tensometer, Mooney viscosity equipment, tear strength tester and abrasion resistance tester.

Table 1. Natural rubber formula RSS-1

No	Ingredients	Phr
1.	RSS-1	100
2.	ZnO	5
3.	Stearic acid	2
4.	Carbon Black N 330	50
5.	Paraffinic oil	5
6.	TMQ	2
7.	TBBS	0,5
8.	Sulfur	2,5

Table 2. Sequence of rubber mastication RSS-1

No	Ingredients	Time, minutes
1	RSS-1	1
2	Stearic acid	1
3	Sulfur	2
4	ZnO	
5	CB_1	3
6	CB_2 + oil	7
7	TBBS	6
8	TMQ	
	Total	20

Procedure

Rubber mixture with the formula listed in Table 1 was masticated using open roll mill with sequence and time taken for each sequence of carbon black filler addition and other chemical ingredients shown on Table 2. Mooney viscosity of rubber compound was then measured.

Curing characteristic of rubber compound was also measured using rheometer at temperature 150 °C. The rheograph indicated the relation between vulcanization time and torque change on curing region. Based on this vulcanization time, the specimen can be cured to measure its physical properties.

Rubber formula in Table 1, especially Carbon Black-1 (CB-1) and Carbon Black-2 (CB-2) added on rubber mastication process were varied. There are four variation of carbon black addition into rubber: B1, B2, B3 and B4. B1 refers to the amount of carbon black filler 10 phr (part per hundred rubber) from the total of 50 phr

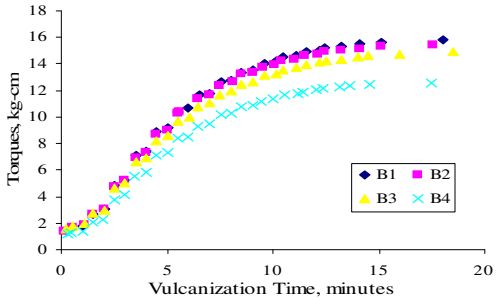

Figure 1. Torque as a function of vulcanization time of natural rubber compound RSS-1 on vulcanization temperature 150 °C

carbon black, added in the beginning of mastication process. Similarly, B2 refers to 20 phr the carbon black filler added in the beginning of mastication process from the total 50 phr, and the remaining carbon black is added afterward. The procedure of B3 and B4 are similar to B1 and B2 with 30 phr and 40 phr carbon black filler first addition, respectively.

Refer to rheograph on Figure 1, vulcanization time and temperature determined from the Figure 1 were used to produce and measure the physical properties of specimen namely elongation at break, abrasion resistance and tear resistance.

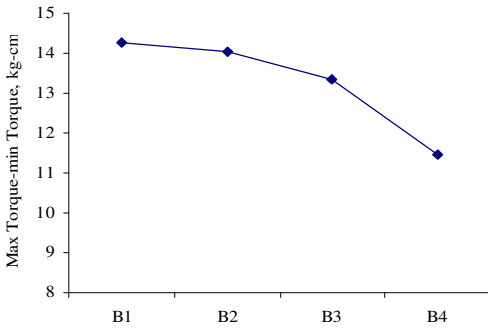

Figure 3. Maximum torque-minimum torque as a function of mastication procedure.

RESULTS AND DISCUSSION

The observation on the change of torque as the function of vulcanization time using rheometer is presented in Figure 1. Figure 1 shows the increase of torque that was in line with the increase of vulcanization time on curing region [12-17]. This torque change was caused by the increase of rubber stiffness that was proportional with the vulcanization reaction occured.

Sample B1 has the highest torque followed by B2, B3, and B4. It significantly indicated there was an influence of mastication procedure upon the physical properties of rubber vulcanizates. The more carbon black filler was added in the beginning of mastication process, the less its influence on the torque change was. It implied that the large number of carbon black filler in the beginning of mastication did not guarantee carbon black filler to be reinforcing filler.

There was a competition between carbon black particles, aggregates or its cluster to function as reinforcing filler. Only those that are closer to rubber backbone could function as reinforcing filler. If the number of carbon black particle was small, it was highly possible that carbon black filler was closer to rubber backbone so that they could function as reinforcing filler.

The relation between scorch time and mastication procedure was illustrated in Figure 2. Figure 2 showed that scorch time tended to increase from B1 to B4. Scorch time is the time required for rubber compound to flow in order to fill the most difficult part of the mould in the molding process of rubber goods industry. The higher the scorch time the slower the vulcanization reaction was, but the more chances for rubber compound to flow to the most difficult part of mould. Scorch time also influenced the lapse between maximum torque and minimum torque. The higher the scorch time was, the smaller the lapse between maximum torque and minimum torque was. A high scorch time indicates that vulcanization reaction proceeds slowly and insignificantly influence the torque of rubber vulcanizates. The lapse between maximum torque and minimum torque is illustrated in Figure 3.

The relation between curing rate and mastication procedure was shown in Figure 4. Curing rate was calculated using Equation (1) as follows [6]:

$$Curing\ rate = \left[\frac{(Torque_{max} - Torqur_{min}}{Opt.Curing - ScorchTime}\right] \quad \text{.....} \quad (1)$$

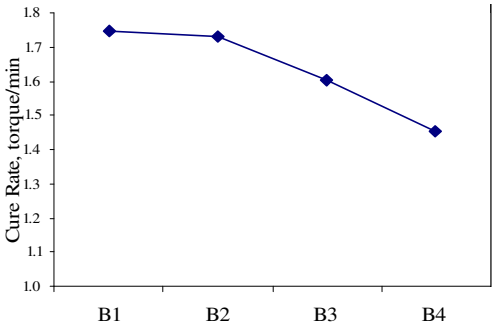

Figure 4. Cure rate as a function of mastication procedure.

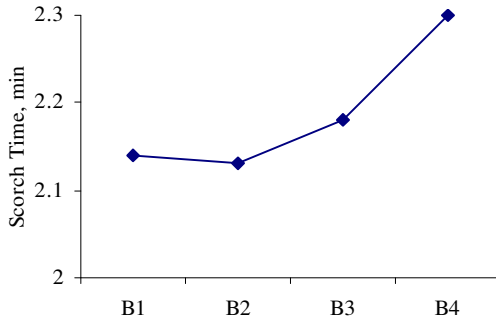

Figure 2. Scorch time as a function of mastication procedure.

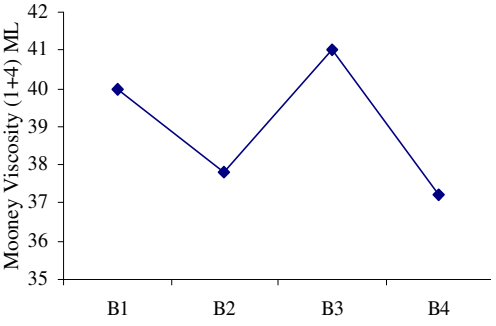

Figure 5. Mooney viscosity as function of mastication procedure.

Vol. 12, No. 2, Februari 2011, hal : 81 - 85
ISSN : 1411-1098

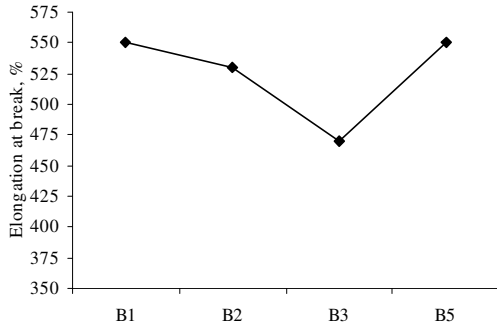

Figure 6. Elongation at break as function of mastication procedure.

Figure 4 indicates the reduction of curing rate starting from B1 to B4. Rubber mastication procedure influenced the curing rate. The more carbon black was added in the beginning process of mastication, the smaller the competition of carbon black filler to function as reinforcing filler was, and the smaller the chance of carbon filler to be closer to rubber backbone. The increase of maximum torque and scorch time caused the low curing rate.

The relation between Mooney viscosity and mastication procedure was illustrated in Figure 5, which showed the tendency of Mooney viscosity to decrease on B1 to B4. Here, the number of carbon black filler plays a significant role in the beginning of mastication process to make rubber softening. Particles of carbon black filler that sheared between rubber backbones in the mastication process can play a role in tearing up the rubber molecule chain besides shearing force of roll mill. Rubber softened and its viscosity decreased.

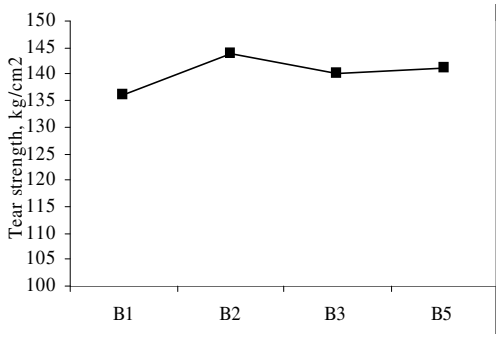

Figure 7. Tear resistance as function of mastication procedure.

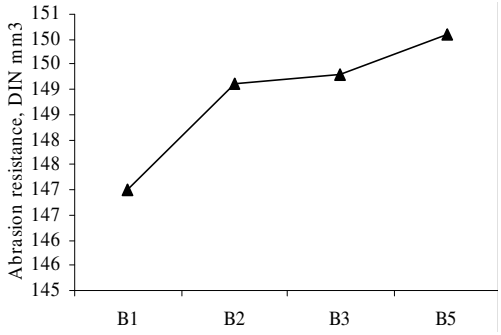

Figure 8. Abrasion resistance as function of mastication procedure

The relation between elongation at break and mastication procedure was illustrated in Figure 6, which showed the decrease of elongation at break starting from B1 to B4. The larger number of carbon black filler added in the beginning process of mastication can cause the spaces between rubber backbones fully filled so that rubber vulcanizates becomes stiffer. The increase of rubber vulcanizates stiffness decreases elongation at break or there are more carbon black filler that cannot function as reinforcing filler on rubber vulcanizates. The increase of stiffness on rubber vulcanizates can increase tear strength and abrasion resistance. High tear resistance and abrasion resistance are required for rubber goods such as shoe sole and tread of tire.

The relation between tear strength and abrasion resistance and mastication procedure are shown in Figure 7 and Figure 8.

CONCLUSION

Mastication procedure of rubber compound B1 to B4 influenced the curing characteristic. Mooney viscosity and the physical properties of rubber vulcanizates. Maximum torque-minimum torque and curing rate tended to decrease while scorch time tended to increase. Mooney viscosity also decreased from B1 to B4. Tear resistance and abrasion resistance tended to increase while elongation at break tended to decrease from B1 to B4. In general, B1 was better than B2, B3, and B4. However, if rubber vulcanizates require high tear resistance and abrasion resistance, such as for shoes sole and tread of tire, B4 is the most appropriate vulcanizate.

ACKNOWLEDGMENT

I would like express my gratitude to Bogor Research Station for Rubber Technology, Polymer Technology Laboratory of Chemical Engineering Department Faculty of Engineering Gadjah Mada University, and Doctor Dissertation Grant from DGHE Republic of Indonesia.

REFERENCES

[1]. J. B. HORN, *Materials for Compounding and Reinforcement and B. B. Boonstra*, *Reinforcement by Fillers in Rubber Technology and Manufacture*, C. M. BLOW and C. HEPHURN, London, Butterworth Scientific, **2nd** (1982) 202-216 and 269-308

[2]. M. J. WANG, *American Chemical Society, Meeting of The Rubber Devision*, Indianapolis, Indiana US, (1998)

[3]. M. J. WANG, *Kautschuk Gummi Kunststoffe*, **61** (2008) 159-165

[4]. M. J. WANG, *International Rubber Conference*, Lyon France, (2006)

[5]. M. J. WANG, *Rubber, Chemistry and Technology*, **71** (1998) 520-589

[6]. M. GERSPACHER, L. NIKIEL, H. H. YANG, C. P. O'FARREL, and G. A. SCHWARTZ, *American Chemical Society, Meeting of the Rubber Division,* Cleveand, Ohio US, (2001)

[7]. N. TRICAS, E. V. ESCALES, S. BARROS, and M. GERSPACHER, *Composite Science and Technology*, **63** (2003) 1155-1159

[8]. C.P. O'FARREL, M. GERSPACHER, and L. NIKEL, *Kautschuk Gummi Kunststoffe*, **53** (2000) 701-710

[9]. S. S. CHOI, *J. Appl. Polym. Sci.,* **93** (2004) 1001-1006

[10]. S. S. CHOI, K. J. HWANG, and B. T. KIM, *J. Appl. Polym. Sci.,* **98** (2005) 2282-2289

[11]. N. TRICAS, E. V. ESCALES, and S. BARROS, *Afinidad,* **59** (2002) 337-342

[12]. R. DING, and A. I. LEONOV, *J. Appl. Polym. Sci.,* **61** (1996) 455-463

[13]. R. DING, A. I. LEONOV and A. Y. CORAN, *Rubber Chem. Technol.,* **69** (1996) 81-91

[15]. P. Y. WANG, H. L. QIAN, H. P. YU, and JIN CHEN, *J. Appl. Polym. Sci.,* **88** (2003) 680-684

[14]. M. A. L. MANCHADO, M. ARROYO, J. HERRERO and J. BIAGIOTTI, *J. Appl. Polym. Sci.,* **89** (2003) 1-15

[16]. P. Y. WANG, H. L. QIAN, and HE-PING YU, *J. Appl. Polym. Sci.,* **101** (2006) 580-583

[17]. P. Y. WANG, Y. CHEN, and H. L. QIAN, *J. Appl. Polym. Sci.,* **105** (2007) 3255-3259

Jurnal Sains Materi Indonesia
Indonesian Journal of Materials Science

Vol. 12, No. 2, Februari 2011, hal : 86 - 90
ISSN : 1411-1098

Akreditasi LIPI Nomor : 452/D/2010
Tanggal 6 Mei 2010

SYNTHESIS AND CHARACTERIZATION OF NATURAL RUBBER-SILICA COMPOSITE

Indra Gunawan[1], Hildayati[2], Sudirman[1,3] and Emil Budianto[3]

[1]Center for Technology of Nuclear Industry Materials-National Nuclear Energy Agency
Kawasan Puspiptek Serpong 15314, Tangerang, Indonesia
[2]Dept. of Physics, Fac. of Math. and Natural Sciences-Sepuluh November Institute of Tech. Surabaya
Kampus ITS Sukolilo, Surabaya 60111, Indonesia
[3]Dept. of Chemistry, Fac. of Math. and Natural Sciences-University of Indonesia
Kampus Baru UI, Depok 16424, Indonesia
e-mail : gindra@lycos.com

ABSTRACT

SYNTHESIS AND CHARACTERIZATION OF NATURAL RUBBER-SILICA COMPOSITE. The composite of natural rubber-silica have been developed with a combination of silica (SiO_2) particles in irradiated natural rubber. This research was conducted with the aim to composite material with irradiated natural rubber as the matrix and silica particles as filler and to study the distribution of silica in the matrix as well as mechanical and physical properties. The results showed that the SiO_2 particles homogenously distributed across the surface of natural rubber matrix as the cluster. The particles are arranged as a cluster by using 3-aminopropyltriethoxysilane (APTES) as a coupling agent. Tensile strength, tensile modulus and elongation at break of composite materials have increased as the addition of SiO_2 on the composition of 9 to 12 percent weight in natural rubber. Additions of SiO_2 composition in the matrix will also increase the hardness of the composite. Structural analysis were performed using FT-IR and SEM. Composite of natural rubber-SiO_2 have a great potential to be applied as a natural rubber base materials mainly as protective products with higher performance.

Key words : Natural rubber, Silica, Composite, Coupling agent

ABSTRAK

SINTESIS DAN KARAKTERISASI KOMPOSIT DARI KARET ALAM-SILIKA. Komposit dari karet alam dan silika telah dikembangkan dalam penelitian ini. Tujuan dari penelitian ini adalah untuk membuat komposit berbasis karet alam teriradiasi sebagai matriks dan partikel silika sebagai pengisi (*filler*) dan untuk mempelajari distribusi dari partikel silika dalam matriks, sifat-sifat fisik dan mekanik dari komposit yang dihasilkan. Hasil penelitian menunjukkan bahwa partikel SiO_2 terdistribusi secara homogen pada permukaan dari matriks karet alam sebagai *cluster*. Partikel dari SiO_2 tertata sebagai *cluster* dengan menggunakan 3-aminopropyltriethoxysilane (*APTES*) sebagai *coupling agent*. Kekuatan tarik, modulus tarik, serta perpanjangan putus dari komposit mengalami kenaikan dengan bertambahnya komposisi SiO_2 (9 %w/w hingga 12 %w/w). Penambahan SiO_2 juga akan menaikkan tingkat kekerasan komposit. Analisis komposit dilakukan menggunakan *FT-IR* dan *SEM*. Hasil penelitian menunjukkan bahwa komposit karet alam-silika memiliki potensi yang baik untuk dipergunakan sebagai material berbasis karet alam terutama sebagai produk protektif dengan performa tinggi.

Kata kunci : Karet alam, Silika, Komposit, *Coupling agent*

INTRODUCTION

Advanced in producing high performance polymer based compositions will in future more likely result from the utilization of new mixtures of polymers and mixtures of polymers with reinforcing components, rather than from new polymer compositions. The term composites is generally applied to fiber reinforced engineering structural materials, in which the fibers are continuous or long enough that they can be oriented to produce enhanced strength properties in one direction [1]. A composite structure is a combination of two or more different component resulting in material having better performance than each individual constituent [2]. Thus the material properties are a function of filler composition

which includes concentration, size, shape and distribution.

As new technologies continue to place increasingly stringent demands on the performance of polymeric materials, it is becoming clear that traditional polymer composites can not meet these requirements. As a result, new material composites are being developed, utilizing multifunctional nature of nano scale materials [3]. The interface between the composite components plays a defining role in the overall composite properties. The available interfacial area is increased by the dispersion of nano sized particles throughout the polymer matrix. So that the material is expected to have an improved properties such as its electrical properties, mechanical and other properties. The main characteristic of the beneficial use of filler particles is to use fewer products to reduce cost.

The wide spectrum of properties available to polymeric materials has afforded numerous practical applications ranging from common household goods to biomedical materials and aerospace components. This is because polymers generally have a distinctive behavior that is printable, lightweight, good insulators and cheap. Plastics, fibers, films, wires and rubber are some examples of polymers commonly used in industry.

In this study, the basic material used as the matrix is natural rubber or latex. Natural rubber is a natural polymer derived from isoprene monomer plant sap from hevea brasiliensis in family of euphorbiceae. Natural rubber could be classified as an elastomer and it can be used as raw material for various types of finished goods such as rubber gloves. Natural rubber is a molecule with a backbone of cis-1 ,4-polyisoprene and color varies from yellow to dark brown, not resistant to hydrocarbon solvents and susceptible to oxidation and thermal degradation. Natural rubber is one of the most important elastomeric materials for diverse industrial applications. However, natural rubber by itself does not possess high enough modulus for most applications and needs to be reinforced with fillers and cross linked with curing agents.

Extensive studies have been carried out in the development of the performance of natural rubber products, such as using black carbon, calcium carbonate, the modified clay, and silica particles as filler materials in the natural rubber. Study of preparation and characterization of self assembled natural rubber/silica nanocomposites as well as effect of filler surface treatment properties of fly ash/natural rubber blend have been done [4,5]. Another research have been carried on covering properties of vulcanized rubber nanocomposites filled with nanokaolin and precipitated silica [6], the effect of filler on epoxidized natural rubber-alumina composite [7] and viscoellastic properties of natural rubber composites reinforced by defatted soy flour and carbon black co filler [8].

In this study, silica particles will be used as filler in natural rubber matrix. Silica is a compound of metal oxide which is widely available in nature, but its presence is bound with other compounds. The nature of the silica is hard, heat resistant and stable. Silica also has a wide surface area, large pore volume, and the ability to absorb another substance such as water, oil and radioactive materials. In general, silica is both hydrophilic and hydrophobic when bonded with other elements in accordance to the structure and morphology.

This research was conducted with the aim, to produce natural rubber based composite materials with silica particles as filler and to study the distribution of silica in the matrix as well as its mechanical and physical properties.

EXPERIMENTAL METHOD

The materials used are irradiated natural rubber with radiation dose of 15 kGy, silica type A275 obtained from UPN Surabaya, 3-aminopropyltriethoxysilane as a coupling agent, distilled water, 0.2 M NaOH and ethanol.

The equipments used in this study are: pipettes, measuring glass, spatula, mortar, sieve, High Energy Milling Machine (HEM) and mixer.

Natural rubber was irradiated priorly to obtain crosslinking to form three dimensional structure and physical properties changes. Silica as a filler first crushed using mortar and sieved using 400 mesh sieves. Silica powder pulverized again by using HEM for 8 hours. 3-aminopropyltriethoxysilane as a coupling agent as much as 10 percent weight mixed with the powder first silana with ethanol. Mixture should be stirred evenly then oven dried at 40 ^{o}C for 1 hour. After drying the mixture at silica and 3-APE dispersed into the water. Already dispersed silica with a pH of latex pH adjusted using NaOH. Furthermore, the dispersed silica was added to natural rubber with varied amounts of 3, 6, 9, 12 and 24 %w/w. The mixture was stirred by using a mixer for 30 minutes and then printed. Sample is left to dry at room temperature for several days, then washed and dried in an oven at a temperature of 70 ^{o}C for 1 hour. After drying the sample was ready for characterizations.

Characterization equipments used were X-Ray Diffractometer (XRD) Phillips PW 1710, PSA Delsa Nano C, Universal Testing Machine, and Fourier Transform Infra Red (FT-IR) Spectrometer.

Measurement of tensile strength, tensile modulus and elongation at break was done by using a Universal Testing Machine (UTM) following ASTM method D4102-9.

RESULTS AND DISCUSSIONS

Figure 1 shows the XRD patterns for SiO_2 powders prior to milling process (0 hours) and after

Vol. 12, No. 2, Februari 2011, hal : 86 - 90
ISSN : 1411-1098

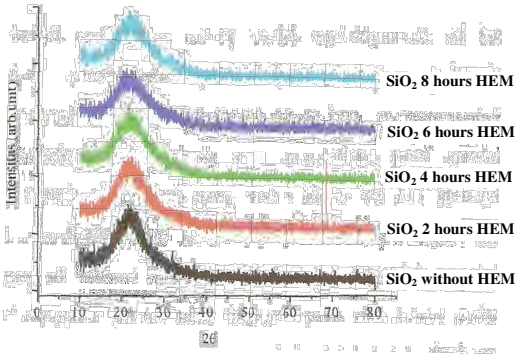

Figure 1. The XRD patterns of SiO_2 powders prior to milling process (0 hours) and after milling of 2, 4, 6 and 8 hours, respectively

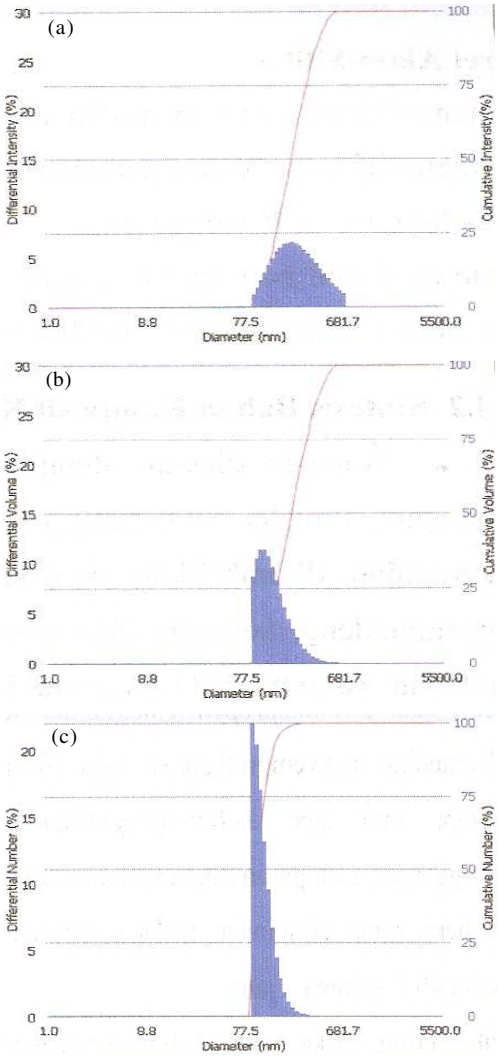

Figure 2. SiO_2 particle size distribution measured by using particle size analyzer (PSA).

consecutive milling time for 2, 4, 6 and 8 hours. From the diffraction pattern shown in Figure 1, it can be concluded that there is SiO_2 phase characterized by diffraction peaks at $2\theta = 10.76°$ and $21.57°$. Amorphous SiO_2 phase is dominating the diffraction pattern characterized by the absence of sharp peaks and the presence of broad diffraction peaks at angles $2\theta = 21.57°$.

Figure 3. SEM images of natural rubber (a), natural rubber-SiO_2 composite with 9 % wt SiO_2 (b), natural rubber-SiO_2 composite with 12 % wt SiO_2 (c) and natural rubber-SiO_2 composite with 24 % wt SiO_2

SiO_2 particle size distribution measured by using particle size analyzer (PSA), are noted in Figure 2. The Figure 2 shows that the use of HEM can reduce the size of SiO_2 powder, which is 266 nm by using the intensity distribution analysis, using volume of distribution is 150 nm and using the sum distribution analysis is 117 nm.

A SEM image of natural rubber is shown in Figure 3. It displays the simple polymer network and there are no voids. The SEM image of natural

rubber-SiO_2 composites reveal homogenously distribution of SiO_2 particles as cluster. The dark image represents the natural rubber and the bright image corresponds to silica particles. From the SEM images the surface roughness increased with increasing filler up to 24 %. It can be observed that the agglomerates increase as the silica content was further added. This may due to the worsening wettability of matrix onto filler surface when ratio of fillers to natural rubber is too high.

Tensile Strength measurement as a function of the addition of SiO_2 in natural rubber shown in Figure 4. Based on these data we can conclude that the tensile strength tends to increase with increasing SiO_2 content until 12 % in natural rubber. By increasing the filler, the chemical bonding between polymer and filler increased, so the force applied can be distributed homogenously by the filler.

The maximum tensile strength was obtained with the SiO_2 composition in natural rubber as much as 12 % with a tensile strength of 19.91 MPa. In SiO_2 addition as many as 24 % tensile strength decreasing compared to tensile strength at 12 % filler addition, because the filler particles are no longer adequately separated or wetted by rubber phase. This result is in agreement with the SEM image obtained.

Tensile modulus measurement at 600 % elongation as effect of SiO_2 addition in natural rubber shown in Figure 5. Mechanical properties of a material can be seen from the modulus of elasticity. The greater the modulus of elasticity, the better mechanical properties of the materials because the material is not easily deformed. Tensile modulus is increasing by the addition of SiO_2 for 12 to 24 %. This strengthening anticipated for dispersing the filler has done well so homogenously distributed in the matrix.

Elongation at break of natural rubber-SiO_2 composite increases with increasing composition of SiO_2 until 12 % and then decreases at 24 %, as shown in Figure 6. At composition of 12 % SiO_2, interaction between filler surface with natural rubber as matrix is strong. This is due to cross-linking between natural rubber. But at the addition of 24 % SiO_2 elongation at break of the composites decrease, caused by slip between SiO_2 particles in natural rubber matrix which weakens the bond and easily broken.

As usually conceived, hardness is a composite property combining concept of resistance to penetration, scratching, marring and so on. Most hardness tests for plastics are based on resistance to penetration by an indentor pressed into the plastic under constant load. Effect of SiO_2 content as filler to composite hardness is shown in Figure 7.

Based on Figure 7 in above, it is concluded that increasing the SiO_2 content in the matrix, will increase the composite hardness. This increasing may be attributed to higher crosslink and good distribution of fillers in the natural rubber matrix.

The FT-IR spectra of SiO_2, natural rubber and natural rubber-SiO_2 composite with addition of 9 wt% SiO_2 could be seen in Figure 8, Figure 9 and Figure 10 respectively. The peak at 1105 cm^{-1} could be ascribed to

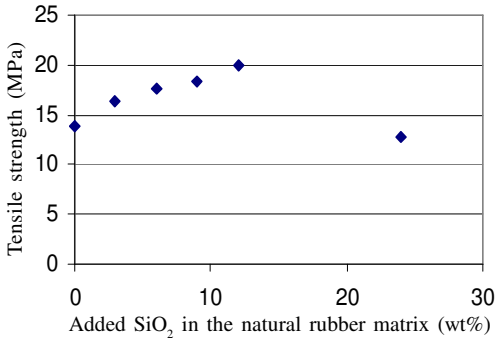

Figure 4. Graph of tensile strength as addition of SiO_2 in the natural rubber matrix

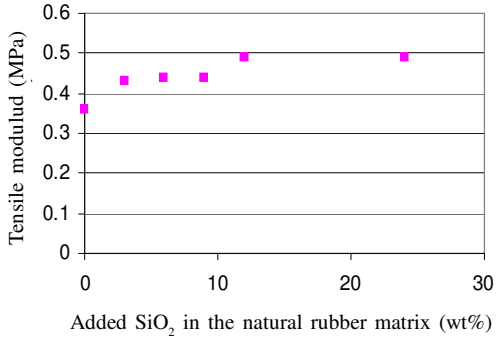

Figure 5. Graph of tensile modulus as addition of SiO_2 in the natural rubber matrix

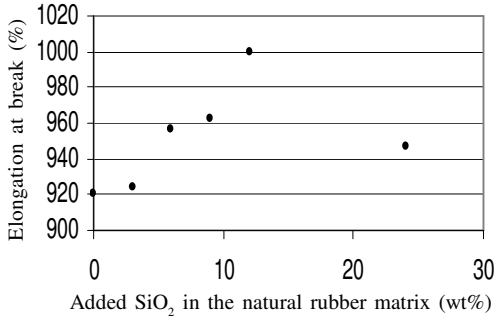

Figure 6. Graph of elongation at break of natural rubber-SiO_2 composites as addition of SiO_2 in the matrix

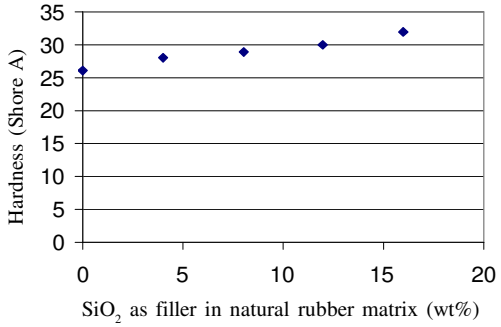

Figure 7. Effect of SiO_2 as filler to composite hardness

Vol. 12, No. 2, Februari 2011, hal : 86 - 90
ISSN : 1411-1098

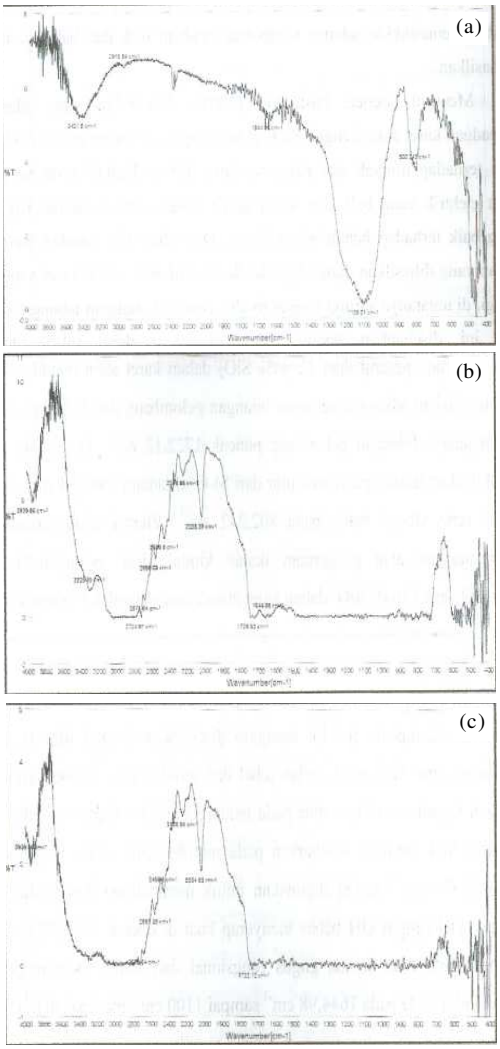

Figure 8. (a) The FT-IR spectra of SiO_2, (b) The FT-IR spectra of natural rubber and (c) The FT-IR spectra of natural rubber-SiO_2 composite

the stretching vibration of Si-O band. While the 3940 cm^{-1}, 3306 cm^{-1}, 2038 cm^{-1} peak were the relative to C-H, O-H and C = C groups, respectively. The FT-IR spectra of natural rubber-SiO_2 composite in Figure 8(c) are different to the Figure 8(a) and Figure 8(b). The difference of FT-IR spectra is loss peak at 1645 cm^{-1} and wave numbers shift occurred from 1730 cm^{-1} to 1722 cm^{-1}. Wave number shift is caused by the interaction of SiO_2 with natural rubber that involving chemical bonding between polymer and filler.

CONCLUSIONS

Natural rubber as the matrix has good elasticity, have been dispersed silica into it to form a composite with the addition of 3-aminopropyltriethoxysilane as coupling agent has good mechanical properties.

Additions of SiO_2 into the natural rubber as much as 12 wt% produce optimum mechanical properties namely tensile strength of 19.91 MPa, tensile modulus at 600% elongation of 3.48 MPa and elongation at break of 1000 %.

REFERENCES

[1]. F.W. BILLMEYER, *Textbook of Polymer Science*, 3rd Ed., John Wiley & Sons, Singapore, (1994)
[2]. K. JANG, W.J. CHO, C.S. HA, *Compos. Sci. and Technol.*, **59** (7) (1999) 995-1001
[3]. G.S. MILLER, Effects of Nanoparticle and Matrix Interface on Nanocomposite Properties, *Thesis The University of Akron*, (2008)
[4]. Z. PENG, L.X. KONG, S.D. LI, Y. CHEN, M.F. HUANG, *J. Compos. Sci. and Technol.*, **67** (2007) 3130-3139
[5]. S. THONGSON, N. NOMBATSOMPOP, *J Pol. Proc. And Flow*, (2005)
[6]. X. LIU, S. ZHAO, *J Appl. Pol. Sci.*, **10** (2008) 1002
[7]. N. MOHAMAD, A. MOCHTAR, *Euro. J. of Sci. Res.*, **24** (4) (2008) 538-547
[8]. L. JONG, *J. Appl. Pol. Sci.*, **106** (2007) 3444-3453

Akreditasi LIPI Nomor : 452/D/2010
Tanggal 6 Mei 2010

ACTIVATION AND PURIFICATION OF BENTONITE FOR THE TREATMENT OF CRUDE PALM OIL AS VEGETABLE OIL

Tutun Nugraha[1,2], Yestine Yuliantina[1] and Supandi Suminta[2]
[1]*Faculty of Life Sciences, Swiss German University, BSD City, Indonesia*
[2]*Center for Technology of Nuclear Industry Material (PTBIN)-BATAN*
Kawasan Puspiptek Serpong 15314, Tangerang
e-mail : yestine.yuliantina@yahoo.co.id

ABSTRACT

ACTIVATION AND PURIFICATION OF BENTONITE FOR THE TREATMENT OF CRUDE PALM OIL AS VEGETABLE OIL. Crude Palm Oil (CPO) to be used for cooking oil requires processing that includes bleaching step which is typically done using bleaching earth made from activated bentonite. Bentonite is a type of mineral that is very rich in montmorillonite. Currently, substantial amount of activated bentonite used by vegetable oil industries are imported. In this research, the bentonite was obtained locally from the region of Leuwiliang (Bogor, West Java). The bentonite was purified using solution of sodium-hexa-meta-phosphate $(NaPO_3)_6$, and was activated using acid reflux methods (H_2SO_4, 100°C). The bentonite activation was done at two different reflux times (1 and 3 hour), and three different acid concentrations (1 M, 2.5 M and 5 M). To assist the interpretation of results, the bentonite samples were also studied using XRF and XRD. Bleaching power of active bentonite was initially studied using adsorption of methylene blue for optimation, which was followed by bleaching of CPO. The results showed that, the purified bentonite and activated at 1 molar H_2SO_4 for 1 hour duration, had the highest bleaching capacity. In addition, the treated oil also showed substantial reduction of peroxide number, and also some reduction of free fatty acid content (FFA) which further improve the quality treated palm oil.

Key words : Bentonite, Bleaching earth, XRD, XRF, Crude palm oil, CPO

ABSTRAK

AKTIFASI DAN PURIFIKASI BENTONIT UNTUK DIGUNAKAN DALAM PEMROSESAN MINYAK SAWIT MENTAH SEBAGAI MINYAK GORENG. Minyak sawit mentah (*CPO*) yang akan dipergunakan untuk minyak goreng memerlukan pemrosesan, termasuk adanya *bleaching* yang dilakukan dengan menggunakan bahan *bleaching earth* yang berasal dari bentonit yang telah diaktifasi. Bentonit merupakan salah satu mineral hasil tambang yang kaya dengan *montmorillonite*. Saat ini, jumlah bentonit aktif yang dipergunakan oleh industri minyak goreng merupakan hasil impor. Dalam penelitian ini, bentonit yang dipergunakan ditambang dari daerah Leuwiliang (Bogor, Jawa Barat). Bentonit ini dipurifikasi menggunakan sodium hexa meta phosphate $(NaPO_3)_6$ dan diaktifasi menggunakan proses refluks asam (H_2SO_4, 100 °C). Proses pengaktifan bentonit dilakukan variasi waktu refluks yang berbeda yaitu 1 jam dan 3 jam dengan konsentrasi asam yang berbeda yaitu 1 M, 2,5 M dan 5 M. Untuk membantu interpretasi dari data yang dihasilkan, sampel bentonit juga dipelajari menggunakan *X-Ray Fluoresence Spetroscopy* (*XRF*) dan *X-Ray Diffractometer* (*XRD*). Kekuatan *bleaching* dari bentonit aktif pada tahap awal diukur menggunakan proses adsorpsi dari *methylene blue* untuk proses optimasi, diikuti dengan *bleaching* langsung terhadap *CPO*. Hasil menunjukkan bahwa bentonit yang telah dimurnikan dan diaktifkan dengan 1 M H_2SO_4 selama 1 jam memiliki kapasitas *bleaching* yang paling tinggi. Selain itu, minyak yang telah memperoleh perlakuan dengan bentonit juga memperlihatkan penurunan bilangan peroksida dan kandungan asam lemak bebas (*FFA*) yang berarti meningkatkan kualitas dari minyak sawit.

Kata kunci : Bentonit, *Bleaching earth*, *XRD*, *XRF*, Minyak sawit mentah, *CPO*

INTRODUCTION

Crude Palm Oil (CPO) is one of the agricultural commodities that are considered important for Indonesia. Indonesia is the world major producer of Crude Palm Oil with a production, in 2008, of about 18.5 million tons [1].

Vol. 8, No. 2, Februari 2007, hal : 91 - 95
ISSN : 1411-1098

In cooking palm oil industries, Crude Palm Oil undergoes some processing to become what is known as commercial frying oil. One of these processes is the bleaching stage. One of the examples of bleaching agent applied is bentonite. To be useful as bleaching earth in the palm oil industries, the bentonite needs to be activated such as through acid reflux treatment. Furthermore, bentonite coming from different places can have different properties, and may or may not be the most appropriate for use as bleaching earth. Because the demand of bentonite for industries is increasing, substantial amount of activated bentonite are currently imported from Malaysia and China. However, bentonite deposits in Indonesia are still quite massive, predicted to be approximately more than 380 million tons. These deposits are found in the Island of Java, Sumatera, Kalimantan and Sulawesi [2].

EXPERIMENTAL METHODS

The raw bentonite from Leuwiliang (Bogor-West Java) was provided in the form of rock pieces by PT. Sumber Alam Makmur (Serang-Banten). Clarified Crude Palm Oil (CPO) used was obtained from PT. Memorintama Perkasa (Cikupa-Banten). In the pretreatment stage of the raw bentonite, all bentonite samples were crushed into small pieces, dried at 105 °C for about 4 hours in the oven, and were finally ground to pass through a mesh size 120 (0.125 mm). The bentonite samples prior to purification, after purification and after acid treatment, were analyzed for their elemental compositions using X-Ray Fluorescence (XRF) and Atomic Absorption Spectrophotometer (AAS). Characterization of the crystalline nature bentonite samples were performed by X-Ray Diffraction (XRD). The bentonite samples were purified using 0.5 % $(NaPO_3)_6$ solution, and was activated using acid reflux method (H_2SO_4, 100 °C). The ratio of bentonite to H_2SO_4 solution was 1:10 (w/v). Different acid concentrations (1 M, 2.5 M and 5 M) and reflux time (1 hour and 3 hours) were used in the activation.

Adsorption of methylene blue (380 ppm) from solution was done by mixing and shaking each of the treated bentonite at 25 °C, 1 hour, 150 rpm. The amount of methylene blue adsorbed onto bentonite was then calculated. Degumming of the CPO, using a solution of 85 % H_3PO_4 at 100 °C for 20 minutes, was carried out prior to the bleaching. In the bleaching, a mixture of 0.5 g of dry bentonite and 50 mL of CPO was heated under continuous stirring (100 °C, 30 minutes). Following the treatment, the bentonite was removed by centrifugation. Color changes in the treated oils were measured by UV-Vis Spectrophotometer. The bleaching capacities were then calculated. As part of quality control, following treatment with bentonite, free fatty acid (FFA) content and peroxide number of the palm oil were also measured. Measurement of FFA was based on titration with NaOH solution, using phenolphthalein as indicator. Peroxide number measurement was based on titration with $Na_2S_2O_3$ solution. Prior to measurement, the oil sample was diluted with acetic acid-isooctane mixture, and then treated with KI. The result was expressed in milliequivalent per kilogram of oil.

RESULTS AND DISCUSSION

Methylene Blue Adsorption Capacity

After purification and acid treatment, the raw bentonite was initially studied for its bleaching capacities using adsorption of methylene blue. Bentonite was found to be able to absorb methylene blue dye from the aqueous solution. Figure 1 showed that there were no substantial performance differences between the purified and non-purified bentonite samples. Treating the bentonite using higher acid concentration, however (i.e. at 2.5 M and 5 M), appeared to reduce the bleaching capacities. Moreover, 1 hour acid reflux time for the

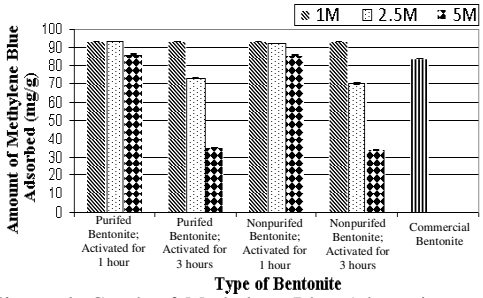

Figure 1. Graph of Methylene Blue Adsorption onto Various Treated Bentonites with a Ratio of Bentonite to Methylene Blue Solution equal to 1:250 (g/mL)

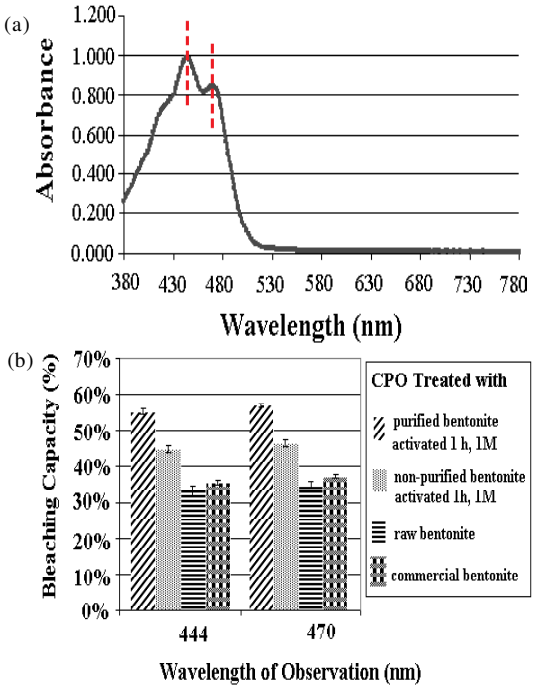

Figure 2. (a) Graph of CPO Absorption Spectra and (b) Bleaching Capacity of Various Treated Bentonites with a Ratio of Bentonite to CPO equal to 1:100 (g/mL)

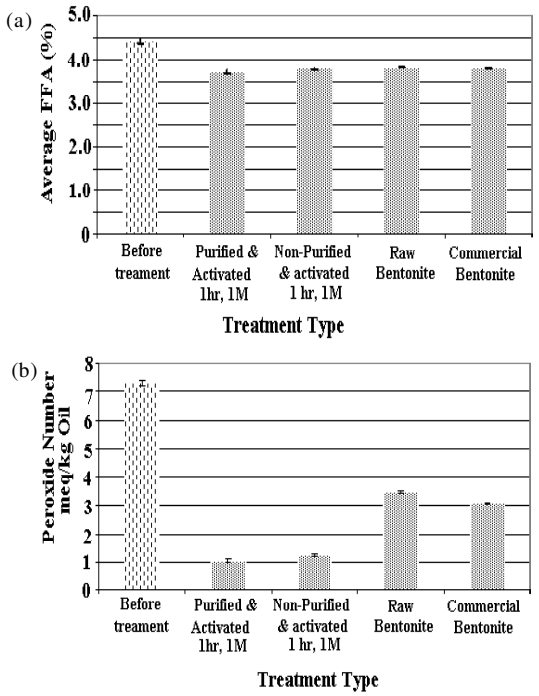

Figure 3. (a) Graph of Free Fatty Acid and (b) Peroxide Number in Crude Palm Oil Samples before and after Bleaching

bentonite appeared to yield better results than the 3 hours reflux time.

Bleaching Capacity

Based on these results, some samples of bentonite that yielded the best results were selected for further studies for their bleaching performance of CPO (1 hour treatment with 1 M H_2SO_4). The results are shown in Figure 2(b). Figure 2(a) showed the maximum absorption spectra of unbleached CPO with peaks that were located at 444 nm and 470 nm. These peaks showed the presence of 13 cis β-carotene that gives the reddish orange color of the natural unbleached CPO.

Figure 2(b) indicated that the purified bentonite; activated with 1 molar H_2SO_4 for 1 hour, had the highest bleaching capacity. Following this, the nonpurified bentonite, treated with the same parameters, had the second highest bleaching capacity. Meanwhile, the commercial and raw bentonites were in the third and fourth place, respectively. It could be concluded that acid activated bentonite was more adsorptive towards the target compounds, and more chemically active than the raw bentonite. The optimum acid concentration needed as found in this study was 1 M H_2SO_4. This finding however does not exclude the possibility of better bleaching performance at acid concentrations lower than 1 M. This is noted for further studies.

Bleaching capacity was related to the adsorption process, which in turn correlated with the surface phenomena. Natural bentonite is rich in surface hydroxyl groups which are responsible for the adsorption process. The presence of these hydroxyl groups could be increased through the acid treatment process. The additional surface hydroxyls were obtained when the octahedral layers of the montmorillonite, which is the principle component of bentonite, were disrupted due to acid attack, leaving behind the hydroxylated segments or silica tails derived from the remaining tetrahedral layer. Surface hydroxyls, acting as the active sites, played important roles in the adsorption of β-carotene. β-carotene was chemisorbed either via electrostatic, or via coordination bonding to the active sites of bentonite structure [3]. These adsorptions of β-carotene resulted in CPO that has lighter color, missing its reddish orange color.

Determination of Free Fatty Acid and Peroxide Number

According to Figure 3, after bleaching, some reduction in the percentage of FFA and substantial reduction of peroxide number were also observed. It should be noted that the percentage of FFA should be checked properly. Acid activated bentonite that was not subjected to proper washing could cause the hydrolysis of triacylglycerol in CPO, resulting in the generation of additional FFA which is not desired. However, the opposite phenomenon was observed, indicated by a slightly decrease in the percentage of FFA.

During bleaching, FFA in the form of palmitic acid interacted through its carbonyl group with the surface hydroxyls present in the montmorillonite via hydrogen bonding. Meanwhile, both acid activated and raw bentonite substantially reduced the peroxide number (Figure 3(b)). The peroxide number was an indicator of the primary oxidation of oil, and hence, it is not desired.

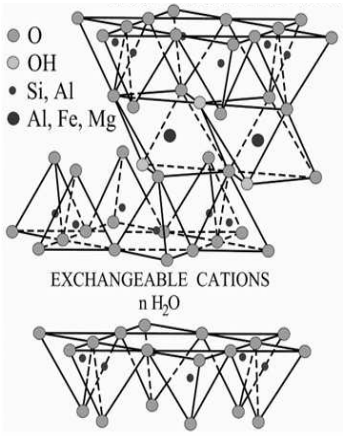

Figure 4. Montmorillonite Structure [5]

Tabel 1. The Elemental Composition of the Raw Bentonite (the Balance being Oxygen and Hydrogen Atoms)

Component	Fe	Ca	K	Si	Al	Mg	Na
Content %	1.783	0.502	0.115	70.469	9.019	6.815	0.0071

Vol. 8, No. 2, Februari 2007, hal : 91 - 95
ISSN : 1411-1098

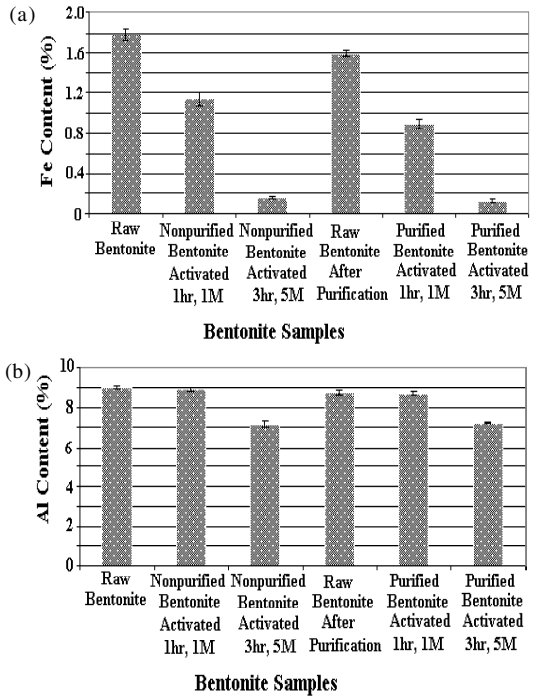

Figure 5. Graph of Iron (a) and Aluminum (b) Analysis in Six Different Bentonite Samples

It was observed that the bleaching using the purified bentonite; activated with 1 molar H_2SO_4 for 1 hour, was the most effective in removing the primary oxidation products. Hence, it can be seen that the bleaching process using acid activated bentonite was a combination of actions, in which the peroxides and FFA were reduced, and accompanied with adsorption of pigments from the oil.

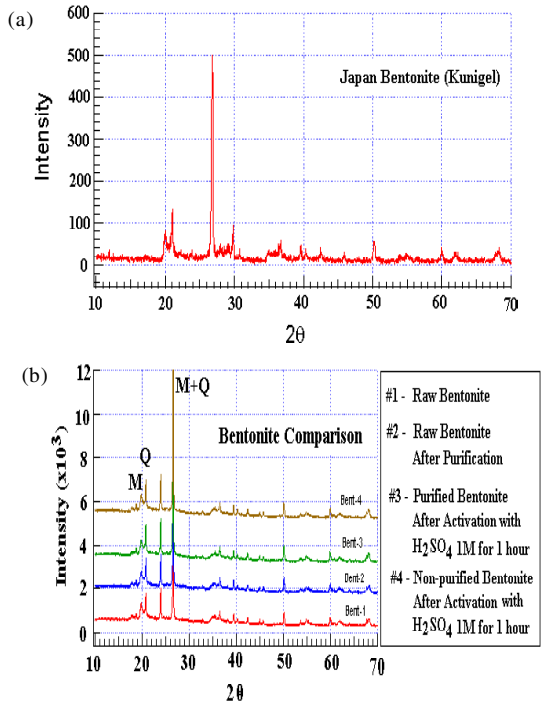

Figure 6. Graph of XRD of Japan Bentonite/Standard (a) and XRD Comparison between Bentonites Produced in this Study. M: Montmorillonite, Q: Quartz (b)

Note :

Bent-1 : raw bentonite before purification
Bent-2 : raw bentonite after purification
Bent-3 : purified bentonite, activated with H_2SO_4 1 molar for 1 hour
Bent-4 : nonpurified bentonite, activated with H_2SO_4 1 molar for 1 hour

Analysis of Bentonite

The results of elemental analysis of the raw bentonite were presented in Table 1. The raw bentonite showed a higher content of calcium compared to sodium, and thus it indicated the presence of calcium bentonite. Montmorillonite was a three-layered sheet of alumino-silicate mineral (Figure 4). Hence, silicone and aluminum comprised higher than 50 % of the bentonite elemental composition. This bentonite also contained iron as one of the main compositions, located in either octahedral or interlayer region of montmorillonite. Iron was present in the interlayer region and might represent impurities that needed to be removed. Note that not all of the data of the elemental analysis were presented here. The complete set of data can be found at Yuliantina (2010) [4].

Any ions present in the interlayer region, for instance Fe, were easier to be removed, and were replaced by sodium due to ion exchange phenomena such as during purification with $(NaPO_3)_6$ solution. Figure 5 confirmed that, after purification, Fe content decreased substantially. Moreover, during acid activation, hydronium ions from the strong acid solution dissolved the octahedral cations (Mg, Fe, and Al). Figure 5 showed that iron and aluminum, decreased after acid treatment. The decrease was more severe when the bentonite was activated with 5 molar H_2SO_4 for 3 hours. This was possible considering that an increase in acid concentrations caused an increase in the damages into the octahedral structure due to acid attack. This finding agreed with previously discussed data and is supported further by the XRD results. When the bentonite was activated with 5 molar H_2SO_4 for 3 hours, it exhibited the lowest methylene blue adsorption capacity.

Characterization of Bentonite with XRD

The main purpose of using XRD in this study was to determine if there were detectable changes of diffraction pattern of the bentonite due to purification and acid activation. The XRD pattern of the raw bentonite before purification indicated that the sample consisted of montmorillonite along with substantial amounts of impurities, namely quartz (Figure 6).

Figure 7 described the example of diffraction pattern of the purified bentonite activated with 5 molar H_2SO_4. It was observed that there were some missing peaks, one of them located in the 2θ of 20 ° which was the signature of montmorilonite [5]. This phenomenon

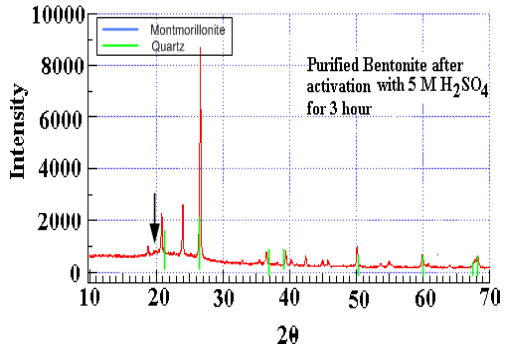

Figure 7. Graph of XRD of Purified Bentonite, Activated with 5 molar H_2SO_4 for 3 hours.

occurred due to the use of high acid concentrations, probably causing some damages in the crystal geometry of the bentonite structure [4,6].

CONCLUSION

The results showed that the optimum activation condition was at constant temperature of 100s °C, using 1 molar of H_2SO_4 and 1 hour acid reflux. The highest bleaching capacity was found to be almost 60s % under optimum condition, which was higher than the adsorption capacity of the available bentonite in the market. If the concentration of acid was too high, the acid would cause damages to the crystal structure of bentonite hindering the bentonite adsorption capacity as shown by the chemical and XRD spectra analysis.

ACKNOWLEDGMENT

The author would like to thank PT. Sumber Alam Makmur as well as PT. Memorintama Perkasa for providing the bentonite samples and the CPO, respectively.

REFERENCES

[1]. Indonesian Crude Palm Oil: CPO Producers see good prices, *Jakarta Post*, (2009)

[2]. Bentonite : Informasi Mineral dan Batubara, Bandung, Pusat Penelitian dan Pengembangan Teknologi Mineral dan Batubara, (2005)

[3]. N. SARIER, C. GULER, *Journal American Oil Chemistry Soc*iety, **65** (1988) 776-779

[4]. YULIANTINA, YESTINE, Activation and Purification of Bentonite for the Treatment of Crude Palm Oil (CPO) As Vegetable Oil, BSD City, Swiss German University, (2010)

[5]. WU ZHANSHENG, LI CHUN, SUN XIFANG, XU XIAOLIN, DAI BIN, LI JIN'E, ZHAO HONGSHENG, *Chinese J. Chem. Eng*., **14** (2) (2006) 253-258

[6]. D. R. TAYLOR and D. B. JENKINS, Society of Mining Engineers of AIME, *Transactions*, **282** (1988) 1901-1910

Jurnal Sains Materi Indonesia
Indonesian Journal of Materials Science

Vol. 12, No. 2, Februari 2011, hal : 96 - 101
ISSN : 1411-1098

Akreditasi LIPI Nomor : 452/D/2010
Tanggal 6 Mei 2010

EFFECT OF NCO/OH RATIO AND MOLD SYSTEM ON PHYSICAL AND MECHANICAL PROPERTIES OF RIGID POLYURETHANE FOAM BASED ON PALM OIL

Evi Triwulandari[1], Agus Haryono[1] and Wiwik Pudjiastuti[2]
[1]*Research Center for Chemistry-Indonesian Institute of Sciences*
Kawasan Puspiptek Serpong 15314, Tangerang, Indonesia
[2]*Center for Chemical and Packaging*
Jl. Pekayon Kalisari, Pasar Rebo, Jakarta Timur, Indonesia
e-mail : vindarie69@yahoo.com

ABSTRACT

EFFECT OF NCO/OH RATIO AND MOLD SYSTEM ON PHYSICAL AND MECHANICAL PROPERTIES OF RIGID POLYURETHANE FOAM BASED ON PALM OIL. A new kind of rigid polyurethane foam (RPUF) was synthesized from palm oil based polyol. Hydroxy methoxy polyol was prepared from epoxidation and hydroxylation process, and called as hydroxyl methoxy glycerolmonostearate (HMGMS) polyol. Synthesis process of rigid polyurethane foam was conducted by reaction between HMGMS polyol and methylene diphenyldiisocyanate (MDI) via one shoot process in the presence of additive i.e. ethylene glycol (chain extender), silicon glycol (surfactant), dimethylcyclohexylamine (amine catalyst), stannous octoate (organometalic catalyst) and water as blowing agent. In this work, we investigated the effect of NCO/OH ratio (1.8 ; 2.0 ; 2.2 ; 2.4) and mold system (closed mold and open mold) on the physical and mechanical properties of rigid polyurethane foam. The physical and mechanical properties of rigid foam were conducted by determining the bulk density, dimensional stability, degree of water absorption and compressive strength. It was found out that NCO/OH ratio and mold type were important variables in making RPUF.

Key words : Polyurethane, Palm oil, Rigid foam, Mold, NCO/OH ratio

ABSTRAK

PENGARUH RASIO DARI NCO/OH DAN SISTEM *MOLD* TERHADAP SIFAT FISIS DAN MEKANIK DARI BUSA KAKU POLIURETAN YANG BERASAL DARI MINYAK SAWIT. Dalam penelitian ini, busa kaku poliuretan tipe baru telah disintesis dari poliol yang berbasis minyak sawit. Hidroksi metoksi poliol telah dipreparasi dari epoksidasi dan proses hidroksilasi dan disebut poliol *Hydroxyl Methoxy Glycerol Mono Stearate* (*HMGMS*). Proses sintesis dari busa kaku poliuretan ini dilakukan dengan mereaksikan poliol *HMGMS* dan *Methylene Diphenyl diisocyanate* (*MDI*) melalui proses *one shoot* dengan disertai keberadaan aditif berupa *ethylene glycol* (pemanjang rantai), *silicon glycol* (surfaktan), *dimethylcyclohexylamine* (katalis amin), *stannous octoate* (katalis organometalik) dan air sebagai *agent* peniup. Dalam penelitian ini, dipelajari pengaruh dari rasio NCO/OH (1,8 ; 2,0 ; 2,2 ; 2,4) dan pengaruh sistem *mold* (*mold* tertutup dan *mold* terbuka) terhadap sifat fisik dan mekanik dari busa yang dihasilkan. Sifat fisik dan mekanik ini ditentukan dengan mengukur densitas *bulk*, stabilitas dimensi, derajat dari absorpsi air serta kekuatan kompresi. Hasilnya menunjukkan bahwa rasio NCO/OH dan sistem *mold* yang dipakai merupakan variabel yang menentukan dalam pembuatan busa poliuretan.

Kata kunci : Poliuretan, Minyak sawit, Busa kaku, *Mold*, Rasio NCO/OH

INTRODUCTION

Rigid polyurethane foam (RPUF) is one of the most efficient, high performance insulation materials, enabling very effective energy savings with minimal occupation of space [1]. It is usually obtained from reaction between polyol polyether or polyol polyester and polyisocyanate forming urethane linkages [2]. Some applications of rigid polyurethane foams are used as shock and thermal insulators and energy absorption material for sensitive electronic components [3]. Rigid polyurethane foam can be manufactured in various shaped and sizes and can also be produced in situ by a variety of methods. RPUF can be poured in place. This involves mixing the chemicals either manually or by mechanical means and pouring into open molds or spaces

where insulation is required. RPUF also can be sprayed directly onto a solid surface using guns that mix and atomize the foam as it is being applied. And also in frothing, the mixture of chemicals is dispensed partially pre expanded, like an aerosol cream [4].

The characteristic of polyurethane foam is affected by the addition of blowing agent to produce bubble and expansion. There are two type of blowing agent i.e. chemical blowing agent (example: carbon dioxide from reaction result between isocyanate and water) and physical blowing agent (example: trichlorofluoromethane and hydrochlorofluorocarbon) [5]. Because of some physical blowing agent impact on ozone depletion, the environmental legislation forces producers to use more environmental friendly substances. Since carbon dioxide is produced by the reaction of water and isocyanate in the polyurethane reaction, it seems to be one of the best choices as an alternative blowing agent. Carbon dioxide used as a blowing agent is a by product of other manufacturing processes and therefore, it has no impact on the global carbon dioxide concentrations [6].

In the producing of rigid polyurethane foam, the properties obtained depend on their structure, the raw materials used and the manufacturing process. Some researches about synthesis of polyurethane foam to enhance its properties has been conducted by using closed mold and open mold [7,8]. However, comparative study about the effect of closed and open mold to the physical properties of polyurethane foam have not been conducted yet. Closed mold correlated with the closed expansion where the foaming process has been conducted under restricted conditions, while open mold correlated with the free expansion under free-rise no restricted [9].

The preparation of polymers from renewable sources such as vegetable oil-based materials is currently receiving increasing attention because of the economic and environmental concerns [10-11]. Therefore, research on the manufacturing of polyurethane based on renewable resources has becoming an important research activities.

Vegetable oils as renewable resources such as soybean oil, canola oil, rapeseed oil, corn oil, palm oil, sunflower, and linseed oil have been studied as polyol source for polyurethane [12-14]. Vegetable oils are triglycerides of fatty acids. In order to use these compounds as starting materials for polyurethane synthesis, it is necessary to functionalize them to form polyols. Epoxidation and ring opening reaction with haloacids or alcohols, ozonolysis and hydration are some of the common methods for functionalization of unsaturated vegetable oils [10].

In this work, rigid polyurethane foam was produced from polyol based on palm oil by using closed mold and open mold method to investigate the effect of mold system on the physical and mechanical properties of rigid polyurethane foam based on palm oil with the carbon dioxide as chemical blowing agent and in the variation of NCO/OH ratio.

EXPERIMENTAL METHOD

Materials

The palm oil based polyols were prepared through epoxidation and hydroxylation process of glycerol monooleate called as Hydroxy Methoxy Glycerol Mono Stearate (HMGMS) polyol, as previously done in the laboratory of polymer chemistry group, RCChem LIPI. The process for the production of polyol has been patented in Indonesia (P00200700238). The properties of the polyol are showed in Table 1.

Additive such as silicon glycol was used as surfactant. Stannous octoate was used as organometallic catalyst. Dimethylcyclohexylamine was used as amine catalyst. Distilled water was used as blowing agent. Ethylene glycol was used as chain extender and Methylene Diphenyl diisocyanate (MDI) were incorporated in the formulation.

Preparation of Rigid Polyurethane Foam

The rigid polyurethane foam was synthesized by using one shoot processing method. In this method component A which consists of mixture of polyol and additives (silicon glycol, stannous octoate, dimethylcyclohexylamine, ethylene glycol and water) was reacted directly with component B which consist of MDI at room temperature.

The effect of mold system (open and closed mold) and variation of NCO/OH ratio to the properties of Rigid Polyurethane Foam (RPUF) were studied in detail. Closed mold used in this research was glass bottle with dimension 45 mm x 80 mm (diameter x height). Procedure for preparing RPUF with closed mold was employed by stirring component A and component B in the glass bottle by using glass spatula for 1 minute and RPUF was molded directly in the bottle and then bottle was closed. Producing of RPUF by using open mold has been conducted in two methods i.e. open mold molded directly in the place by using polypropylene cup mold and open mold poured by using paper box mold.

For the first method of open mold, component A and component B was stirred in the polypropylene cup by using glass spatula for 1 minute and then allowed to rise freely. While, for the second method of open mold, component A and component B was stirred in the polypropylene cup for 1 minute and then at the creamy

Table 1. Properties of the palm oil based polyol (HMGMS polyol)

Hydroxyl value (mg KOH/g)	161
Iod value (mg I_2/100 g)	28,2

stage (the mixture turning creamy), the mixture was poured into an open mold (paper box mold) and allowed to rise freely. Study of the effect of NCO/OH ratio was conducted with variation ratio 0.8; 1.0; 1.2; 1.8; 2.0; 2.2; 2.4 for closed mold and for open mold start from NCO/OH ratio 1.8. The NCO/OH ratio is given by Equation (1) as follows:

$$[NCO]/[OH]\,ratio = \frac{M_{MDI}\, x W_{MDI}}{M_{HMGSMSpdlyo}\, x W_{HMGMSpdlyo} + M_{ethyleneglycol}\, x W_{ethyleneglycol} + W_{water}\, x \frac{1000}{9}} \quad \ldots\ldots\ldots\ldots\ldots\ldots \quad (1)$$

Where :

M_{MDI} = Content of the isocyanate group in MDI (6.78 mmol/g)
$M_{HMGMS\ polyol}$ = Content of the hydroxyl group in HMGMS polyol
$M_{ethylene\ glycol}$ = Content of the hydroxyl group in HMGMS ethylene glycol (hydroxyl number/56.1: 2.87 mmol/g and 4.55 mmol/g)
W_{MDI} = Weight of MDI
$W_{HMGMS\ polyol}$ = Weight of HMGMS polyol
$W_{ethylene\ glycol}$ = Weight of ethylene glycol
W_{water} = Weight of water

The formula of additive used for preparation of RPUF with variation of mold is presented in Table 2.

Characterization and Property Measurements of RPU Foam

The physical and mechanical properties of RPUF were characterized by determining its dimensional stability, bulk density, degree of water absorption and compressive strength. The chemical structure of palm oil based polyol used was characterized using an FT-IR Spectrophotometer (IRPrestige 21 SHIMADZU).

Dimensional Stability

Dimensional stability was determined by measuring of shrinkage level for five days. For open mold method, shrinkage level was calculated after curing for 24 hours. While for closed mold method shrinkage level was determined after glass bottle was opened and foam was cured (glass bottle was opened after 24 hours and then cured for 24 hours). The shrinkage degree of RPUF was calculated according to the following Equation (2) :

$$\text{Shrinkage degree (\%)} = \frac{V_{initial} - V_{final}}{V_{initial}} \text{ x } 100 \quad .... \quad (2)$$

Where :

$V_{initial}$ = RPUF volume before curing
V_{final} = RPUF volume after curing

Bulk Density

For density measurement, the PU foams were cut into specimens with dimension of about (20 x 20 x 10) mm^3 (width x length x thickness) for the open mold method and 45 mm x 10 mm (diameter x height) for closed mold method.

The specimens were accurately weighed to determine their densities using the equation, density = mass/volume. The density for each foam was ascertained using the average value from five specimens.

Degree of Water Absorption

The samples of foam (25 x 25 x 15) mm^3 (width x length x thickness) for the open mold method and 45 mm x 10 mm (diameter x height) for closed mold method) were immersed in 250 mL Beaker glass, containing water and kept for 6 days in room temperature. The samples were removed from water and weight with an analytical balance. The samples mass change resulting from the water uptake (expressed as a gram/volume percentage) was calculated according to the following Equation (3) :

$$\text{Water absorption (g/v \%)} = \frac{m_w - m_d}{v_{foam}} \text{ x } 100 \quad .... \quad (3)$$

Where :

m_d = Masses of dry sample
m_w = Masses of wet sample
v_{foam} = Volume of RPUF foam

RESULTS AND DISCUSSION

In this work rigid polyurethane foam was produced from polyol based on palm oil (called as HMGMS polyol) by using water as chemical blowing

Table 2. The formula of additive used for preparation of RPUF with variation of mold system

Raw Materials	Type	Closed Mold	Open Mold-Molded Directly	Open Mold-Poured
Polyol	Palm oil based polyol (HMGMS)	8.5 g	10 g	20 g
Surfactant	Silicon glycol	2.04 pphp	2.04 pphp	2.04 pphp
Catalyst	dimethylcyclohexylamine	0.2 pphp	0.2 pphp	0.2 pphp
Blowing agent	water	2.67 pphp	2.67 pphp	2.67 pphp
Chain extender	ethylene glycol	1 pphp	1 pphp	1 pphp

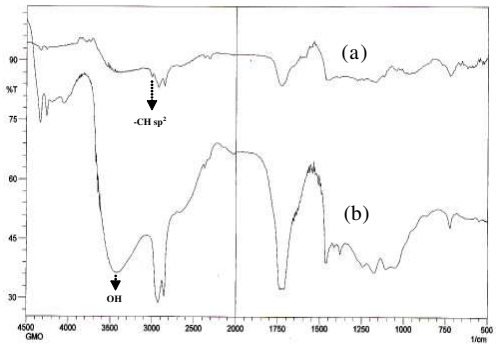

Figure 1. FT-IR spectra of derivative of Palm oil (a) and HMGMS polyol (b).

agent. Polyol based on palm oil has tendency to produce rigid polyurethane foam, due to its shorter chain than that of petrochemical based polyol. The characterization of the effect of mold system and NCO/OH ratio on the physical and mechanical properties has been conducted by determining its dimensional stability, bulk density, degree of water absorption and compressive strength.

Characterization of Palm Oil Based Polyol

Characterization of palm oil-based polyol was employed by using FT-IR technique to analyze the functional groups of palm oil based polyol (HMGMS polyol). Figures 1(a) and 1(b) showed the spectra of derivative of palm oil and HMGMS polyol, respectively. FT-IR spectrum of derivative of palm oil, showed absorption bands at 2924-2852 cm^{-1} assigned to C-H sp^3 vibration and 3005.1 cm^{-1} assigned to C-H sp^2. The characteristic absorption band attributed to carboxylic acid was shown at 1728 cm^{-1} assigned to C=O carbonyl from carboxylic acid and at 1282 -1220 cm^{-1} assigned to C-O group.

The significant distinguish FT-IR spectrum of derivative of palm oil and HMGMS polyol was showed by appearance of absorption at 3427-3332 cm^{-1} in the product which assigned to O-H group. The presence of O-H group in the product suggests that hydroxylation has taken place.

Furthermore, another information which shown that hydroxylation has taken place was disappearance absorption band at 3005.1 cm^{-1}. It was shown that unsaturated bond converted into saturated bond.

Characterization of Rigid Polyurethane Foam

Dimensional Stability

The dimensional stability of an insulation material is a property that is absolutely necessary for the faultless function of an insulation system. Poor dimensional stability can cause shrinkage. Shrinkage is reduction in linear size during cooling from molding to room temperature. Because of polymers have high thermal expansion coefficients, so

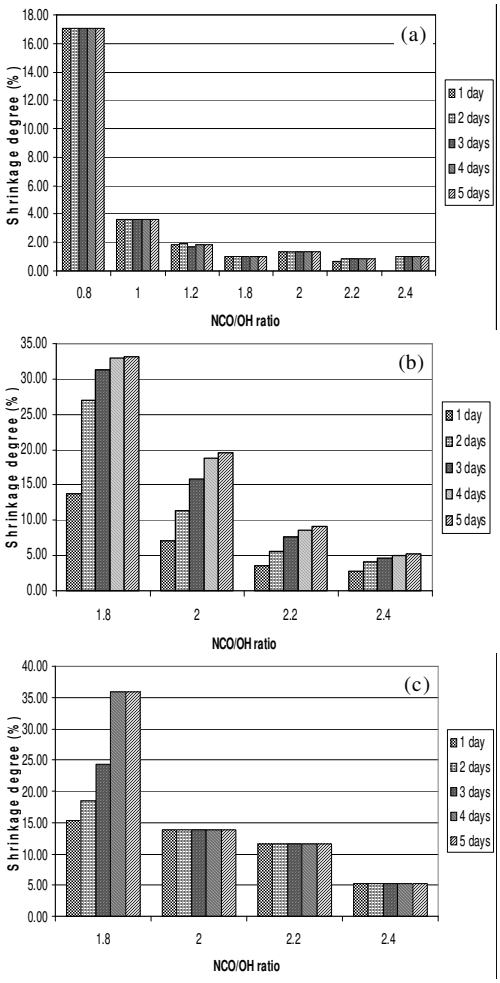

Figure 2. The shrinkage data of RPUF obtained by using (a) closed mold, (b) open mold-poured and (c) open mold-molded directly.

significant shrinkage occurs during solidification and cooling in mold.

Beside that, shrinkage can be caused by the mix ratio being incorrect. One factor that can reduce the foam shrinkage is by adding higher pressures force, more material into mold cavity and study formulated ratio of RPUF. Foam shrinkage of RPUF was investigated and compared between RPUF which produce by using closed mold (in the presence of pressure) and open mold (allow rise freely).

The foam shrinkage data of RPUF obtained by using closed mold, open mold-poured and open mold molded directly were shown in the Figure 2. RPUF which was produced by using closed mold has smaller shrinkage than open mold poured and open mold molded directly.

The foam shrinkage for closed mold method, start from NCO/OH ratio 1.0 until 2.4, the foam shrinkage was not more than 5 %. In other side, shrinkage data of RPUF which produced by using open mold poured and open mold molded directly showed the smallest shrinkage (under 5 %) when the NCO/OH ratio 2.4. These data showed that the

Vol. 12, No. 2, Februari 2011, hal : 96 - 101
ISSN : 1411-1098

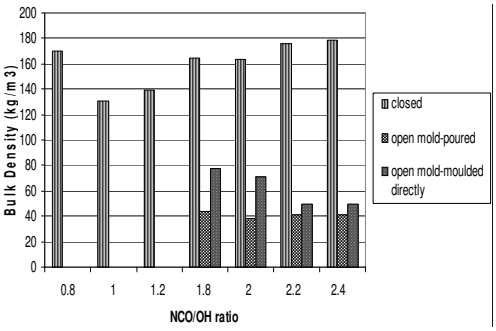

Figure 3. Bulk density of RPUF with variation of mold type and NCO/OH ratio

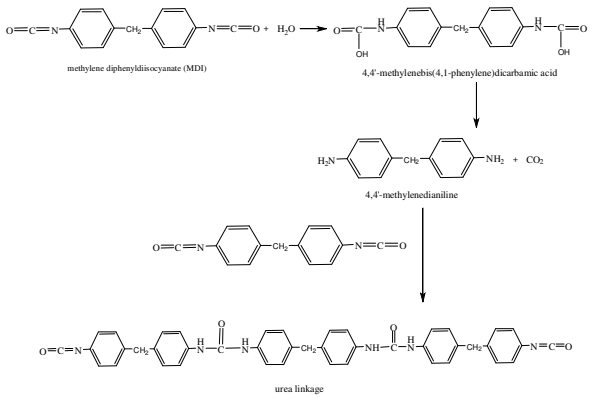

Figure 4. Reaction of methylene diphenyldiisocyanate (MDI) and water

shrinkage degree of RPUF can be reduced in the presence of pressure.

Bulk Density

Density is a most important parameter to control the mechanical and thermal properties of cell foams. Bulk density of RPUF with variation of mold type and NCO/OH ratio were shown in the Figure 3. Bulk density analysis of RPUF obtained by using open mold was started from NCO/OH ratio 1.8 not from 0.8 like in the closed mold. This is due to RPUF using open mold with ratio start from 1.8 has poor dimensional stability so it is supposed that for NCO/OH ratio under 1.8 will have more poor dimensional stability.

The bulk density of open mold method showed that the bulk density decrease with the increasing of NCO/OH ratio. This is due to the increasing of blowing efficiency and additional blowing as the NCO/OH ratio increases by the CO_2 produced from the reaction between the isocyanate groups and water (Figure 4). The additional of blowing gas caused the increasing of diameter cell wall and affect decreasing of the mass of RPUF.

The bulk density of closed mold method was increased with increasing of NCO/OH ratio. This was in contrary with the bulk density of closed mold method. This is due to the different expansion with the

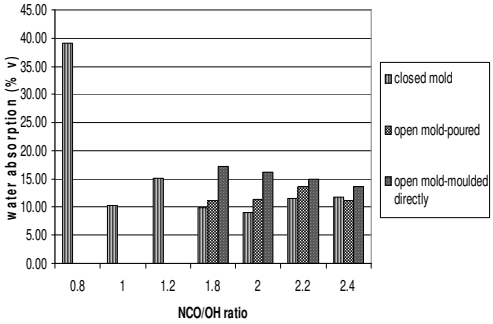

Figure 5. Histogram of water absorption of RPUF with variation of NCO/OH ratio and mold system

open mold method. The expansion in the open mold method is free, while in the closed mold method the expansion is closed. The increasing of additional blowing gas with the increasing of NCO/OH ratio in the closed expansion affected the increasing of pressure. Furthermore the increase of the pressure caused the cell diameter decreased and the mass of RPUF compressed.

Water Absorption

Water absorption is the amount of water picked up over a specific period of time. Water absorption of RPUF with variation of NCO/OH ratio and mold system was shown in the Figure 5. Water absorption of RPUF from open mold and closed mold system has tendency to decrease with increasing of NCO/OH ratio. The increasing of NCO/OH ratio affected the decreasing of hydrophilicity of foam, thus the penetration of water into bulk of polymer decreased. Water absorption of RPUF using closed mold system in the range of NCO/OH ratio from 1.8 until 2.4 showed smaller percentage. This can be explained as RPUF using closed mold system had higher bulk density than RPUF using open mold system. In the higher density, diameter of cell was smaller and this affected on the reducing penetration of water into foam.

Compressive Strength

Mechanical properties of RPUF was determined by analyzing of compressive strength. Compressive strength of RPUF with variation of NCO/OH ratio and mold system was showed in the Figure 6. The data showed that compressive strength of RPUF using closed method was increasing with the increasing of NCO/OH ratio. While the compressive strength of RPUF using open mold method was decreasing with the increasing of NCO/OH ratio. It is generally known that the mechanical properties of a cellular material mainly depend on its density [7]. Therefore, when the RPUF produced using closed mold method, the increasing of the compressive strength may be due to the increase of foam density. And for RPUF produced using open mold

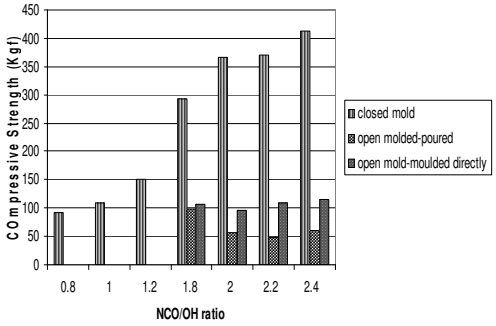

Figure 6. Histogram of compressive strength of RPUF with variation of NCO/OH ratio and mold system

method, the decreasing of the compressive strength may be due to the decreasing of foam density.

CONCLUSION

From the study of the effect of NCO/OH ratio and mold system in the producing rigid polyurethane foam based on palm oil, it was found that NCO/OH ratio and mold system were important variables in making polyurethane foam especially on their physical properties. In order to obtain good properties (good dimensional stability) the appropriate ratio of producing RPUF using open mold system and closed mold was different. In the closed mold system, NCO/OH ratio was started from ratio 1.0 but in the open mold NCO/OH ratio was started from ratio of 2.4.

ACKNOWLEDGEMENTS

This work was supported by the Indonesia Toray Science Foundation (ITSF) Research Grant (15th, 2008). Author also gratefully acknowledge to Ms. Animira Hikmawati, Ms. Yulianti Sampora and Mr. Agustinus Edi Susilo for their help and fruitful discussion.

REFERENCES

[1]. A.E.V. NIEUWENHUYSE, Thermal Insulation Materials Made of Rigid Polyurethane foam (RPUF/PIR) Properties-Manufacture, *Report No. 1, Federation of European Rigid Polyurethane Foam Associations, 1160 Brussel-Belgium*, (2006)

[2]. T. WANG, L. ZHANG, D. LI, J. YIN, S. WU, Z. MAO, *Bioresource Technology*, **99** (2008) 2265-2268

[3]. D. JACKOVICH, B. O'TOOLE, M. C. HAWKINS and L. SAPOCHAK, *Journal of Cellular Plastics,* **41** (2005) 153

[4]. S. DOROUDIANI, C. E. CHAFFEY, M.T. KORTSCHOT, *Journal of Polymer Science*, *Part B: Polymer Physics*, **40** (2002) 723-735

[5]. S. CHUAYJULJIT, T. SANGPAKDEE and O. SARAVARI, *Journal of Metals, Materials and Minerals*, **17** (1) (2007) 17-23

[6]. ROBERT C. HARPER, *Method of Producing Closed Mold Polyurethane foam Molding Free of Surface Voids By Flushing The Mold With a Vaporized Halogenated Hydrocarbon*, United States Patent 3,666,848 (1972)

[7]. H. YEGANEH, P. J. TALEMI, *Polymer Degradation and Stability*, **92** (2007) 480-489

[8]. S. CHUAYJULJIT, S. SANGPAKDEE and O. SARAVARI, *Journal of Metals, Materials and Minerals,* **17** (1) (2007) 17-23

[9]. Z. S. PETROVIC, I. CVETKOVIC, D. HONG, X. WAN, W.ZHANG, T. ABRAHAM and J. MALSAM, *J. Applied Polymer Science*, **108** (2008) 1184-1190

[10]. Z. S. PETROVIC, W. ZHANG and I. JAVNI, *Biomacromolecules*, **6** (2005) 713-719

[11]. R. ALFANI, S. IANNACE, and L.NICOLAIS, *J. Applied Polymer Science*, **68** (1998) 739-745

[12]. X. KONG, J. YUE and S. S. NARINE, *Biomacromolecules*, **8** (2007) 3584-3589

[13]. X. KONG and S. S. NARINE, *Biomacromolecules*, 8 (2007) 2203-2209

[14]. A. HARYONO, E. TRIWULANDARI, D. SONDARI, Development of Polyurethane Rigid Foam from Palm Oil Polyols, *Proceeding of Annual Meeting of SPSJ*, Yokohama, Japan, (2008)

Jurnal Sains Materi Indonesia
Indonesian Journal of Materials Science

Vol. 12, No. 2,Februari 2011, hal : 102 - 105
ISSN : 1411-1098

Akreditasi LIPI Nomor : 452/D/2010
Tanggal 6 Mei 2010

GRAFTING OF CELLULOSIC PALMITATE-METHYL METHACRYLATE BY ELECTRON BEAM IRRADIATION AND CHARACTERIZATION OF THEIR MEMBRANES MECHANICAL PROPERTIES

Asep Riswoko[1] and Tri Suryanti[2]

[1] *Center for Material Technology-Agency for the Assessment and Application of Technology*
Jl. M.H. Thamrin No. 8, Jakarta 10340, Indonesia
[2] *Faculty of Math. and Natural Science-State University of Jakarta*
Jl. Rawamangun Muka, Jakarta 13220, Indonesia
e-mail : asepriswoko@webmail.bppt.go.id

ABSTRACT

GRAFTING OF CELLULOSIC PALMITATE-METHYL METHACRYLATE BY ELECTRON BEAM IRRADIATION AND CHARACTERIZATION OF THEIR MEMBRANES MECHANICAL PROPERTIES. A cellulose derivative membrane, cellulosic palmitate, has been modified to give a better mechanical properties of composite membranes. Modification has been carried out by adding methyl methacrylate (MMA) onto cellulosic palmitate with volume ratio 1:1 and then irradiated by electron beam at dosage of 3, 5, 7, 9, and 10 kGy. The best performance of MMA grafted cellulosic membrane was successfully obtained for irradiation dose at 5 kGy which has a tensile strength of 76,92 Kg/cm^2 (stronger than that of the original cellulosic palmitate membrane up to 75%). This result is supported by FT-IR spectra which showed that grafting methyl methacrylate onto cellulosic palmitate increased the intensity of absorbance of -CH_2- group (1468.47 and 1450.47 cm^{-1}). In addition, there are also strong absorption in region 1068.64 and 1014.56 cm^{-1} which is absorption for C-O-C (ether linkage) between cellulosic palmitate and methyl methacrylate. X-Ray Diffraction and SEM analysis were also revealed that adding of MMA on cellulosic palmitate affected a degree of crystalline and morphology membrane.

Key words : Cellulosic palmitate, Methyl methacrylate, Electron beam, Grafting

ABSTRAK

***GRAFTING* SELULOSIK PALMITAT-METIL METAKRILAT MENGGUNAKAN IRADIASI BERKAS ELEKTRON DAN HASIL KARAKTERISASI SIFAT MEKANIK MEMBRAN**. Membran yang merupakan turunan dari selulosa, yaitu selulosa palmitat, telah dimodifikasi dalam penelitian ini untuk memperoleh sifat mekanik yang unggul dari sebuah komposit membran. Modifikasi ini dilakukan dengan menambahkan metil metakrilat (MMA) kepada selulosa palmitat pada rasio volume 1 : 1, kemudian diiradiasi dengan berkas elektron pada dosis 3 kGy, 5 kGy, 7 kGy, 9 kGy dan 10 kGy. Kinerja terbaik dari membran selulosa yang telah di*grafting* dengan MMA didapat pada dosis iradiasi 5 kGy, yang memiliki kekuatan tarik sebesar 76,92 kg/cm^2 (lebih kuat dari material orisinil sebelum proses *grafting* sebesar 75 %). Hasil ini didukung oleh data spektrum *FT-IR* yang memperlihatkan bahwa proses *grafting* dari MMA kepada selulosa palmitat telah meningkatkan intensitas dari absorbansi gugus -CH_2- (1468,47 cm^{-1} dan 1450,47 cm^{-1}). Selain itu, ditemukan juga absorpsi yang kuat pada daerah 1068,64 cm^{-1} dan 1014,56 cm^{-1} yang merupakan absorpsi dari C-O-C (ikatan eter) antara selulosa palmitat dengan MMA. Analisis *XRD* dan *SEM* juga menunjukkan bahwa penambahan MMA telah menambah sifat kristal dan morfologi dari membran.

Kata kunci : Selulosa palmitat, Metil metakrilat, Berkas elektron, *Grafting*

INTRODUCTION

Modification of natural polymers such as cellulose and its derivatives have been widely carried out in order to enhance their possibilities in industrial application by formation of cellulose esters, grafting and crosslinking with another synthetic monomers [1], and so on. In the application for separation of racemate, cellulosic palmitate membrane was used to separate the racemic mixture of ibuprofen with a very good separation

ratio [2]. However cellulosic palmitate membrane has low mechanical strength. Efforts can be done to improve the mechanical properties of cellulose is by adding supporting materials such as methylmethacrylate (MMA) monomer and polymerized by radiation techniques [3].

Radiation techniques that widely used for the modification of polymers is gamma rays and Ultra Violet (UV). Radiation technique using electron beam machine also has been used for long years ago to modify the polymer [4]. Electron beam as a source of radiation is very competitive when compared with gamma rays. The radiation energy utilization efficiency is very high because the electron beam has a lower energy level than that of the gamma rays. With the low energy level it will not damage the irradiated material. Whereas, comparing with the UV polymerization, irradiation by the electron beam does not require initiator.

In this study, preparation will be carried out from blending between cellulosic palmitate with MMA monomer, then irradiated by electron beam at various radiation doses. Mechanical properties of cellulosic palmitate-MMA membrane will be evaluated using tensile strength instrument. Meanwhile, structural characterization will be performed using FT-IR spectroscopy, the membrane morphology by Scanning Electron Microscope (SEM), and degree of crystallization by X-Ray Diffractometer (XRD).

EXPERIMENTAL METHOD

Synthesis

Synthesis of cellulosic palmitate has been carried out by reacting activated cellulose and palmitoyl chloride using mixed solvent of piridine and DMF at 70 °C for 3 hours. Membrane was casted by blending cellulosic palmitate and MMA monomer with volume ratio 1 : 1 using methylenechloride solvent. Radiation onto membrane was carried out by electron beam machine at total doses 3, 5, 7, 9, and 10 kGy.

Characterization

Characterization of structure and properties of the membrane were carried out by FT-IR spectroscopy, SEM, XRD and tensile strength instrument.

RESULTS AND DISCUSSION

A cellulose derivative membrane, cellulosic palmitate, has been synthezed and grafted with methylmethacrylate by electron beam irradiation. Based on data in Table 1, it is known that cellulosic palmitate-MMA membranes irradiated at doses of 5 and 7 kGy give better tensile strength compared with cellulosic palmitate membrane. This shows that methylmethacrylate has an impact on the increase of membrane's strength. The result of FT-IR analysis (Figure 1) also showed that grafting has occurred between cellulosic palmitate with methylmethacrylate.

Table 1. Characterization of the irradiated membranes

Characterization of Product			
Membrane	Radiation Dose (KGy)	Tensile Strength (Kg/cm^2)	Crystallinity by XRD (%)
Cellulosic Palmitate	0	69.42	42.39
Cellulosic Palmitate	1	66.25	-
Cellulosic Palmitate-MMA	3	45.15	-
Cellulosic Palmitate-MMA	5	76.92	64.3
Cellulosic Palmitate-MMA	7	72.14	-
Cellulosic Palmitate-MMA	9	63.77	-
Cellulosic Palmitate-MMA	10	63.42	-

At doses of 9 and 10 kGy the tensile strength of the cellulosic palmitate-MMA was lower than cellulosic palmitate membrane. This indicates that both doses of radiation are too high for grafting the membrane, and tend to cause the degradation. This is in accordance

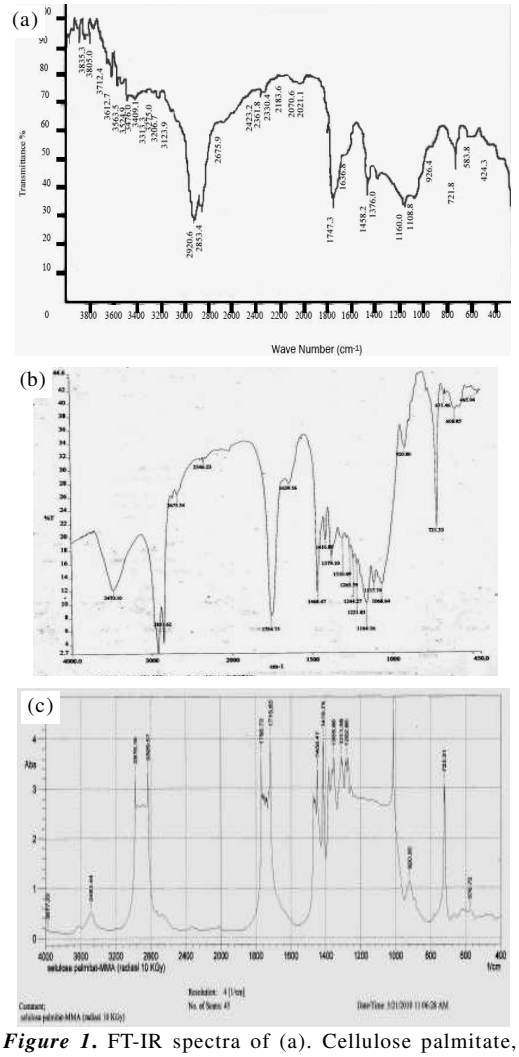

Figure 1. FT-IR spectra of (a). Cellulose palmitate, (b). Cellulose-MMA palmitate 5 kGy radiation dose and (c). Cellulose-MMA Palmitate 10 kGy radiation dose

Vol. 12, No. 2,Februari 2011, hal : 102 - 105
ISSN : 1411-1098

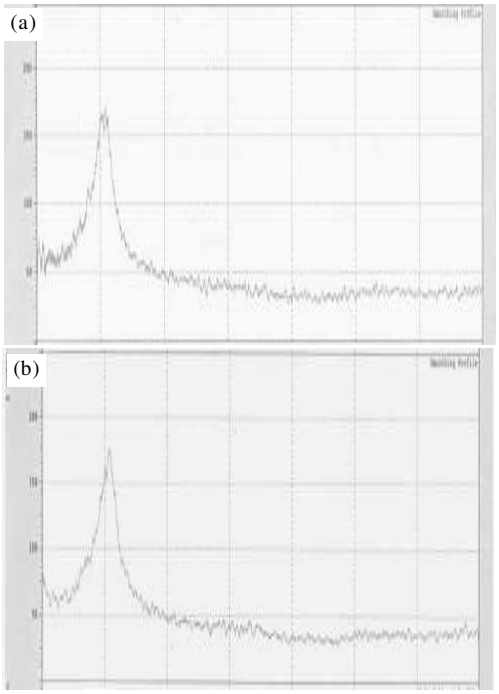

Figure 2. XRD Diffractogram of (a). Cellulosic Palmitate Membrane XRD and (b). Cellulosic Palmitate-MMA Membrane Irradiation by Electron Beam at Doses 5 kGy

with the literature that says that vinyl polymers irradiated with electron beam will experience two types of main reaction, crosslink and degradation. In general, both happen simultaneously, though at high-dose the degradation is more dominant [5]. In addition, the reduction in mechanical strength is affected by the disruption of the crystalline structure of polymers. Grafting of an amorphous polymer on the crystalline region can cause a decrease or an increase of mechanical properties. Grafting which occurs in the amorphous can increase the mechanical properties [1].

Grafting of methylmethacrylate onto cellulosic palmitate increased the intensity of absorbance of $-CH_2-$ group. This can be seen on the irradiated membrane in which the intensity of the absorbance at 1468.47 and 1450.47 cm^{-1} increased. Figure 1 also shows that large doses of radiation can destroy membrane structures. This can be seen from the loss of C-O group absorption peak of the glycoside bond in the membrane which is subjected to doses of 10 kGy. These results are also in accordance with the strength change of membrane due to high radiation dosage as discussed in above.

X-Ray technique also can be used to detect structural changes that occurred due to grafting. Grafting between cellulosic palmitate and MMA produce a higher density and well regulated of polymer structure (crystalline phase). The increase in degree of crystallization as shown in Figure 2, reveals that dose of 5 kGy is the optimum dosage for the occurrence of grafting.

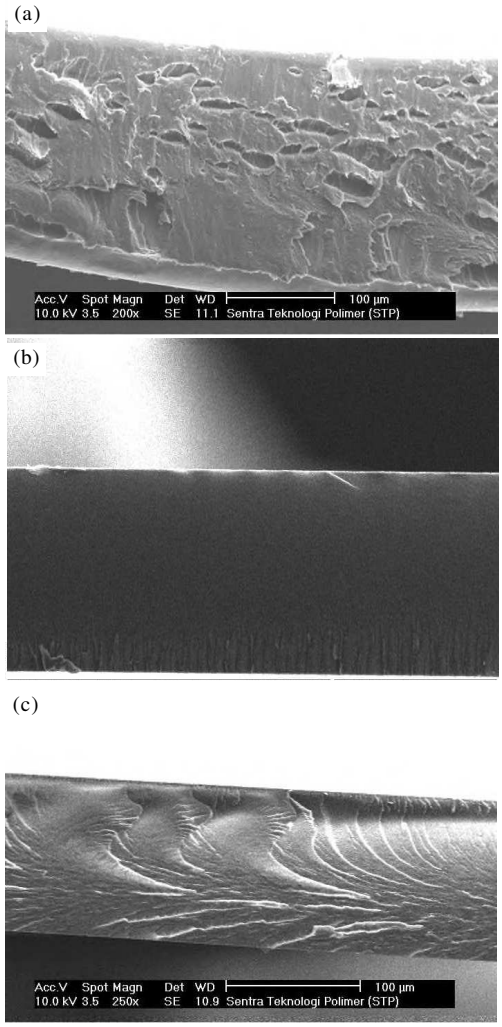

Figure 3. Cross Section imaging of SEM Membrane (a). Cellulosic Palmitate, (b). Cellulosic Palmitate-MMA 5 kGy and (c). Cellulosic Palmitate-MMA 10 kGy

Figure 3 shows the differences in morphology of the three membranes. Cellulosic palmitate-MMA membrane with irradiation dose of 5 kGy (Figure 3(b)) has a tighter structure than that of the cellulosic palmitate membrane (Figure 3(a)) and cellulosic palmitate-MMA membrane with dose of 10 kGy (Figure 3(c)). Therefore, the cellulosic palmitate-MMA membrane with irradiation dose of 5 kGy has greater tensile strength than that of the four other membranes as well as the cellulose palmitate membrane.

CONCLUSIONS

From the above results it can be concluded that, cellulosic palmitate has been succesfully to be blended with methylmethacrylate at the a volume ratio of 1 : 1 using methylenechloride solvent at room temperature. Irradiation by electron beam could cause grafting reaction of cellulosic palmitate membranes with methylmethacrylate or degradation. The optimum radiation dose for the occurrence of grafting was 5 kGy. Grafting that occurs between cellulosic palmitate with

methylmethacrylate increased the mechanical properties of membrane. The degradation of the structure was found when the membranes were irradiated by a high dosage result in the decrease of the mechanical strength.

REFERENCES

[1]. A. BHATTACHARYA, J.W. RAWLINS, P. RAY, *Polymer Grafting and Crosslinking*, John Wiley & Sons, Inc., New York, (2008)

[2]. NURHAYATI, Uji Kemampuan Selulosa Palmitat Pada Pemisahan Campuran Enansiomer, *Skripsi FMIPA UNJ Jakarta*, (2007)

[3]. HORIO, MASAO, O GAMI, KAZUO, KONDO, TAKASHI, SEKIMOTO, KENICHI, *Polymerization of Styrene, Methyl Methacrylate and Acrylonitrile onto Wool by Gamma Irradiation*, Kyoto University, Japan, (1963)

[4]. PUDJORAHARDJO dan S. DJOKO, *Aplikasi Mesin Berkas Elektron di Pusat Teknologi Akselerator dan Proses Bahan-BATAN*, P3TM BATAN, Yogyakarta, (2006)

[5]. STEVENS and P. MALCOLM, *Kimia Polimer,* diindonesiakan oleh IIS SOPYAN, Pradnya Paramita, Jakarta, (2001)

Jurnal Sains Materi Indonesia
Indonesian Journal of Materials Science

Vol. 12, No. 2, Februari 2011, hal : 106 - 109
ISSN : 1411-1098

Akreditasi LIPI Nomor : 452/D/2010
Tanggal 6 Mei 2010

THE EFFECTS OF IMPACT MODIFIERS ON THE PROCESSABILITY AND THE TOUGHNESS OF POLY VINYL CHLORIDE PROFILES

Nutt Lumpikanond and Sirijutaratana Covavisaruch
Department of Chemical Engineering, Faculty of Engineering-Chulalongkorn University
Bangkok 10330, Thailand
e-mail : fchscv@hotmail.com

ABSTRACT

THE EFFECTS OF IMPACT MODIFIERS ON THE PROCESSABILITY AND THE TOUGHNESS OF POLY VINYL CHLORIDE PROFILES. Extruded Poly Vinyl Chloride (PVC) door profile and window profiles often fail at the bend. This research aims to reduce such problem by enhancing the toughness of the PVC profiles while still maintaining their load bearing function and stiffness. Three impact modifiers namely methacrylate-butadiene-styrene (MBS), chlorinated polyethylene (CPE) and nano-scaled nitrile butadiene rubber (NBR) were employed in the PVC profiles at 1-11 phr. The processability assessed by rheometric study revealed only a slight increase in the torque required to process the melt PVC dosed with CPE and nano NBR while that required for the PVC with MBS was raised quite significantly. Although the PVC modified with MBS melted faster at a lower temperature, a rapid rise of temperature was observed during processing. The heat was probably due to the higher friction and shear induced by the rather viscous PVC melt dosed with MBS. Mechanical tests in terms of impact energy, stiffness and hardness revealed that the toughening efficiency of all three impact modifiers were close at low content, but at around 9 and 11 phr, the MBS and the CPE enhanced the impact energy quite rapidly by four folds while their corresponding hardness and stiffness were lowered considerably.

Key words : Impact modifier, Processability, Toughness, Poly vinyl chloride

ABSTRAK

EFEK DARI *IMPACT MODIFIER* PADA KEMUDAHAN PROSES DAN KEULETAN DARI PROFIL POLIVINIL KHLORIDA. Profil Pintu dan jendela dari Polivinil khlorida (*PVC*) hasil ekstrusi seringkali gagal pada bagian lengkungan. Penelitian ini bertujuan untuk mengurangi masalah kegagalan hasil ekstrusi dengan meningkatkan keuletan dari profil berbahan *PVC* dengan tetap menjaga kemampuan menerima beban dan kekakuannya. Tiga jenis bahan untuk memodifikasi kemampuan menerima impak (*impact modifier*) yaitu *methacrylate-butadiene-styrene* (*MBS*), *chlorinated polyethylene* (*CPE*) dan *nano-scaled nitrile butadiene rubber* (*nano-NBR*) digunakan dalam profil *PVC* pada 1 *phr* hingga 11 *phr*. Kemudahan proses torsi yang terukur dari hasil studi rheometrik menunjukkan bahwa hanya sedikit peningkatan *torque* yang diperlukan untuk memproses lelehan *PVC* yang telah ditambahi dengan *CPE* dan *nano-NBR*. Namun untuk *PVC* yang telah ditambahi dengan *MBS* dibutuhkan peningkatan torsi yang lebih tinggi. Meskipun *PVC* yang dimodifikasi dengan *MBS* meleleh lebih cepat pada suhu yang lebih rendah, peningkatan suhu yang lebih cepat terobservasi selama pemrosesan. Panas ini mungkin terjadi karena gesekan yang lebih besar serta *shear* yang disebabkan oleh lelehan *PVC-MBS* yang lebih kental. Tes mekanik dalam bentuk energi impak, kekakuan dan kekerasan menunjukkan bahwa efisiensi peningkatan keuletan dari ketiga jenis *impact modifier* memiliki kemiripan pada konsentrasi rendah, namun pada sekitar 9 *phr* hingga 11 *phr*, *MBS* dan *CPE* meningkatkan energi impak secara lebih cepat hingga empat kali lipat, sedangkan tingkat kekerasan serta kekakuannya menjadi lebih rendah.

Kata kunci : *Impact modifier*, Kemudahan proses, Keuletan, Polivinil khlorida

INTRODUCTION

PVC profiles formed by extrusion gain added value when they are employed in the building and construction sector to replace wood or aluminum door and window frames. Problems arised during the use of such PVC profiles in the form of cracks at the bent corners. As a remedy, impact modifiers are generally added to

PVC compound to improve the impact properties. Current commercial impact modifiers include methacrylate-butadiene-styrene (MBS) and chlorinated polyethylene (CPE), they are available in particles of micro scaled. Earlier studies remarked that they tend to affect the processability of the PVC as well by reducing the fusion time and changing the torque required for processing [1-2].

The present study proposed to use elastomeric nano NBR to improve the toughening of the PVC profiles. NBR was selected because of its flexibility and its extremely low glass transition temperature. Two types of the commercial impact modifiers namely MBS and CPE were applied to toughen the PVC and to compare their toughening efficiencies with the nano-scaled NBR particles.

EXPERIMENTAL METHOD

Materials and Sample Preparation

The raw material used in this study was PVC compound (K66) with melting temperature ranges from 160 to 190 °C. It composed of $CaCO_3$ 5 phr, TiO_2 1 phr, processing aid 1.5 phr, stabilizer 5.5 phr and lubricant 1.4 phr. Three types of impact modifiers to be applied to the PVC at 1, 3, 5, 7, 9 and 11 phr were MBS, CPE and NBR. The commercially available MBS and CPE were both of micro-scaled with average particle sizes of 50 µm and 10 µm respectively while that of the nano NBR was 90 nm.

The PVC compound was firstly mixed with each impact modifier by using a high speed laboratory mixer (Thermo electron, PRISM Pilot 3) at the speed of 3,000 rpm at 30 °C. PVC compound was devided for processability assessment by rheometric test and for further blending by using 2-roll mill at 160 °C. Test specimens were compression-molded and notched for izod impact test according to the dimensions specified by ASTM D256-06.

Thermal and Mechanical Tests

The degradation temperature of the PVC compound and of each impact modifier was evaluated by Thermo-Gravimetric Analyzer (Diamond TG/DTA) in nitrogen atmosphere. The processability was studied by using a Torque rheometer (Brabender, type 815606). Notched impact strengths were measured at room temperature by using an impact tester (Yasuda Impact Tester) according to ASTM D256-06.

RESULTS AND DISCUSSION

Degradation

The degradation temperature of the PVC and of each impact modifier was shown in Figure 1.

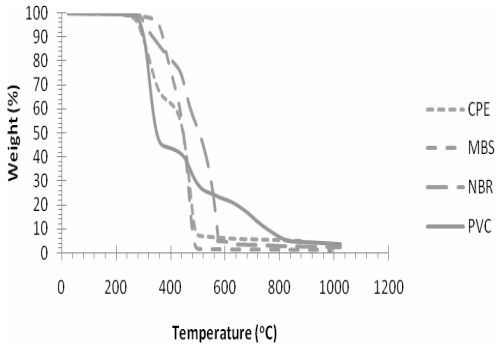

Figure 1. Degradation temperature of PVC and each impact modifier.

The first range of degradation of the PVC compound occurred between 260 and 360 °C, it was associated with the release of HCl and was accompanied by 55% of weight loss. The CPE degraded at 260-360 °C, this was associated with the release of HCl which was accompanied by 35% of weight loss. The decomposition of the MBS appeared at 320-480 °C. The NBR was found to degrade at 300-560 °C.

Processability

Figure 2(a) shows that the torque required for processing the modified-PVC melt increased with the content of the impact modifiers. The processing torque for the melt PVC modified with CPE and nano NBR increased only slightly while that for the PVC with MBS was raised quite significantly.

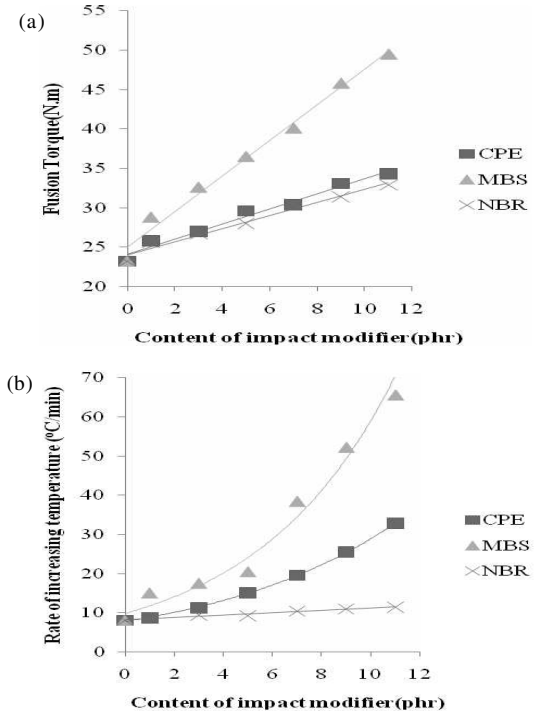

Figure 2. Influences of MBS, CPE and nano NBR impact modifiers and their content on (a) the torque required to process and (b) the rate of temperature rising in the modified-PVC melt.

Vol. 12, No. 2, Februari 2011, hal : 106 - 109
ISSN : 1411-1098

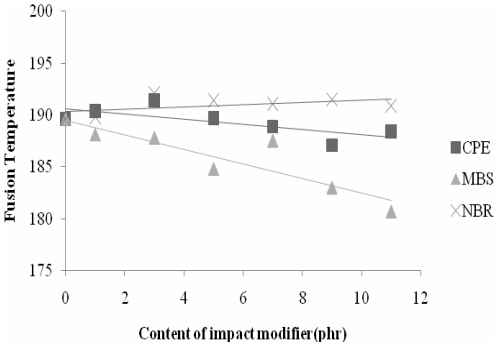

Figure 3. Melting temperatures of the impact- modified PVC.

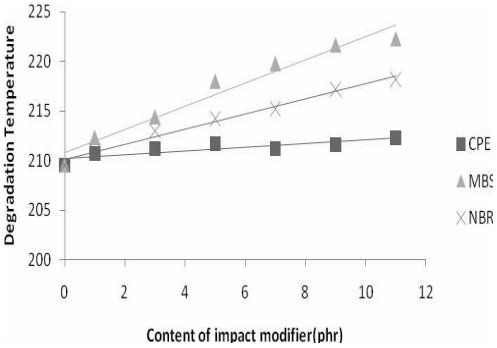

Figure 4. Degradation temperature obtained from rheometric study of the PVC modified with MBS, CPE and nano NBR impact modifiers.

During processing, the MMA shell of the MBS was believed to have melted first and reacted with the PVC molecules through polar-polar interactions [3]. The higher torque suggested that the melt PVC modified with MBS had greater melt viscosity [4] and was more difficult to process.

As a result, the rate of temperature rising in the MBS-modified PVC melt was found notably high, as demonstrated in Figure 2(b), due to the extra heat arised from the friction and shear between the viscous PVC melt and the rheometric test chamber.

The melting temperature of the PVC with each impact modifier is shown in Figure 3. The temperature required for melting the PVC modified with MBS was lowered rather significantly with the MBS content while those for the PVC dosed with CPE or NBR hardly changed.

The degradation temperatures detected upon processing the impact-modified PVC by rheometric study are shown in Figure 4. The degradation temperature increased with the modifier content because the degradation of all modifiers were inherently higher than that of the PVC compound.

The degradation temperatures detected by the rheometric study were lower than those obtained from the TGA because the degradation of the modified PVC in the rheometric study was induced by both the heat applied and the heat arised from frictional shear force while the that in the TGA occurred purely from the heat applied.

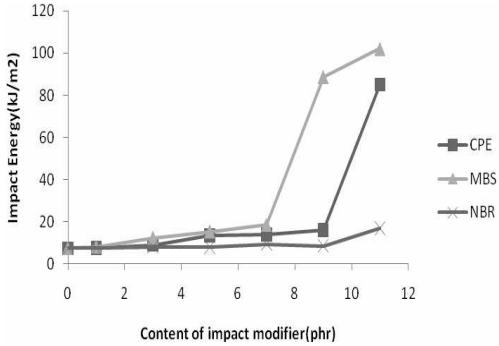

Figure 5. Influences of MBS, CPE and nano NBR impact modifiers and their content on the impact strength of modified PVC.

Impact Property

The impact energy at 30 °C, as shown in Figure 5, depicts clearly the efficiency of each modifier. The fracture of the PVC modified with 9 phr of MBS and 11 phr of CPE clearly transformed from a brittle mode with rather low impact energy to a more ductile one with the impact energy enhanced by ten and eight folds respectively. At 11 phr, the nano NBR improved the impact energy only slightly.

CONCLUSION

The MBS impact modifier influenced the processability by raising the torque required. MBS was the most efficient impact modifier among those studied, yielding toughened PVC with the highest impact energy as compared with CPE and NBR.

ACKNOWLEDGMENT

The authors acknowledge the research grant (MRG-WI525E010) from The Thailand Research Fund (TRF). Thanks are extended to Nawa Plastic Industries Company Limited for facilitating the torque rheometer and to and Siam Extek Company Limited for the provision of the nano-scaled NBR.

REFERENCES

[1]. E. FREIRE, O. BIANCHI, E. E. C. MONTEIRO, R. C. R. NUNES, M. C. FORTE, *Materials Science and Engineering C,* **29** (2009) 657-661

[2]. A. A. BAKAR, A. HASSAN and A. F. M. YUSOF, *Journal of Vinyl and Additive Technology*, **14** (2008) 204-210

[3]. X. XU, S. GUO and Z. WANG, *Journal of Polymer Research*, **2** (1995) 233-238

[4]. Q. WANG, X. ZHANG, S. LIU, H. GUI, J. LAI, Y. LIU, J. GAO, F. HUANG, Z. SONG, B. H. TAN, JINLIANG QIAO, *Polymer*, **46** (2005) 10614-10617

[5]. C. WAIKRUT, Enhancing Impact Properties of Wood Composites by Rubber, *Master Thesis Chulalongkorn University*, (2009)

[6]. F. PRUNEDA, J. J. SUÑOL, F. ANDREU-MATEU and X. COLOM, *Journal of Termal Analysis and Calorimetry*, **80** (2005) 187-190

[7]. Z. LIU, X. ZHU, L. WU, Y. LI, Z. QI, C. CHOY, F. WANG, *Polymer*, **42** (2001) 737-746

[8]. Q. ZHOU, W. YANG, Q. WU, B. YANG, J. HUANG, J. SHEN, *European Polymer Journal*, **36** (2000) 1735-1740

Jurnal Sains Materi Indonesia
Indonesian Journal of Materials Science

Vol. 12, No. 2, Februari 2011, hal : 110 - 113
ISSN : 1411-1098

Akreditasi LIPI Nomor : 452/D/2010
Tanggal 6 Mei 2010

THE APPLICATION OF BENTONE AS NANOFILLER IN POLYPROPYLENE NANOCOMPOSITES

Ariadne L. Juwono[1], Seto Roseno[2] and Andes T. Agnelia[1]

[1]Department of Physics, Faculty of Mathematics and Natural Sciences-University of Indonesia
Kampus Baru UI, Depok 16424, Indonesia
[2]Center of Material Technology-Agency for Assessment and Application Technology
Jl. M.H. Thamrin No. 8, Jakarta 10340, Indonesia
e-mail : ariadne@fisika.ui.ac.id

ABSTRACT

THE APPLICATION OF BENTONE AS NANOFILLER IN POLYPROPYLENE NANOCOMPOSITES. For the last two decades, thermoplastic polymer based nanocomposites have been developed because of their superior properties. The benefits of these materials are light weight, high stiffness, and good resistance. With an addition of a small amount of filler, some properties improved significantly. This paper presents the tensile and flexural properties of a polypropylene with a dispersion of commercial Bentone clay in the matrix. Bentone polypropylene nanocomposites were successfully prepared by a melt intercalation method. The melting process was initiated by the addition of a modifier and an initiator. Bentone polypropylene nanocomposites with the variation of bentone contents were then analyzed. A pattern of clay morphology typically found in polypropylene based nanocomposites was observed using an X-Ray diffraction and a transmission electron microscope. These findings showed that an intercalated structure was formed. Furthermore, the value of tensile and flexural modulus as well as the value of tensile strength increased by an addition of 1 wt% bentone.

Key words : Bentone, Polypropylene nanocomposites, Tensile modulus, Flexural modulus

ABSTRAK

APLIKASI DARI *BENTONE* SEBAGAI *NANOFILLER* DALAM NANO KOMPOSIT POLIPROPILEN. Dalam dua dekade terakhir ini, nano komposit yang berbasis polimer termoplastik telah banyak dikembangkan karena keunggulan karakteristiknya. Keuntungan dari material ini diantaranya adalah ringan, kaku serta memiliki sifat ketahanan yang baik. Dengan ditambahkannya material pengisi (*filler*), beberapa sifatnya dapat ditingkatkan. Makalah ini memaparkan sifat kekuatan tarik dan kelenturan dari polipropilen dengan dispersi tanah liat *bentone* komersil dalam matriksnya. Nano komposit dari *bentone* polipropilen telah berhasil dibuat dengan menggunakan metode pelelehan dan interkalasi. Proses pelelehan dimulai dengan penambahan *modifier* dan *initiator*. Komposit dari *bentone* polipropilen dengan variasi konsentrasi dari *bentone* kemudian dianalisis. Pola morfologis tanah liat yang biasa ditemukan dalam nano komposit berbasis polipropilen dapat ditemukan dengan menggunakan difraksi sinar-X dan *TEM*. Temuan ini memperlihatkan bahwa struktur interkalasi telah terbentuk. Nilai dari modulus tarik dan lentur, serta nilai dari kekuatan tarik mengalami kenaikan dengan ditambahkannya 1% w/w *bentone*.

Kata kunci : *Bentone*, Nano komposit polipropilen, Modulus tarik, Modulus lentur

INTRODUCTION

For the last two decades, the organic inorganic nanocomposites have been widely studied and some of these potential materials have been used for a wide range of application. These materials, such as polymer layered silicate nanocomposites (PLSNs), have some benefits such as lighter weight, enhanced mechanical and thermal properties, as well as better fire resistance compared to the pristine polymers [1-4]. It is reported that a broad range of polymer have been used for these materials, such as epoxy, polyurethane, polyimide, polyester, polypropylene and polystyrene [5]. The role of nanofiller is important in the nano level of the materials. Being of 1 nm thickness clay silicate layers, the nanofiller is uniformly dispersed throughout the polymer matrix. Having a large surface ratio, the PLSNs show a significant change in mechanical and thermal properties. Only with less than 10 %nanofiller addition, these properties increase dramatically [6].

Polypropylene (PP) is one of the most widely used polymers since PP has a relatively simple structure and is easily recycled. Two methods have been developed to produce clay-PP nanocomposites, namely melt intercalation and intercalating polymerization [7]. One method to obtain a better mixing process during clay dispersion in a melt intercalation process is by the addition of a compatibilizer [6]. It has been studied that the compatiblizer promotes the formation of clay-PP nanocomposites. The presence of a compatibilizer, such as maleic anhydride (MA), reduces the viscosity of the PP during the clay dispersion. An optimum amount of MA can be added to the clay-PP mixture so that the PP molecules can easily enter the clay galleries or the clay particles can easily dispersed in the PP matrix.

Two different structures are formed when the clay is mixed with polymers, namely the intercalated and exfoliated structures. XRD is one effective method to characterize the nanocomposite structures. At least a peak is seen in the diffractogram of clay and from this peak, the (001) d-spacing can be identified. This peak will be shifted to the left as the d-spacing increases and this relates to the intercalated structure formation. When the peak disappears, an exfoliated structure may be formed. Moreover, Transmission Electron Microscope images also provide a better characterization since the clay layer separation can be observed. When the clay particles form aggregates in the matrix, the material obtained is identified as a composite.

In this study, a compatibilizer maleic anhydride and an initiator were added into the mixture of polypropylene (PP) and a commercial SD1 bentone to produce bentone-PP nanocomposites. The objectives of this research were to observe the structures of the materials using X-Ray Diffraction and Transmission Electron Microsope and to study the role of bentone in the tensile and flexural properties of the nanocomposites.

EXPERIMENTAL METHOD

The materials used in this experiment were polypropylene (PP) as the PLSNs matrix, maleic anhydride (MA) as the coupling agent, diphenylamine (DPA) as the initiator and a commercial SD1 bentone as the nanofiller.

A melt intercalation method was applied to synthesize the PLSNs. The PP, MA, DPA and Bentone were mixed using a rheomix machine at a temperature of 190 ^{o}C for 20 minutes with a 120 rpm rotor speed. The bentonite content varied of 1, 3, 5 and 7 wt%, while the weight percentage of MA was double of the bentonite percentage. The blending material was crushed and was then pressed using a compression moulding machine at a temperature of 180 ^{o}C and a pressure of 1 bar for 30 minutes.

An X-Ray Diffraction machine was used to observe the commercial bentone, the pristine PP and the PLSN materials.

The nanocomposites morphology structure was observed using a Transmission Electron Microscope after the specimens were prepared by a microtome. The tensile tests for the PLSNs materials were conducted according to ASTM D638 type IV, whereas the bending tests were followed ASTM 790.

RESULTS AND DISCUSSION

Figure 1 shows the results of XRD observation of the bentone, the pristine polypropylene (PP) and the bentone- PP nanocomposites with the variation of bentone loading. The first diffractogram has the diffraction angle of 2 θ = 4.54° equals to the (001) d-spacing of 1.98 nm. This peak is a characteristic peak of the SD1 bentone clay. The second diffractogram does not have any peak and this indicates a typical curve for non-crystalline polymers. There is no peak in the 1 wt%, 3 wt% and 7 wt%bentone-PP nanocomposite diffractograms. It is believed that exfoliated structure was formed.

However, an intercalated structure was formed in the 5 wt%bentone-PP nanocomposite. The peak at the diffraction angle of 2θ = 3.64° corresponds to the intercalated structure with a d-spacing of 2.41 nm. The XRD results indicated that formation of nanocomposite structures were achieved through the melt intercalation process.

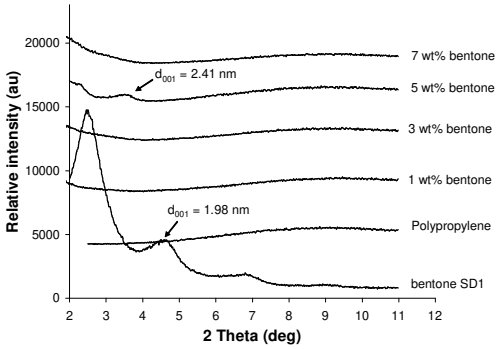

Figure 1. Diffractogram of bentone, polypropylene, and nanocomposites with different clay contents

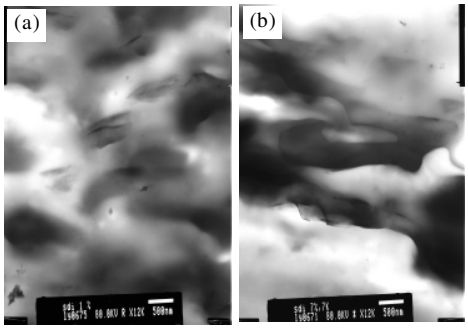

Figure 2. TEM images of (a). 1 wt%bentone-PP and (b). 7 wt%bentone-PP nanocomposites

Vol. 12, No. 2, Februari 2011, hal : 110 - 113
ISSN : 1411-1098

The TEM images of 1 wt% and 7 wt%bentone-PP nanocomposites are shown in Figure 2 (a) and Figure 2(b) respectively. The TEM image of 1 wt%bentone-PP nanocomposite is a typical image for intercalated nanocomposites where the clay layers can be seen in this image. While the TEM image of 7 wt%bentone-PP nanocomposite does not show any layer separation. This indicates that neither intercalated nor exfoliated structure was formed in this sampel. Even there is no XRD peak in the 7 wt%bentone-PP nanocomposite diffractogram which relates to an exfoliated structure, the TEM observation confirmed that the 7 wt%bentone-PP nanocomposite was a nanocomposite material with clay agglomerations. A similar image was obtained by Marchant and Jayaraman [8]. It is evidence for the 7 wt%bentone-PP systems that some amount of clay was dispersed in the matrix in which the PP penetrated into the clay galleries, however, some other amount of clay were identified as agglomerations.

Figure 3 demonstrates the tensile modulus and tensile strength of bentone-PP nanocomposites with a variety of bentone loadings. It is clear that the addition of 1wt% bentone in PP enhances the tensile properties. The values of both tensile modulus and tensile strength increases 20 %. It is also clear that the addition of 7 wt%bentone reduces the tensile strength by %. This reduction because the addition of high content of bentone addition produce brittle material [9]. From this result, it can be said that the effective amount of bentone in this nanocomposite systems to provide an enhanced tensile property is 1wt%.

Figure 4 shows the flexural modulus and flexural strength of bentone-PP nanocomposites with different bentone contents. It can be seen that an improvement in flexural modulus was achieved by the 1 wt%bentone-PP nanocomposite materials. While the flexural strength decreases as the clay content increases.

The presence of clay usually causes more brittle materials [9]. The flexural stress was not effectively transferred from the polymer matrix to the inorganic nano filler and this resulted the decreasing of flexural strength.

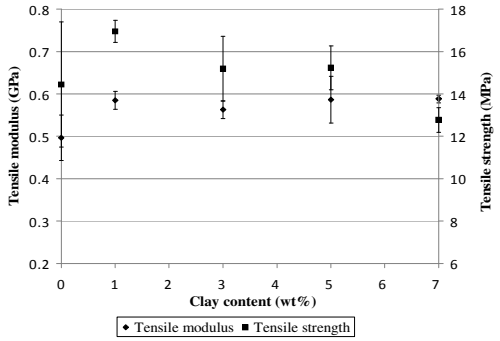

Figure 3. Tensile modulus and tensile strength of bentone-PP nanocomposites versus bentone contents.

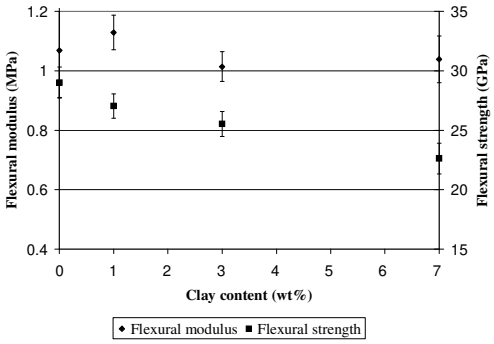

Figure 4. Flexural modulus and flexural strength of bentone-PP nanocomposites versus bentone contents.

Similar to the tensile test results, the most effective clay loading for flexural properties is 1 wt%.

From the structure observation and mechanical testing results, it can be said that 1wt% clay content is the most effective content for this bentone-PP nanocomposite material. The values of both tensile and flexural strength of these bentone-PP nanocomposite materials decrease significantly when the clay content was 7 wt%. Based on the TEM image of the 7 wt%bentone-PP nanocomposite, it is believed that the material obtained was composite, in which the bentone did not play as a nano filler. A further research on how the mechanism of high clay contents are dispersed in this bentone-PP systems should be carried out.

CONCLUSION

The addition of 1wt% bentone improves significantly the tensile modulus, tensile strength and flexural modulus of bentone-PP nanocomposite materials. Exfoliated and intercalated structure were found in the 1wt%, 3wt% and 5 wt%bentone-PP nanocomposite respectively. While the 7 wt%bentone-PP system was nanocomposite material with clay agglomerations in it.

ACKNOWLEDGMENT

This research was financially supported by the Incentive Research Program, Agency for Assessment and Application Technology. The authors thank to Nuning Aisyah and Henny Purwati from the Center of Material Technology, Agency for Assessment and Application Technology for their work contribution.

REFERENCES

[1]. M. GRASIA, G. VAN VLIET, S. JAIN, B.A.G. SCHRAUWEN, A.E. SARKISSOV, W. VAN ZYL and B. BOUKAMP, *Rev. Adv. Mater. Sci*., **6** (2004) 169-175

[2]. K. H. CHEN and S. M. YANG, *Journal of Appl. Sci*, **86** (2002) 414-421
[3]. Q.H. ZENG, A.B. YU, Q (MAX) LU and D.R. PAUL, *Journal of Nanosci Nanotech*, **5** (2005) 10
[4]. P. C. LE BARON, Z. WANG and T.J. PINNAVAIA, *Applied Clay Science*, **15** (1999) 11-29
[5]. M. KAWASUMI, N. HASEGAWA, M. KATO, A. USUKI and A. OKADA, *Macromolecules*, **30** (1997) 6333-6338
[6]. F. CHIU and P. CHU, *Journal of Polymer Res*., **13** (2006) 73-78
[7]. Y. ZHANG, J. LEE, J.M. RHEE and K.Y. RHEE, *Composites Sci and Tech*., **64** (2004) 1383-1389
[8]. D. MARCHANT and K. JAYARAMAN, *Ind. Eng. Chem. Res*., **41** (2001) 6402-6408
[9]. S.S. RAY and M. OKAMOTO, *Prog. Polym. Sci*., **28** (2003) 1539-1641

Jurnal Sains Materi Indonesia
Indonesian Journal of Materials Science

Vol. 12, No. 2,Februari 2011, hal : 114 - 119
ISSN : 1411-1098

Akreditasi LIPI Nomor : 452/D/2010
Tanggal 6 Mei 2010

SYNTHESIS AND CHARACTERIZATION OF SUPERABSORBENT POLYMER COMPOSITES BASED ON ACRYLIC ACID, ACRYLAMIDE AND BENTONITE

A. Zainal Abidin, I. Noezar and Ridhawati

Dept. of Chemical Engineering, Faculty of Industrial Technology-Bandung Institute of Technology
Jl. Ganesha No. 10, Bandung 40132, Indonesia
e-mail: zainal@che.itb.ac.id

ABSTRACT

SYNTHESIS AND CHARACTERIZATION OF SUPERABSORBENT POLYMER COMPOSITES BASED ON ACRYLIC ACID, ACRYLAMIDE AND BENTONITE. Superabsorbent polymer (SAP) is a hydrogel material which is capable of absorbing and or storing liquid up to a hundred times of its dry weight. SAP was synthesized from monomers of acrylic acid and acrylamide. Beside that a superabsorbent polymer composite (SAPC) was also made by grafting the SAP with bentonite. The polymerization processes were carried out using a chemical method of a ammonium persulphate (APS) as chemical initiator and N,N-methylene bisacrylamide (MBA) as crosslink forming materials at temperature of 70 ^{o}C in the 500 mL round flask. The homogeneity of the mixture was achieved by an adjustable magnetic stirrer. The result of polymer formed was identified using a FT-IR spectroscopy and the characteristic of absorption was studied using demineral water and 0.9 % NaCl solution. The maximum absorption capacity obtained from SAP is 339 g/g in water and 65 g/g in NaCl solution, while the maximum absorption rate obtained from SPAc is 19.43 g/min in water and 7.3 g/min in NaCl solution. It is interesting to note the absorption characteristic of SAP and SAPc above, the SAP is better in capacity of absorption while the SAPC is better in the rate of absorption. This phenomenon is supported by the result of morphology identification of SEM that shows the micro porous structure of SAP is bigger in number but smaller in pore sizes, while the micro porous structure of SAPC is smaller in number but bigger pore sizes.

Key words : Superabsorbent polymer, Acrylamide, Acrylic acid, Bentonite, Grafting, Absorption capacity

ABSTRAK

SINTESIS DAN KARAKTERISASI KOMPOSIT POLIMER SUPERABSORBEN BERBASIS ASAM AKRILAT, AKRIAMIDA DAN BENTONIT. Polimer superabsorben (*SAP*) merupakan material hidrogel yang mampu menyerap dan/atau menyimpan cairan hingga ratusan kali lipat dari berat keringnya. *SAP* disintesisdari monomer berupa asam akrilat dan akril amida. Kemudian, komposit polimer superabsorben (*SAPC*)-nya dibuat dengan metode *grafting* dari SAP itu dengan bentonit. Proses polimerisasi dilakukan dengan metode kimia yang menggunakan inisiator ammonium persulfat (*APS*) dan *crosslinker* (bahan pemicu *crosslink*) N,N-methylene bisacrylamide (*MBA*) pada suhu 70 ^{o}C dalam sebuah labu 500 mL. Homogenitas dari campuran dicapai dengan memanfaatkan pengaduk magnetik. Polimer yang dihasilkan diidentifikasi dengan spektroskopi *FT-IR* dan sifat absorpsinya dipelajari dengan menggunakan air tanpa mineral (*aqua DM*) serta larutan garam 0,9 % NaCl. Kapasitas absropsi maksimal diperoleh dengan *SAP* ini ialah 339 g/g terhadap air, dan 65 g/g untuk larutan 0,9 % NaCl, sedangkan kecepatan absorpsi maksimal diperoleh dengan *SAPC* 19,43 g/min untuk air dan 7,3 g/min untuk larutan 0,9 % NaCl. Satu hal yang menarik di sini adalah bahwa *SAP* memiliki kapasitas yang lebih baik, sedangkan *SAPC* memiliki kecepatan absorpsi yang lebih baik. Hal ini didukung oleh hasil dari identifikasi morfologi dengan *SEM* yang memperlihatkan bahwa struktur pori mikro dari *SAP* menunjukan jumlah pori-pori yang lebih banyak tetapi ukurannya lebih kecil. Sedangkan pada *SAPC* jumlah pori lebih sedikit, namun dengan ukuran yang lebih besar

Kata kunci : Polimer superabsorben, Akrilamida, Asam Akrilat, Bentonit, *Grafting*, Kapasitas Absorpsi

INTRODUCTION

Superabsorbent polymer (SAP) is a hydrogel material which is capable of absorbing and or storing liquid up to a hundred times of its dry weight. The fluids that can be absorbed by SAP are

water, body fluids such as urine and blood, or other liquids. The advantage of using hydrogel in comparison to other absorbent materials such as paper, cellulose and cotton is the ability of its absorption more than its weight, better in pressure resistant, and it can be described as environmental friendly materials [1,2]. SAP is a polymeric product that can be naturally degraded by microbes to be small molecules such as CO_2, H_2O dan nitrogen and hence safe for use.

The polymer is also sensitive to direct sunlight because it can break the polymer bond and then become some oligomers.The hydrophilicity, swelling in aqueous media, nonsoluble nature in aqueous fluids, and ionic aspect are basic requirements of a good SAP. Because of their unique properties, SAP has a great potential of applications in various systems. For example, since SAP could absorb water in a rainy season and slowly releases it for plants in a dry season, it would help them to survive under dry condition and increases the survival rate of afforestation [4]. Some of their applications include novel moisture sensors, fire protection materials, hygienic products, horticulture, gel actuators, drug delivery systems, as well as water blocking tapes and coal dewatering [5].

However, superabsorbent has negative features in some application fields because of high production cost and low gel strength. To overcome these, inorganic substances can be added as low cost material and a filler to improve the strength properties in the polymer matrixes. In the field of SAP, much attention has recently been paid to a layered silicate in order to improve mechanical properties of SAP by producing a superabsorbent composite (SAPC). Clays, such as kaolin, montmorillonite, and attapulgite have all been used as well in the preparation of SAPC. Pillared clays are modified clays that protect the layered silicate structure [6,7].

In this research, SAP was synthesized from monomers of acrylic acid and acrylamide, while SAPC was made by grafting the SAP with bentonite. Acrylic acid is usually used to produce plastics of homopolymer or copolymer. Acrylamide is a kind of nonionic monomer and has a great advantage as a raw material of SAP due to good salt-resistant. Bentonite is a layered silicate with reactive groups –OH on the surface and was added to SAP in order to reduce costs and improve the properties of compression and rate of its waterabsorbtion. Grafting process carried out by chemical methods, i.e. by using ammonium persulphate (APS) as the initiator and N,N-methylene-bisacrylamide (MBA) as the cross linker. Initiator and cross linker are important components that affect the properties of the final polymerization product.

EXPERIMENTAL METHOD

Materials

Acrylic acid (AA) chemically pure, Merck Factory was distilled under reduced pressure before use. Acrylamide (AM) chemically pure, Merck Factory was used as purchased. Ammonium persulphate (APS) Merck Factory was recrystallized from water. N,N-methylene bisacrylamide (MBA) chemically pure, Merck Factory was used as purchased. Bentonite micro powder (DIY, Indonesia), milled through 320-mesh screen, followed by treatment with 37 % hydrochloric acid for 48 hours and washed with distilled water until pH 7 to remove any residual hydrochloric acid, was dried at 105 °C for 8 hours prior to use. All solutions were prepared with distilled water.

Preparation of Superabsorbent

The polymerization of SAP were carried out using a chemical method of a chemical initiator as APS and crosslink forming material as MBA at temperature of 70 °C in the 250 mL round flask [8-11]. The homogeneity of the mixture was achieved by an adjustable magnetic stirrer. A series of SAP formulas was prepared by the following procedure: AA (23 mL) was dissolved in 75 mL distilled water and then neutralized with 20.8 mL of sodium hydroxide solution (5 M) in a four-neck flask equipped with a stirrer, condenser and thermometer. AM (10.65 g) and MBA were then added to the above partial neutralized monomer solution. The mixture was stirred at room temperature for about 30 minutes. The water bath was heated slowly to 70 °C with effective stirring. After that APS was introduced to the mixed solution and allowed the reaction to take place. 3 hours later, the resulting product was washed several times with distilled water, dried at 70 °C to a constant weight, then milled and screened.

Preparation of Superabsorbent Composite

SAPC was prepared in the same way as that of SAP, instead bentonite was also added when MBA was introduced into the 250 mL round flask. The addition of bentonite was varied in order to study the effect of the filler to the properties of SAPC.

Absorption Capacity Measurement

A weighted quantity of the SAP or SAPC was immersed in distilled water or saline solutions at room temperature to reach the swelling equilibrium. Swollen samples were then separated from unabsorbed water by filtered over a 100-mesh screen. The absorption capacity (Q_{H_2O}) of superabsorbent composite was determined by weighting the swelled samples, and the Q_{H_2O} of

Vol. 12, No. 2,Februari 2011, hal : 114 - 119
ISSN : 1411-1098

the samples was calculated using the following Equation (1) [12] :

$$Q_{H_2O} = \frac{m_2 - m_1}{m_1} \quad \text{..... (1)}$$

Where :

m_1 = Weights of the dry sample
m_2 = Weights of the water-swollen sample
Q_{H2O} = Calculated as grams of water per gram of sample

Absorption Rate Measurement

The absorption rate measurement was done by pouring SAP or SAPC samples (1.0 g, 50-60 mesh) into 10 Erlenmeyer flasks of 1 liter distilled water or desired solution and dispersing them with mild stirring [13]. Then observed the change of sample weight at various interval times by taking out the sample from the flask one by one at consecutive time intervals, and weighted according the procedure above. The absorption rate was obtained from the slope of the curve of sample weight changes against the interval time.

Characterization

The IR spectra of the SAP and SAPC were recorded on a FT-IR-8400 SHIMADZU using KBr pellets. The morphology of the dried samples was examined using a SEM instrument after coating the sample with gold film.

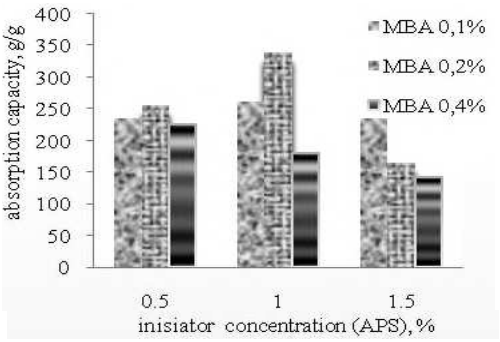

Figure 1. Water absortive capacity of SAP

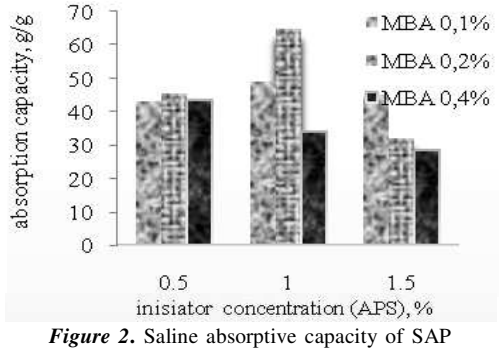

Figure 2. Saline absorptive capacity of SAP

RESULTS AND DISCUSSION

Absorption Characteristics

Absorption capacity of SAP is the ability of SAP to absorb certain liquids by immersing the SAP in the liquid. There are two types of liquid used in determining the absorption capacity i.e. distilled water and 0.9 % NaCl solution. These are the types of fluids expected to represent the application of SAP in the field of agriculture and health such as baby diapers and sanitary napkins.

Figure 1 and Figure 2 show that absorption capacity depends on MBA and salt concentrations. The maximum absorption capacity is obtained at 0.2 % MBA concentration for both distilled water (339 g/g) and saline solution (65 g/g), which means that the density of crosslinking has significant effects on the absorption capacity of SAP. At low crosslinking density (0.1 % MBA), the SAP is weak to hold water molecules and at high crosslinking density the SAP has a little space to accommodate water molecules.

The relationship between absorption capacity of the polymer network structure has been described by Equation (2) as following [14],

$$Q^{5/3} = \frac{(i/2v_u S^{*1/2})^2 + (1/2 - \chi)/V_1}{v_e/V_0} \quad \text{..... (2)}$$

In the Equation (2), the crosslink density is an important element that controls the capacity of the superabsorbent polymer.

Similar trend is shown with the effect of APS concentration, which may indicate that increasing number in short chain SAP will decrease the absorption capacity of SAP. The relationship between absorption capacity and the number of initiators are described by the following Equation (3) [14].

$$v = \frac{[k_p/2v(fk_dk_t)^{1/2}][M]}{[I]^{1/2}} \quad \text{..... (3)}$$

Increasing the amount of the initiator will decrease the polymer molecular weight and increase the number of single polymer chain. Single polymer chain does not contribute to the absorption capacity. Thus the absorption capacity decreases with the increase in the number of initiators. However, if the initiator is too small, the absorption capacity will also decrease. This is because the number of free radicals

Table 1. Water absorptive capacity of SAPC

Variabel		Kapasitas absorbsi, (g/g)					
Jumlah APS (%)		0,5%		1%		1,5%	
MBA (%)	0,1	184,365	A	207,363	B	126,735	C
	0,2	242,690	C	304,085	A	198,589	B
	0,4	165,655	B	187,766	C	208,697	A

A = bentonit concentration 5% ; B = 10% and C = 15%

Table 2. Saline absorptive capacity of SAPC

Variabel		Kapasitas absorbsi, (g/g)					
Jumlah APS (%)		0,5%		1%		1,5%	
MBA (%)	0,1	28,025	A	41,464	B	25,208	C
	0,2	32,545	C	48,112	A	30,612	B
	0,4	26,814	B	30,753	C	36,984	A

A = bentonit concentration 5% ; B = 10% and C = 15%

generated by initiator is small and hence reduces the number of chains formed.

Figures above also show that the present of NaCl reduces a lot the absorption capacity of SAP. This is due to increasing external ionic strength of NaCl, resulting in decrease of osmotic pressure differences between SAP and saline solution.

Table 1 and Table 2 add some more information that increasing concentration of Bentonite in the SAPC will decrease the absorptive capacity of the material. However, the experiment showed that the presence of bentonit in the SAPC increased the rate of water absorption in the beginning, 17 g/g.minutes for 0 % Bentonite and 35 g/g.minutes for 5 % bentonite. This characteristic of SAP and SAPC has opened opportunity of their application, for example SAP may be good for application in agriculture field due to high absorptive capacity while SAPC may be good for application in health field (such as baby diapers) due to fast absorption in the beginning.

FT-IR and SEM Characteristics

Functional group analysis of the sample was carried out using a FT-IR machine and basically done by comparing the absorption band formed in the infrared spectrum using the correlation table [15]. The bentonite FT-IR spectroscopy test result is shown in Figure 3.

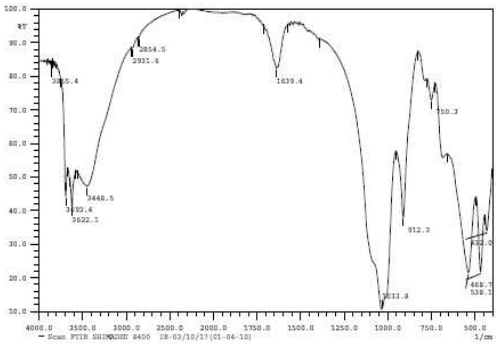

Figure 3. FT-IR spectra of bentonite

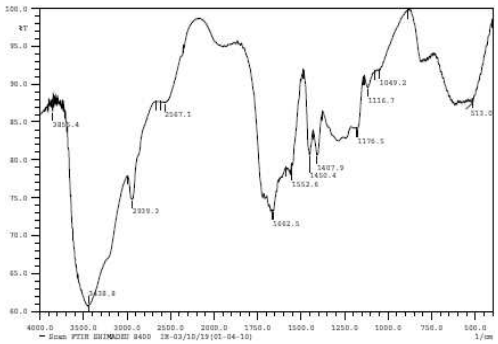

Figure 4. FT-IR spectra of SAP

Table 3. The end groups indentified from SAP sample

Sample	Isolated wave number (cm^{-1})	Theoritical wave number (cm^{-1})	Groups
SAP	3438,8	3310-3500	-OH
	2939,3	2700-3000	-CH
	1662,5	1640-1680	-C=O
	1176,5	1110-1180	$-NH_2$
	1407,9	1350-1470	-NH
	1552,6	1550-1680	-C=O
	1450,4	1400-1480	-NH

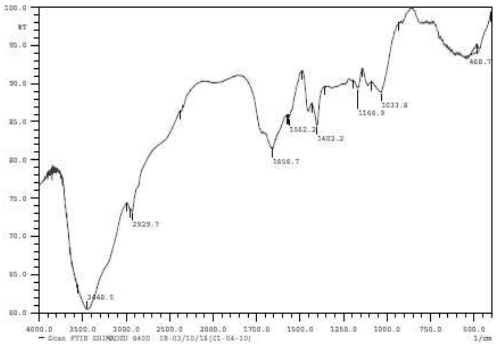

Figure 5. FT-IR spectra of SAPC

Table 4. The end groups indentified from SAP sample

Sample	Isolated wave number (cm^{-1})	Theoritical wave number (cm^{-1})	Groups
SAPC`	3436,9	3310-3500	-OH
	2927,7	2700-3000	-CH
	1656,7	1550-1680	-C=O
	1164,9	1110-1180	$-NH_2$
	1402,2	1350-1470	-NH
	1562,2	1550-1680	-C=O
	1033,8	685-1040	Si-O (bentonite)

It can be seen from Figure 3 that the infra-red spectrum of bentonite are on the wave number 3622.1, which refers to -OH groups, and the wave number 1033.8, which refers to Si-O clusters. These two groups, -OH and Si-O, are the main characteristics of bentonite, which has the sharpest intensity band.

Figure 4 shows the FT-IR spectroscopy result of SAP. All wave numbers representing groups in the SAP are given in Table 3. There are 7 groups identified in the spectrum, i.e. -OH group originally from AA monomer, $-NH_2$ group from AM monomer, -CH and -C=O groups from AA and AM monomers, and -NH group from MBA cross linker. These are all hydrophilic groups that make the polymer having high capability of absorbing water or saline solution.

Figure 5 shows the infra-red spectrum of SAPC. All wave numbers representing groups in the SAPC are given in Table 4. This FT-IR spectrum of SAPC clearly shows that the material is combination between SAP and bentonite, as indicated by the regional SAPC of 1033.8 wave number which is a characteristic absorption of Si-O clusters derived from bentonite.

Vol. 12, No. 2,Februari 2011, hal : 114 - 119
ISSN : 1411-1098

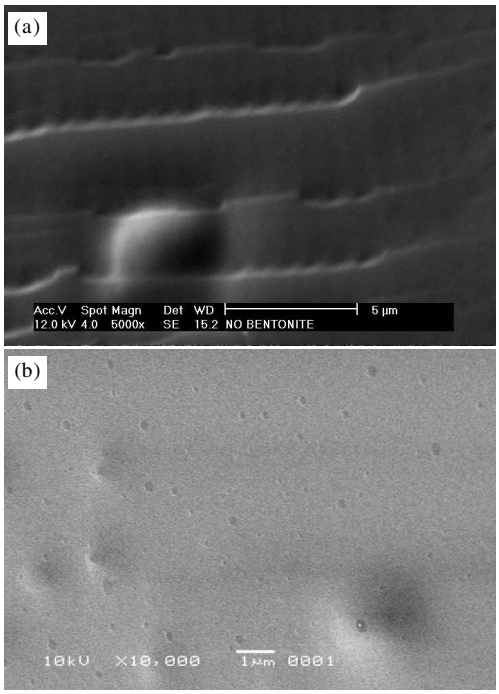

Figure 6. Scanning electron micrographs of SAP (a). 5000x and (b). 10.000x

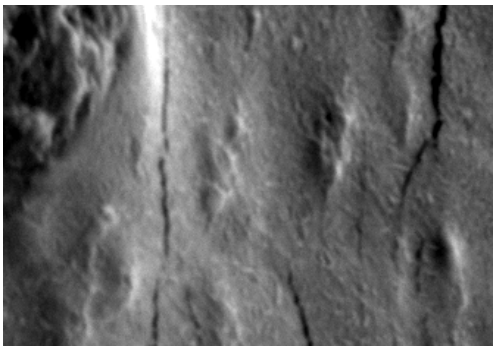

Figure 7. Scanning electron micrographs of SAPC 5000x

SAP and SAPC morphologies were identified by SEM in order to analyze the surface and micro pore of the material. The morphology is believed to have an effect on the absorptive characteristics of SAP and SAPC, either on their absorptive capacity or absorptive rate. The surface and micro pore are places where water and saline solution interact with hydrophilic groups. Hence, their form and number are important to observe.

Figure 6 shows the surface microstructure of SAP is very smooth, having many small pores (200-230 nm). This has made SAP having a higher absorptive capacity but a slower absorptive rate compared to those of SAPC. Further look to the surface of SAPC in Figure 7, the surface looks rough and has many strains, which indicate that the surface area and pore cavities of SAPC are larger than those of SAP. This may contribute to the faster absorption rate of SPAC. Additionally, bentonite of SAPC may cause many small pores closed and hence reduce its absorptive capacity.

CONCLUSIONS

This research has already showed that superabsorbent polymer (SAP) and superabsorbent polymer composite (SAPC) synthesized using chemical method of MBA cross linker and APS initiator having good absorptivity, which are significantly different between those in distilled water and saline solution. In addition, introduction of bentonite to the SAP can produce SAPC that has faster absorptive rate in the beginning and slightly lower absorptive capacity than SAP has. Therefore, SAP may suitable for application in agriculture area and SAPC in health area.

ACKNOWLEDGEMENT

We would like to thank Dr Aditianto from Department of Material Engineering, ITB, and to Dr Pramono Nugroho from LIPI, Bandung, for providing help and enlighten discussion during SEM analysis.

REFFERENCIES

[1]. AN LI, JUNPING ZHANG, AIQIN WANG, *Bioresource Technology*, **98** (2007) 327-332
[2]. AN LI, AIQIN WANG, *European Polymer Journal*, **41** (2005) 1630-1637
[3]. DEYU GAO, J. LERCHNER, *Journal of Material Science*, **36** (2001) 4567-4571
[4]. DOUGLAS R. CHAMBERS, JR. HUBERT H. FOWLER, YOJI FUJIORA and FUSAYOSHI MASUDA, Super Absorbent Polymer having Improved Absorbency Properties, *US Patent number 5145906*, (1992)
[5]. DAYO GAO, Superabsorbent Polymer Composite (SAPC) Materials and their Industrial and High Tech Applications, *Dissertation Der Technischen U ätBergakademie Fiberg University*, (2003)
[6]. DENI SWANTOMO, KARTINI MEGASARI, RANY SATAAJI, Pembuatan Komposit Polimer Superabsorben dengan mesin Berkas Elektron, *Seminar Nasional IV SDM Teknologi Nuklir Yogyakarta*, Sekolah Tinggi Teknologi Nuklir-BATAN, (2008)
[7]. FLORY PJ, *Principle of Polymer Chemistry*, NY. Cornell University Press, Ithaca, New York, (1953) 576-594
[8]. MARK ELLIOT, *Superabsorbent Polymers*, BASF Product Development Scientist, (1997)
[9]. MEHR ZOHURIAN J. MOHAMMAD, KABIRI KOUROSH, *Iranian Polymer Journal*, **17** (6) (2008) 451-477
[10]. Nasir Muhammad, Pembuatan Komposit Hidrogel berbasis Selulosa untuk Pertanian di Lahan Kering, *Penelitian Laboratorium Bidang Ilmu Teknik Material*, LIPI Bandung, (2010)

[11]. SOO CHEONG CHANG and JIN SUNG YOO, *Korean Journals Chemical Engineering*, **16** (1999) 581-584

[12]. TAO WAN, LAN WANG, JIE YAO, *Polymer Bulletin*, **60** (2008) 431-440

[13]. SILVERSTEIN R.M., BASSLER G.C. and MORRILL T.C., *Spectrometric Identification of Organic Compound*, Fourth Edition, John Wiley and Sons, (1981) 248-283

[14]. SUDA KIATKAMJORNWONG, *Science Asia*, **33** (Supplement 1) (2007) 39-43

[15]. YIAN ZHENG, PING LI, JUNPING ZHANG, *European Polymer Journal*, **43** (2007) 1691-1698

Jurnal Sains Materi Indonesia
Indonesian Journal of Materials Science

Vol. 12, No. 2, Februari 2011, hal : 120 - 124
ISSN : 1411-1098

Akreditasi LIPI Nomor : 452/D/2010
Tanggal 6 Mei 2010

PHASE TRANSITION IN Fe_3O_4/Fe_2O_3 NANOCOMPOSITES BY SINTERING PROCESS

Muhammad Ghufron, Malik Anjelh Baqiya, Mashuri, Triwikantoro and Darminto
Dept. of Physics, Fac. of Math. and Natural Sciences-Sepuluh November Institute of Tech. Surabaya
Kampus ITS Sukolilo, Surabaya 60111, Indonesia
e-mail : darminto@physics.its.ac.id

ABSTRACT

PHASE TRANSITION IN Fe_3O_4/Fe_2O_3 NANOCOMPOSITES BY SINTERING PROCESS. Fe_3O_4 powders have been successfully produced by using coprecipitation method. The characterization using X-Ray Diffraction method resulted in the size of Fe_3O_4 powders of 9.1 ± 0.3 nm. Samples were then formed into pellete and powders. Heat treatment at temperature 600 °C of powder samples for 1 hour and 2 hours give maghemite and hematite phases, but heat treatment at temperature 700-800 °C for 1 hour, 2 hours and 3 hours give only one phase namely hematite. Heat treatment at temperature 600 °C, 700 °C and 800 °C of pelletes for 1 hour, 2 hours and 3 hours give also only one phase which is hematite. Quantitative analysis using MAUD program resulted in Fe_3O_4/Fe_2O_3 composites with changing crystal size at increasing temperature.

Key words : Coprecipitation, Fe_3O_4/Fe_2O_3 composites, XRD, Phase transition, Fe_3O_4 powder

ABSTRAK

TRANSISI FASA PADA KOMPOSIT NANO Fe_3O_4/Fe_2O_3 DENGAN PROSES *SINTERING*. Dalam riset ini serbuk Fe_3O_4 telah berhasil disintesis dengan menggunakan proses kopresipitasi. Karakterisasi dengan menggunakan metode difraksi sinar-X memperlihatkan ukuran kristal dari serbuk Fe_3O_4 sebesar 9,1 ± 0,3 nm. Sampel ini kemudian dibentuk menjadi pelet dan serbuk. Perlakuan panas pada suhu 600 °C pada serbuk selama 1 jam dan 2 jam menghasilkan fasa *maghemite* dan *hematite*, namun perlakuan panas pada suhu 700 °C hingga 800 °C pada 1 jam, 2 jam dan 3 jam menghasilkan fasa tunggal yaitu *hematite*. Perlakuan panas pada 600 °C, 700 °C dan 800 °C pada pelet selama 1 jam, 2 jam dan 3 jam juga menghasilkan fasa tunggal yaitu *hematite*. Analisis kuantitatif dengan menggunakan program *MAUD* menghasilkan komposit Fe_3O_4/Fe_2O_3 dengan perubahan ukuran kristal bila suhu dinaikkan.

Kata kunci : Kopresipitasi, Komposit Fe_3O_4/Fe_2O_3, *XRD*, Transisi fasa, Serbuk Fe_3O_4

INTRODUCTION

Many researchers have recently employed various methods to obtain magnetic nanocrystal with size reduction and dimensional modification. They have tried to examine magnetic, optic, and electronic properties, and even the surface reactivity of these materials. Iron oxides are common compounds which are widespread in nature and readily synthesized in laboratories. Iron oxides in nano crystal size can improve and repair materials performance. That is why it is very important to control particle size, its morphology and texture, shape, and distribution of synthesized iron oxides [1].

Magnetite (Fe_3O_4) is one of iron oxide phase and member of inverse spinel structure, in which the divalent ions are on octahedral sites, and the trivalent ions are equally divided between tetrahedral and octahedral sites [2]. Its general chemistry name is *ferrous-ferric oxide*. Magnetite's chemical formula is often written in $FeO.Fe_2O_3$ form with one part is wustite (FeO) and another part is hematite (Fe_2O_3).

Research shows there is phase transformation from γ-Fe_2O_3 to α-Fe_2O_3 in Fe_3O_4/Fe_2O_3 nanocomposites at temperature 550 °C [3]. Another study discuss the temperature effect in α-Fe/Fe_3O_4 composite at range 100 °C to 400 °C [4]. In present study, it is shown that Fe_3O_4 powder and bulk (pellete) will transform completely to Fe_2O_3 (hematite) in different temperature of heat treatment. In this paper, Fe_3O_4/Fe_2O_3 composites were obtained from heating process of Fe_3O_4 nanopowders and their bulk form in the range from 100 °C to 400 °C. The goal is to study the different phase transition in powder and bulk related to structural properties based on XRD analysis.

EXPERIMENTAL METHOD

Synthesis of Fe_3O_4 Nanopowders

Fe_3O_4 nanopowders were synthesized by coprecipitation technique using HCl as solvent and NH_4OH as precipitate agent without calcinations. This method can be done at low temperature and give an easy and simple technique to produce nanocrystal materials quickly. Extracted iron sand was used as raw materials. It was solutted in HCl at ~ 70 °C under constant stirring. The resulted solution was added slowly with NH_4OH. After 30 minutes of the digestion at the same temperature and stirring speed, the black precipitates were formed. These particles were initially washed with distilled water and then dried at 70 °C for five hours.

Synthesis of Fe_3O_4/Fe_2O_3 Composites

Fe_3O_4 nanopowders were divided into two type of samples, powder and bulk (pellete). Each sample was sintered at several temperature, that were 600 °C, 700 °C and 800 °C for 1 hour, 2 hours and 3 hours. The samples were also sintered at temperature 300 °C, 400 °C and 500 °C.

Characterisation of Fe_3O_4/Fe_2O_3 Composites

After sintering process, both Fe_3O_4/Fe_2O_3 powder and bulk samples were analyzed by XRD. (Cu Kα 1,54 Å, 40 kV, 30 mA) for determination of phase, crystal structure and average crystal size using search match and MAUD program.

RESULTS AND DISCUSSION

Fe_3O_4 nanoparticles from iron sand have been synthesized using simple coprecipitation method [5]. According to qualitative analysis (search and match program), there is only one phase obtained which is magnetite (Fe_3O_4) with PDF Number 11-0614. XRD pattern of this initial phase is shown in Figure 1.

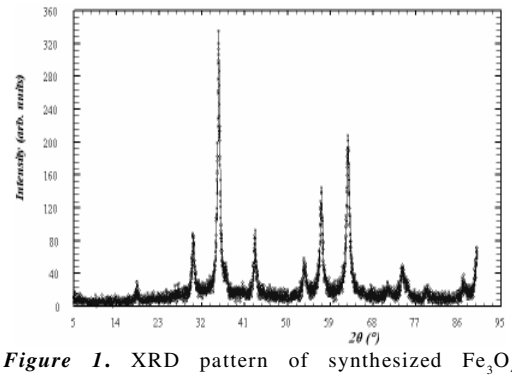

Figure 1. XRD pattern of synthesized Fe_3O_4 nanoparticles.

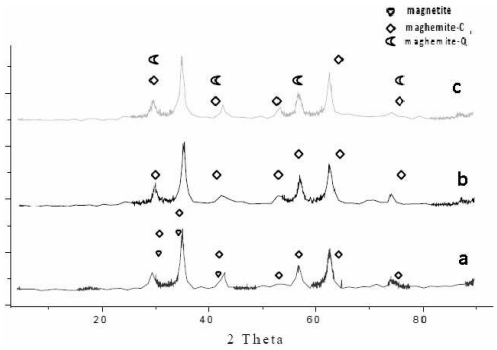

Figure 2. XRD result for pellete samples (a) sintering at temperature 300 °C, (b) sintering at temperature 400 °C, and (c) sintering at temperature 500 °C for 1 hour.

Based on quantitative analysis using MAUD Program [6], it is known that magnetite phase has crystal size 9.10 ± 3.25 nm. This initial sample was then formed into two kinds, powder sample and pellete sample. Both samples were sintered at different duration time and temperature. The sintering temperature variations are 300 °C, 400 °C, 500 °C, 600 °C, 700 °C and 800 °C.

Figure 2 shows XRD result for pellete samples sintered at temperature 300 °C, 400 °C and 500 °C for 1 hour. It is known that there is phase transformation because of increasing temperature from magnetite (Fe_3O_4) to maghemite, γ-Fe_2O_3 phases. When specimen is heated, the particle which initialy have Fe_3O_4 phase gets thermal energy from furnace. The increasing of heating temperature causes the increasing of thermal energy which is given so that atom will vibrate and diffuse at grain boundary.

Phase transformation process start when Fe^{2+} ion is oxidated into Fe^{3+} ion.These Fe^{3+} ions diffuse so that formed γ Fe_2O_3. At temperature 300 °C, magnetite phase in pellete sample was partially oxidated, thus there are two phases in the sample, magnetite and maghemite. It might be said that composite was formed in the sample because of increasing temperature at certain value.

Maghemite-C resulted in pellete sample in Figure 2(a) and Figure 2(b) can be indexed using PDF data number 39-1346. New possible phase, maghemite-Q, seems appeared in pellete sample at sintering 500 °C and can be analized using PDF data number 25-1402. Maghemite-Q is maghemite with tetragonal crystal structure. Phase composition exists in this temperature equal to 65.23 % for maghemite-C

Table 1. Crystal size of pellete samples after sintering

T (°C)	Crystal size (nm) at holding time 1 hour		
	Magnetite	Maghemite-C	Maghemite-Q
300	19.2 ±1.7	5.1 ± 0.5	(none)
400	(none)	9.8 ± 0.5	(none)
500	(none)	20.9 ± 2.1	8.1 ± 0.9

Vol. 12, No. 2, Februari 2011, hal : 120 - 124
ISSN : 1411-1098

and 34.77 % for maghemite-Q. It should be a nanocomposite here.

From quantitative analysis using MAUD Program, phase composition of pellete sample sintered at 300 °C are magnetite and maghemite phase of 37,96 % and 62,04 %, respectively. Crystal sizes of pellete samples after sintering at 300 °C, 400 °C and 500 °C for 1 hour are shown in Table 1. Crystal size tends to increase as sintering temperature increase.

Higher sintering temperature, higher diffusion occur in all of the sample, thus higher crystal size. At constant temperature, for example 600 °C in Figure 3, diffusion took place between particle at grain boundary and resulted in larger grain. Phase transformation from magnetite to hematite happened at temperature < 500 °C for pellete samples. Below 500 °C, the phase transform slowly until reaching temperature around ~450 °C. At temperature 500 °C, crystallization of hematite will be initiated and grown to hematite phase rapidly [7]. XRD pattern of samples sintered at temperature 600 °C with different sintering time can be seen in Figure 3 and Figure 4 for powder and pellete specimen respectively.

According to Figure 3 and Figure 4, it can be observed that there are differences in the diffraction pattern between pellete (bulk) and powder sample. In bulk sample, sintering at 600 °C for 1 hour even for 2 hours, etc, will result in direct transformation from magnetite (initial) to hematite phase (PDF Number 13-0534). While for the powder sample sintering at

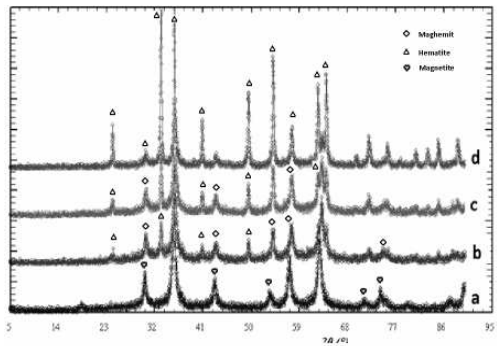

Figure 3. XRD pattern for (a) initial powder; powder sample sintered at 600 °C during (b) 1 hour, (c) 2 hours and (d) 3 hours.

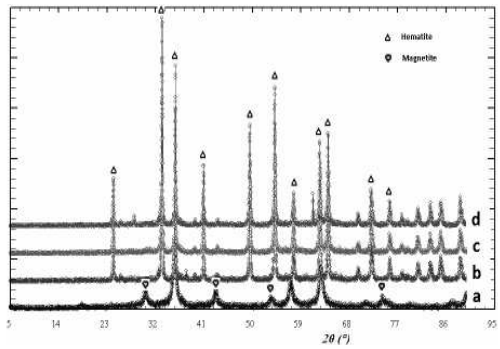

Figure 4. XRD pattern for (a) initial powder; pellete/bulk sample sintered at 600 °C during (b) 1 hour, (c) 2 hours and (d) 3 hours.

Table 2. Phase Transformation for bulk and powder samples sintered at different temperature and holding time.

T (°C)	t (h)	Initial Phase	Phase after sintering	
			Pellete (Bulk)	Powder
600	1	Magnetite	Hematite	Maghemite and Hematite
600	2	Magnetite	Hematite	Maghemite and Hematite
600	3	Magnetite	Hematite	Hematite
700	1	Magnetite	Hematite	Hematite
700	2	Magnetite	Hematite	Hematite
700	3	Magnetite	Hematite	Hematite
800	1	Magnetite	Hematite	Hematite
800	2	Magnetite	Hematite	Hematite
800	3	Magnetite	Hematite	Hematite

600 °C for 1 hour and 2 hours, will give two phases, that is maghemite and hematite. But for 3 hours sintering, the powder transform to hematite entirely. This phase transition occurs even in the same temperature because duration of sintering time also responsible for ionic diffusion in the material. Longer sintering time, it makes possible ionic arrangement to form other crystal structure which more stable in the current temperature. If the phase already reach its stability, then longer sintering time can increase crystal size. This condition can occur because of ionic vibration at grains and their boundaries.

Percentage of maghemite and hematite phase are 33.01 % and 66.99 % respectively for powder sample sintering at temperature 600 °C during 1 hour. While for sample sintered at temperature 600 °C for 2 hours, maghemite and hematite phase of 10.32 % and 89.68 % respectively are obtained. The forming of these two phases expresses that the two powder samples have come to be nanocomposite, with maghemite phase as filler and hematite phase as matrix.

Table 2 shows the result of qualitative analysis using search-match program for samples with sintering temperature of 600 °C, 700 °C, and 800 °C for 1 hour, 2 hours and 3 hours. Table 2 shows that Fe_3O_4 nanoparticles (magnetite phase) will transform to hematite phase perfectly after sintering at temperature above 600 °C for 3 hours.

Figure 5 and Figure 6 represents that for both samples (powder and bulk), increasing temperature may cause in increasing crystal size which is signed by decreasing of FWHM values in each peak of XRD patterns. Once again, ionic (atomic) diffusion and vibration take place here.

Tables 3-4 show crystal size value for both sample (powder and bulk) analyzed using MAUD Program.

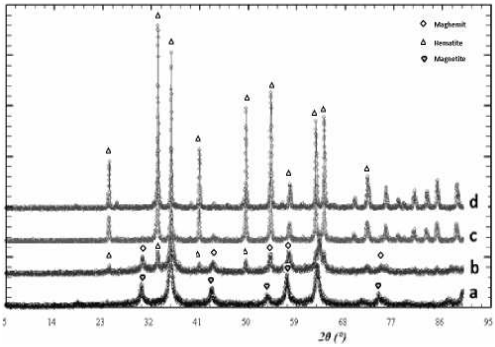

Figure 5. XRD pattern for (a) initial sampel without sintering, powder samples sintered for 1 hours at (b) 600 °C (c) 700 °C and (d) 800 °C.

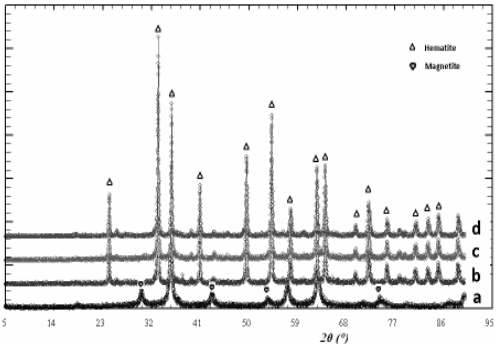

Figure 6. XRD pattern for (a) initial sampel without sintering; pellete / bulk samples sintered for 1 hour at (b) 600 °C (c) 700 °C (d) 800 °C

According to Tables 3-4, it can be observed clearly as mentioned before that the increasing of sintering temperature causes the increasing of crystal size. The increasing of holding time also yields the increasing of crystal size. Pellete samples have smaller crystal size than powder samples at the same temperature and sintering time. This may occur because pellete samples have fixed form and there is internal pressure (residual stress) in bulk samples caused by compaction, while the powder one do not have residual stress and they are not limited by room. When pellete samples are sintered at higher temperature, thermal energy activation for diffusion energy is distributed more rapid so they transform to hematite phase quicker than powder samples.

When the particle sintered at the same temperature, they have same energy for diffusion process. It should cause crystal size progressively increase, but at certain size, this increasing will reach maximal value. If the sintering still continues, pellete samples which are limited by certain available space may have large microstrain and the grain will brake (known *broken grain*) so that grain becomes apart. The higher microstrain value in pellete sample was proved by MAUD analysis. Effect of this broken grain is crystal size of pellete sample become smaller than powder sample at the same temperature with longer sintering time. This case is clearly observed at sintering

Table 3. Powder sample crystal size after sintering analyzed using MAUD software

T (°C)	Crystal size (nm)		
	1 hour	2 hours	3 hours
600°C	Maghemite 35.53 ± 0.04	Maghemite 43.70±0.03	71.5 ± 0.02
	Hematite 55,30 ± 0,03	Hematite 67,80±0,02	
700°C	88.12 ± 0.04	123.8 ± 6.30	193.5 ± 0.02
800°C	171.20 ± 0.03	205.6 ± 0.02	206.8 ± 0.03

Table 4. Pellete sample crystal size after sintering analyzed using MAUD software

T (°C)	Crystal size (nm)		
	1 hour	2 hours	3 hours
600	126.0 ± 0,03	168.8 ± 0.04	193.5 ± 0.02
700	88.5 ± 0.20	100.0 ± 0.03	119.5 ± 0.03
800	148.6 ± 0.03	176.9 ± 0.01	178.3 ± 0.01

temperature 800 °C during 1 hour, 2 hours and 3 hours for both samples.

CONCLUSION

Fe_3O_4 nanoparticles synthesized from iron sand by copresipitation technique result in nanomaterial which crystal size value is 9.1 ± 0.03 nm. This material was used as raw material to obtain Fe_3O_4 / Fe_2O_3 composites. The formed phases in the powder are hematite and maghemite-C which may occur at sintering temperature below 600 °C for 2 hours. Sintering the pellete samples at temperature between 300 °C to 500 °C may cause the formation of maghemite-C, maghemite-Q and hematite phase. Sintering the sample at temperature above 600 °C during 3 hours will result in entirely transformation of the sample to hematite phase without any other phases. Sintering at elevated temperature and sintering time can increase crystal size of the obtained phase(s). It is caused by thermal activation which affect diffusion and atomic vibration of the sample.

REFERENCES

[1]. M. BALASIOU, M. V. AVDEEV, V. L. AKSENOV, *Crystallography Report,* **52** (3) (2007) 505-511

[2]. C. KITTEL, *Introduction to Solid State Physics*, John Willey & Sons, Inc., New York, (1996)

[3]. M. VASQUEZ-MANSILLA, R.D. ZYSLER, C. ARCIPRETE, M. DIMITRIJEWITS, D. RODRIGUEZ-SIERRA, C. SARAGOVI, *Journal of Magnetism and Magnetic Material*, **226-230** (2) (2001) 1907-1909

Vol. 12, No. 2, Februari 2011, hal : 120 - 124
ISSN : 1411-1098

[4]. LIJUN ZHAO, HUA YANG, SHUIMING LI, LIANXIANG YU, YUMING CUI, XUEPING ZHAO, SHOUHUA FENG, *Journal of Magnetism and Magnetic Materials*, **301** (2006) 287-291

[5]. MALIK A. BAQIYA and DARMINTO, *Indonesian Journal of Materials Science*, **Edisi Khusus Desember 2009** (2009) 74-77

[6]. L. LUTTEROTI, *MAUD: Material Analysis Using Diffraction*, Available: [http://www.ing.unitn.it/~maud], (2006)

[7]. P.S. SIDHU, *Clays and Clay Mineral*, **36** (1) (1988) 31-38

Akreditasi LIPI Nomor : 452/D/2010
Tanggal 6 Mei 2010

INVESTIGATING THE NANOCRYSTALLINITY OF SOL GEL DERIVED TiO_2 NANOPARTICLES UPON ANNEALING AND POST HYDROTHERMAL TREATMENTS

Akhmad Herman Yuwono, Alfian Ferdiansyah, Arif Rahman and Wulandari Handini
Dept. of Metallurgy and Materials Engineering, Faculty of Engineering-University of Indonesia
Kampus Baru UI, Depok 16424, Indonesia
e-mail : ahyuwono@metal.ui.ac.id

ABSTRACT

INVESTIGATING THE NANOCRYSTALLINITY OF SOL GEL DERIVED TiO_2 NANOPARTICLES UPON ANNEALING AND POST HYDROTHERMAL TREATMENTS. The present study is aimed at investigating the major factor causing the low nanocrystallinity nature of the sol gel derived TiO_2 nanoparticles. For this purpose, TiO_2 nanoparticles of different nanocrystallinity was synthesized by various hydrolysis ratio (R_w) of 0.85; 2.00 and 3.50 upon sol solution preparation, followed with subsequent drying, conventional annealing and post-hydrothermal treatments. The resulting nanoparticles were studied by dynamic light scattering, XRD and FT-IR spectroscopy which confirm that the highly amorphous state of TiO_2 is related to the fast development of stiff Ti-OH networks during hydrolysis and condensation upon sol gel process. A post hydrothermal treatment involving high-pressure water vapor has been successfully devised to enhance the nanocrystallinity of TiO_2 nanoparticles. It has been found in this study that R_w value of 2.00 was the optimum hydrolysis ratio during sol solution preparation of TiO_2 precursor to result in the most enhanced nanocrystallinity as represented with the biggest crystallite size of 12.46 nm.

Key words : TiO_2 nanoparticles, Sol gel, Nanocrystallinity, Annealing, Post hydrothermal

ABSTRAK

INVESTIGASI NANOKRISTALINITAS NANOPARTIKEL TiO_2 TERDERIVASI SOL GEL DENGAN PERLAKUAN *ANNEALING* DAN *POST HYDROTHERMAL*. Penelitian ini bertujuan untuk menginvestigasi faktor utama yang menyebabkan rendahnya nanokristalinitas struktur nanopartikel TiO_2 hasil derivasi sol gel. Untuk tujuan tersebut, telah disintesis berbagai nanokristalinitas dari nanopartikel TiO_2 dengan variasi rasio hidrolisis (R_w) 0,85, 2,00 dan 3,50 dengan preparasi larutan sol diikuti dengan pengeringan, *annealing* konvensional dan penanganan *post hydrothermal*. Nanopartikel yang dihasilkan selanjutnya dipelajari dengan *dynamic light scattering*, *XRD* dan spektroskopi *FT-IR* yang mengkonfirmasi bahwa tingkat amorf yang tinggi dari TiO_2 berhubungan dengan perkembangan *network* yang cepat dari *stiff* Ti-OH selama hidrolisis dan kondensasi dalam proses sol gel. Penanganan *post hydrothermal* menggunakan uap air bertekanan tinggi telah berhasil meningkatkan nanokristalinitas nanopartikel TiO_2. Telah diketemukan bahwa nilai R_w 2,00 adalah rasio hidrolisis optimum selama preparasi larutan sol *precursor* TiO_2 untuk menghasilkan nanokristalinitas yang paling tinggi sebagaimana ditunjukkan dengan ukuran kristalit terbesar yakni 12,46 nm.

Kata kunci : Nanopartikel TiO_2, Sol gel, Nanokristalinitas, *Annealing*, *Post hydrothermal*

INTRODUCTION

Sol gel process has been widely practiced to respond to the demand for advanced ceramics of high purity, well controlled homogeneity, and properly tailored properties as well as various nanostructured materials [1]. This is mainly due to its versatility i.e.: (i). a lowered processing temperature, (ii). high purity and (iii). feasibility of employing various post forming processes [2]. Sol gel process is basically a wet chemical route which involves the evolution of a system from a colloidal suspension (the sol) into a solid/semi solid (the gel) phase. Upon the phase evolution, two important reactions namely hydrolysis and condensation are involved. This process was developed initially as a technique to prepare pure ceramic precursors and inorganic glasses at low temperatures. For the synthesis of TiO_2 nanoparticles, however, the sol gel process has a major limitation, which is the low crystallinity in the resulting TiO_2 phase, as a consequence of the relatively

Vol.12, No. 2, Februari 2011, hal : 125 - 128
ISSN : 1411-1098

low processing temperatures. In connection with this case, Brinker and Hurd [3] and Langlet et al. [4] proposed that the low nanocrystallinity of sol gel derived TiO_2 phase could be due to the fast development of a stiff Ti-O-Ti network, which in turn hinders the densification during post-solution treatments.

Structural changes of TiO_2 can be induced by the treatment in a high humidity environment at temperatures above 100 °C [5,6]. Furthermore, reported that exposure of sol gel derived TiO_2 films to water vapor induced rearrangement of Ti-O-Ti network leading to formation of anatase phase at 180 °C [7,8].

Therefore, it is thus of interest in the current work to investigate the factor causing the amorphous nature of sol gel derived TiO_2 nanoparticles. For this purpose, a variation in hydrolysis ratio or amount of water to inorganic precursor (R_w) of 0.85; 2.00 and 3.50 upon sol solution preparation will be performed. The resulting gel is furthermore subjected to drying, conventional annealing and post hydrothermal treatments in order to observe the nanocrystallinity of TiO_2 phase under investigation.

EXPERIMENTAL METHOD

TiO_2 nanoparticles in the current study were synthesized through a well controlled sol gel process using titanium tetra isopropoxide (TTIP) as inorganic precursor. First, TTIP was mixed carefully with ethanol in a container and stirred for 30 minutes. A mixture of deionized water and hydrochloric acid (HCl) was then added under stirring condition into the transparent solution to promote hydrolysis. The TTIP concentration in the solution was controlled at 0.4 M with the ratio of water to TTIP (R_w) was varied as 0.85, 2.00 and 3.50 while the pH value of all solution was kept to be consistent as low as ~1.30 for obtaining a stable highly transparent solution.

The solution was further stirred overnight and poured into a petri-dish to form thick film. The thick film was subjected to drying at room temperature for 1 week and 60 °C for 3 days, followed with conventional annealing in dry atmosphere at 150 °C for 24 hours and subsequent post hydrothermal treatment with highly pressurized water vapor at 150 °C for 24 hours.

For the post hydrothermal treatment, a Teflon lined stainless steel autoclave (Parr, Moline, IL) was used where a specially designed stand was placed inside the autoclave in order to prevent the samples from direct contact with liquid water. In order to confirm the effect of different treatments on the TiO_2 nanostructures, the resulting sol solution and powders were further characterized by particle size analyzer (Delsa TM Nano Submicron dynamic light scattering), X-Ray diffraction (XRD, Bruker AXS θ–2θ diffractometer) and Fourier transform infrared spectroscopy (Bio Rad QS-300 spectrometer).

RESULTS AND DISCUSSION

Figure 1 shows the result of dynamic light scattering of TiO_2 sol solution with different hydrolysis ratio, R_w. It can be seen that with the increase of hydrolysis ratio (R_w), i.e. the amount of water content added to the inorganic precursor (TTIP) upon sol gel process, the particle size has increased significantly. It should be noted, however, that the presented values here are not the real size of the solid nanocrystalline TiO_2. Instead, they still represented the size of Ti-OH and Ti-O-Ti networks as the species resulted from the hydrolysis and condensation reactions of inorganic precursor. It is highly possible that they formed clusters or particle like networks among the random and entangled chains of inorganic molecules.

In order to further analyze, the results of dynamic light scattering will be compared with the crystallite size measurement obtained through XRD on the resulting TiO_2 powders after drying, annealing and post hydrothermal treatments.

Figure 2 shows the XRD traces of the resulting TiO_2 powders derived from the sol gel process with various hydrolysis ratios after drying, conventional annealing and post hydrothermal treatment.

It can be seen that all as dried samples are not crystalline yet as indicated by a very broad hump in the 2θ range of 20°-35° in traces (a), (b) and (c). The

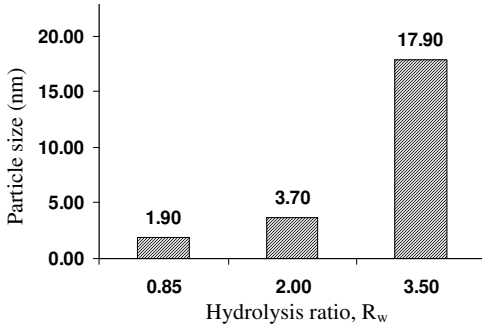

Figure 1. The result of particle size measurement by dynamic light scattering for TiO_2 sol solution with various R_w

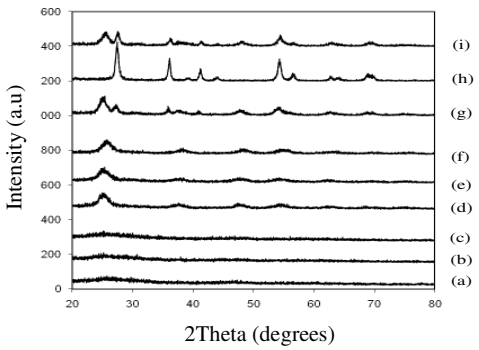

Figure 2. XRD traces of TiO_2 derived from sol-gel with hydrolysis ratio, R_w of 0.85; 2.00 and 3.50 at drying (traces (a), (b) and (c)), conventional annealing (traces (d), (e) and (f)), and post-hydrothermal (traces (g), (h) and (i)) conditions, respectively.

crystallinity enhancement started to occur when the conventional annealing were applied on all the samples. This can be seen from a slightly increase in the intensity for the diffraction peaks at 2θ angles of 25 °-26 °, 38 °, 48 ° and 54 ° in traces (d), (e) and (f). A much more significant enhancement, as demonstrated with further increase in the above mentioned peaks, was apparently shown by the post hydrothermally treated samples (traces (g), (h) and (i)). Among the post hydrothermally treated samples, the most enhanced nanocrystallinity was achieved by TiO_2 derived from the sol gel process with R_w of 2.00 (trace (h)).

In order to obtain a more quantitative data, Scherrer's formula was applied on the above XRD traces and the result of crystallite size estimation is given in Figure 3. It should be noted that throughout the use of Scherrer's formula, all the additional broadening on the XRD peaks due to non uniform strain and instrument effect has been excluded [9]. It can be seen that the increase of hydrolysis ratio from 0.85 to 2.00 has increased the crystallite size of TiO_2 nanoparticles at both annealed and post hydrothermal conditions from 3.10 and 4.84 nm to 4.07 and 12.46 nm, respectively.

However, a further R_w increase to 3.50 has adversely decreased the crystallite size down to 3.81 and 7.21 nm, although these values are still higher than those shown by R_w of 0.85. It is also apparently

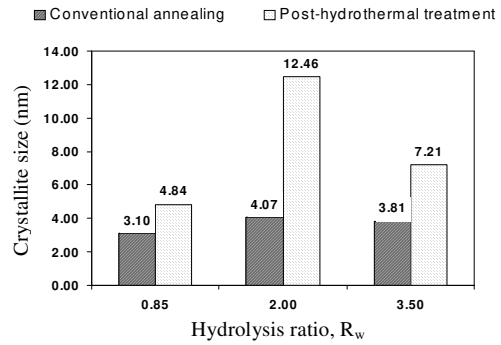

Figure 3. The result of crystallite size estimation by using Scherrer's formula for sol gel derived TiO_2 nanoparticles with R_w of 0.85; 2.00 and 3.50 at conventional annealing and post hydrothermally treatment conditions

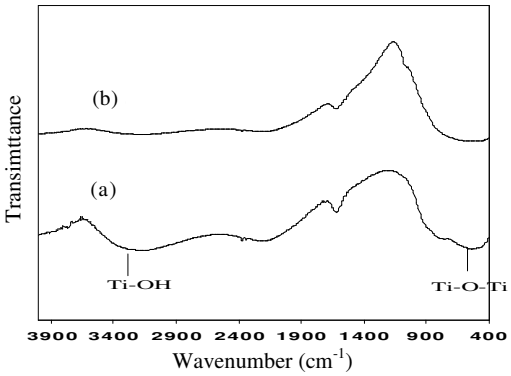

Figure 4. FT-IR spectra of (a). conventionally annealed and (b). post hydrothermally treated TiO_2 nanoparticles derived from the sol gel technique

demonstrated that the post hydrothermally treated sample with R_w of 2.00 provides a much more pronounced nanocrystallinity enhancement as represented with a significant increase in the crystallite size up to 12.46 nm.

In order to further understand the phenomenon behind the observed results, FT-IR spectroscopy was performed on both conventionally annealed and post hydrothermally treated TiO_2 nanoparticles. Figure 4 shows obviously the existence of broad absorption bands located at ~3400-3500 cm^{-1}, which is assigned to hydroxyl groups of Ti-OH [10]. In addition, there exists also an absorption band in the range of ~400-900 cm^{-1}, which is accounted for by stretching vibrations of Ti-O-Ti groups [11].

From the Figure 4, it can be apparently demonstrated that the conventionally annealed sample (spectrum (a)) provides a high intensity Ti-OH absorption band, but with a weak intensity in Ti-O-Ti absorption band. By contrast, a reverse phenomenon is resulted by the post hydrothermally treated sample (spectrum "b') where the intensity of Ti-OH absorption band is decreased significantly, accompanied with an increase in the intensity of Ti-O-Ti absorption band.

By correlating the above XRD and FT-IR analyses, it was known that the crystallinity enhancement of the sol gel derived TiO_2 phase is represented with an increase in the intensity of Ti-O-Ti absorption band and a decrease in intensity of Ti-OH absorption band. The stretching vibration of Ti-O-Ti absorption band is regarded as the characteristic peak for TiO_2 nanocrystalline [11]. Water vapor exposure in the post hydrothermal treatment can successfully enhance the nanocrystallinity of TiO_2 phase as a result of cleavage mechanism of strained Ti-OH networks by high pressure water molecules to provide much more flexible Ti-O-Ti networks which can further densify to form nanocrystalline TiO_2 [7,8].

R_w of 2.00 is the optimum hydrolysis ratio that can lead to a proper number of Ti-OH species which function as flexible nuclei for the formation of TiO_2 nanocrystalline, both at annealed and post hydrothermal conditions, while the R_w value of 3.50 caused an excessive formation of stiff Ti-OH networks which could not densify further to form TiO_2 nanocrystalline, although the cleavage mechanism has been applied on this sample through post hydrothermal treatment [3,4]. This mechanism is highly possible causing the decrease in the crystallite size of TiO_2 from 12.46 nm to 7.21 nm when the hydrolysis ratio was increased from R_w 2.00 to 3.50 upon sol solution preparation.

CONCLUSION

A systematic investigation has been conducted into TiO_2 nanoparticles derived from sol gel process, aimed at understanding the mechanisms responsible for the occurrence of the largely amorphous state in TiO_2 nanoparticles. The results confirm that the low

Vol.12, No. 2, Februari 2011, hal : 125 - 128
ISSN : 1411-1098

nanocrystallinity of TiO_2 is shown to relate to the fast development of stiff Ti-OH networks during hydrolysis and condensation upon sol gel. A post hydrothermal treatment involving high pressure water vapor has been successfully devised to enhance the nanocrystallinity of TiO_2 nanoparticles. The nanocrystallinity enhancement is related to the cleavage of stiff Ti-O-Ti bonds by water molecules, which effectively increases the number of flexible Ti-OH groups and rearranges Ti-O-Ti bonds promoting crystallization of TiO_2. In this study, the R_w value of 2.00 has been found to be the optimum hydrolysis ratio for the sol solution preparation of TiO_2 precursor to provide the most enhanced nanocrystallinity of 12.46 nm.

ACKNOWLEDGMENT

The authors would like to thank the financial support from Hibah Riset Strategis Nasional Tahun 2009 with contract No : 407CB/DRPM-UI/A/N1.4/2009. Some part of research was also supported by Indonesian Toray Science Foundation (ITSF) Research Grant Year 2008.

REFERENCES

[1]. K.N.P. KUMAR, K. KEIZER, A.J. BURGRAAF, T.OKUBO, H. NAGAMOTO and S. MOROOKA, *Nature*, **358** (1992) 48

[2]. J.D. MCKENZIE, *In Ultrastructure Processing of Ceramics*, Ed. by L.L. HENCH and D.R. ULRICH, Wiley, New York, (1984)

[3]. C.J. BRINKER and A.J. HURD, *J. Phys. III France*, **4** (1994) 1231

[4]. M. LANGLET, M.BURGOS, C. COUTIER, C.JIMENEZ, C.MORANT and M. MANSO, *J. Sol-Gel. Sci. Technol.,* **22** (2001) 139

[5]. A. MATSUDA, Y. KOTANI, T. KOGURE, M.TATSUMISAGO and T. MINAMI, *J. Am. Ceram. Soc*., **83** (2000) 229

[6]. Y. KOTANI, A. MATSUDA, T.KOGURE, M. TATSUMISAGO and T. MINAMI, *Chem. Mat*., **13** (2001) 2144

[7]. H. IMAI, H. MOROMOTO, A. TOMINAGA and H. HIRASHIMA, *J. Sol-Gel. Sci. Technol.,* **10** (1997) 45

[8]. H. IMAI and H.HIRASHIMA, *J. Am. Ceram. Soc*., **82** (1999) 2301

[9]. B.D. CULLITY, *Elements of X-Ray Diffraction*, 2nd Ed., Addison-Wesley Reading, Massachusetts, 1978.

[10]. L. H. LEE and W.C. CHEN, *Chem. Mater*., **13** (2001) 1137

[11]. S.X. WANG, M.T., WANG, Y.LEI and L.D.ZHANG, *J. Mater. Sci. Lett*.,**18** (1999) 2009

Akreditasi LIPI Nomor : 452/D/2010
Tanggal 6 Mei 2010

PREPARATION OF ELECTROCHEMICALLY IMMOBILIZED IRON ON THIN FILM FAUJASITE-NANOZEOLITE MODIFIED GLASSY CARBON

Yuni K. Krisnandi, Ivandini T. Anggraningrum, Hanny Tovina and Aminah
Department of Chemistry, Faculty Mathematics and Science-University of Indonesia
Kampus Baru UI, Depok 16424, Indonesia
e-mail : ykrisna@ui.ac.id

ABSTRACT

PREPARATION OF ELECTROCHEMICALLY IMMOBILIZED IRON ON THIN FILM FAUJASITE-NANOZEOLITE MODIFIED GLASSY CARBON. Metal iron that electrochemically immobilized on thin film faujasite type of nanozeolite (FAU-nanozeolite) grown on polyelectrolyte (PDDA, PSS, PDDA layers) modified glassy carbon has been prepared. Thin film of FAU-type nanozeolite was synthesized using seeding method. The seeded modified-glassy carbon then was immersed in FAU colloidal suspension at 100 °C for certain period. XRD patterns of the seed and as-synthesized zeolite powder have similarity with the patterns from standard NaY zeolite. SEM images of thin film nanozeolite also show the appearance of crystals with homogeneous size of about < 1 μm. The best spread thin film was obtained when using 3 ml seed and immersion in colloidal FAU solution for 20 hours. The thin film then was utilized for metal iron synthesis, in which Fe(III) from $FeNO_3$ solution containing Na-citrate of that adsorbed on the surface of thin film was electrochemically reduced to (Fe^0). SEM image shows some aggregates (size > 100 nm) of the nanozeolite thin film. However, it can also be seen that the crystals actually consist of smaller particles with size < 100 nm. The EDS mapping of the surface indicates that after electrochemical treatment, the surface of thin film consists of about 0.30% (w/w) iron that spread evently both on the surface covered by nanozeolite thin film and that from modified glassy carbon.

Key words : Nanozeolite, Faujasite (FAU), Seeding, Glassy carbon, Iron, Electrochemistry

ABSTRAK

PREPARASI BESI TERIMOBILISASI ELEKTROKIMIA PADA KARBON GELAS TERMODIFIKASI LAPISAN TIPIS *FAUJASITE-NANOZEOLITE*. Telah dipreparasi logam besi yang diimobilisasi secara elektrokimia pada lapisan tipis nanozeolit tipe *faujasite* (*FAU*) yang ditumbuhkan pada karbon gelas termodifikasi dengan polielektrolit (lapisan *PDDA*, *PSS*, *PDDA*). Lapisan tipis nanozeolit tipe *FAU* disintesis menggunakan metode *seeding*. Karbon gelas termodifikasi dalam bentuk *seed* dicelupkan ke dalam suspensi koloid *FAU* pada 100 °C selama waktu tertentu. Pola *XRD* dari *seed* dan serbuk zeolit awal memiliki kemiripan dengan zeolit NaY standar. Gambar *SEM* dari nanozeolit lapisan tipis juga menunjukkan keberadaan kristal dengan ukuran homogen sekitar < 1 μm. Penyebaran lapisan tipis terbaik diperoleh apabila menggunakan *seed* 3 mL dan dicelupkan ke dalam koloid *FAU* selama 20 jam. Lapisan tipis kemudian digunakan untuk mensintesis logam besi, dimana Fe(III) dari larutan $FeNO_3$ mengandung Na sitrat yang terabsorsi pada permukaan lapisan tipis tereduksi secara elektrokimia menjadi Fe(0). Gambar *SEM* menunjukkan beberapa agregat lapisan tipis nanozeolit (ukuran > 100 nm). Tetapi, terlihat juga bahwa kristal tersebut mengandung partikel kecil berukuran < 100 nm. *Mapping EDS* terhadap permukaan menunjukkan bahwa setelah penanganan elektrokimia, permukaan lapisan tipis mengandung sekitar 0,30 % (w/w) besi yang tersebar rata pada kedua sisi, yakni permukaan yang tertutup lapisan tipis nanozeolit dan permukaan dari karbon gelas termodifikasi.

Kata kunci : Nanozeolit, *Faujasite*, *Seeding*, Karbon gelas, Besi, Elektrokimia

INTRODUCTION

Nanosized metals have drawn many attention as their catalytic properties increase significantly as well as many other potential application in microelectronic research and optic and magnetic device [1]. So far, several methods in nanometal synthesis have been developed, such as reduction by chemical reaction, photoreduction, thermal decomposition, and electrochemical reduction [2]. The important factor in all above methods

Vol. 12, No. 2, Februari 2010, hal : 129 - 133
ISSN : 1411-1098

is the prevention of nanoparticle agglomeration during and after synthesis [3]. Organic compounds such as ligands, polymers or surfactants are usually used as protecting agent to maintain the stability of nanoparticle so that they are separated from each other [4].

However, the use of organic compounds as dispersing agent sometimes limit the applications of metal nanoparticles, e.g. as catalysts and electrodes. Zeolite is an inorganic aluminosilicate material having orderded and homogeneous pores and/or nanochannels that can trap nano metal into its structure. Preparation of Ag nanoparticle have been done using FAU type zeolite as template [1]. The zeolite was grown on Pt-electrode having surface modified by some layers of polyelectrolytes in order to give positive charge to its surface. In our previous work, mordenite type of zeolite was synthesized on the surface of modified glassy carbon electrode, then was used to immobilize Fe(III) cations. The application of this Fe(III)-immobilized glassy carbon electrode as arsen sensor is promising. The detection limit achieved for arsen, so far, is 6.75 ppb [5].

In this work, iron nanoparticle was synthesized by electrochemical reduction method from iron nitrate solution containing sodium citrate, dispersed inside the pores of FAU nanozeolite modified glassy carbon surface (ZGC). Thus, the electrochemical reduction of iron(III) to iron(0) is expected to occur inside the pores. To the best of our knowledge the use of FAU nanozeolite as dispersing agent and glassy carbon electrode as support for iron nanoparticle preparation has not yet been reported.

Modification on preparation of nanozeolite and the process of electrochemical reduction of Fe(III) to Fe(0) are discussed in this paper.

EXPERIMENTAL METHOD

Synthesis of FAU Nanozeolite

Colloidal nanocrystal FAU type zeolites was synthesized following procedure reported by Lassinati et.al [6] with some modification [7]. Seeds was prepared in homogeneous solution with molar composition of 2.46 $(TMA)_2O$, 0.032 Na_2O, Al_2O_3, 3.40 SiO_2, 400 H_2O, by pouring aluminium isopropoxide solution (in ethanol/ water = 1 : 10), TMAOH and 0,1 M NaOH into TEOS solution (in water) with vigorous stirring. After aging overnight, the mixture then was refluxed at 100 °C for 7 days. The seed formed then was washed three times and redispersed in 0.1 M ammonia solution.

FAU nanozeolite then was prepared by adding certain amount of seed into homogeneous mixture with molar composition of Na_2O, Al_2O_3, 10 SiO_2, 798 H_2O, 3Na_2SO_4 followed by hydrothermal treatment at 80 °C for 24 hours. The product was then washed with solution of 0.1 N NH_3 and aquadest and redispersed in aqueous suspension.

Nanozeolite Immobilization [5, 7]

Glassy carbon was modified with nanozeolite using self assembly method through electrostatic interaction as thin films of three layers of polyelectrolyte PDDA/PSS/PDDA applied giving positive charge to the final layer. Then the nanozeolite seed was added into the surface of modified glassy carbon in solution of 01 M NaCl at pH 9.5 for 20 minutes. Afterward, the modified glassy carbon was immersed in the colloidal FAU nanozeolite suspension for certain period at 100 °C. The FAU nanozeolite modifed glassy carbon was then labelled ZGC.

Synthesis of Iron Nanoparticle

Fe(III) solution 2 x 10^{-3} M containing Na-citrate 5 x 10^{-2} M was prepared from $FeNO_3.9H_2O$. Na-citrate is a capping agent to avoid coagulation and precipitation of Fe(III) cations [8]. Thin film nanozeolite on modified glassy carbon was immersed in $FeNO_3$ solution of 2 x 10^{-3} M, and dried at room temperature. The modified glassy carbon then immersed in Fe(III) solution 1 x 10^{-3} M containing Na-citrate 5 x 10^{-2} M at pH 8.7 and then electrochemically reduced under condition of potential = 2000 mV to -2000 mV, reference electrode = Ag/AgCl, counter electrode = Pt. The result was then called Fe-ZGC.

RESULTS AND DISCUSSION

Synthesis of Seeds and Immobilization of FAU Nanozeolite on Modified Glassy Carbon

Modification in seed synthesis (using mixed solvent ethanol/water (1 : 10) was applied in order to slow down the hydrolisis of Al-isopropoxide to $Al(OH)_3$ so that it was easier to form tetrahedral network with SiO_4^- in zeolite framework.

XRD pattern of as-synthesised nanozeolite is similar to that of nanozeolite prepared using commercial NaY as seed (Figure 1), and resemble to nanozeolite reported by Holmberg et.al [9]. Observation with EDAX gives Si/Al ratio within 2.5-2.8 range, which falls into Si/Al ratio for FAU zeolite type Y.

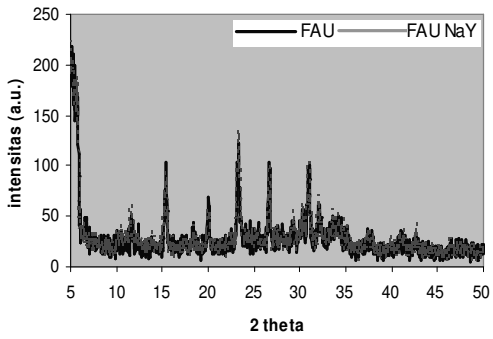

Figure 1. XRD pattern of nanozeolite

Morphology of the as-prepared FAU-nanozeolite, both seeds and bulk are shown by Figure 2. It can be seen that the size and shape of seeds and NaY added-seeds, shown by Figure 2(a) and Figure 2(c), are quite similar. While the shape of bulk powder is rather poor compared to that of NaY-added bulk powder.

Thin films of nanozeolite immobilized on polyelectrolyte modified glassy carbon were then prepared as summarized in Table 1. Only one layer or seed applied to every sample as based on our previous

Table 1. Thin films of nanozeolite grown on modified glassy carbon

No.	Sample name	Details
1	ZGC1-20	Nanozeolite on glassy carbon: 1 mL seed immersion time 20 hours
2	ZGC3-20	Nanozeolite on glassy carbon: 3 mL seed immersion time 20 hours
3	ZGC1-40	Nanozeolite on glassy carbon: 1 mL seed immersion time 40 hours
4	ZGC3-40	Nanozeolite on glassy carbon: 3 mL seed immersion time 40 hours

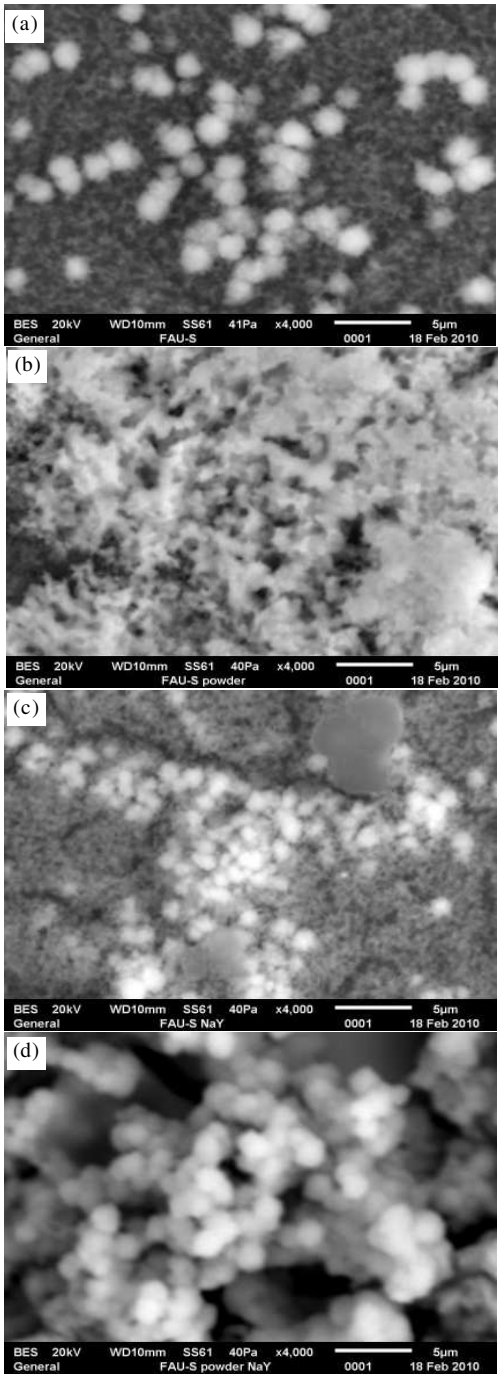

Figure 2. SEM of as-prepared FAU nanozeolite (a). seeds, (b). bulk powder, (c). NaY added seeds and (d). NaY added bulk powder at 4 kx magnification

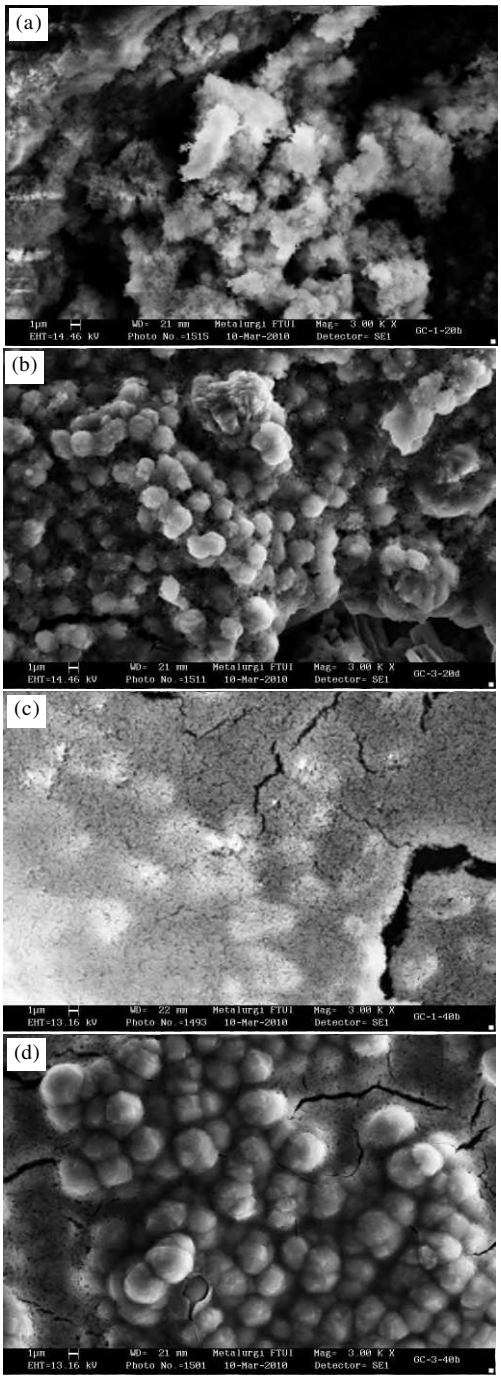

Figure 3. SEM images of (a). ZGC1-20, (b). ZGC3-20, (c). ZGC1-40 and (d). ZGC3-40 with 3 kx magnification

Vol. 12, No. 2, Februari 2010, hal : 129 - 133
ISSN : 1411-1098

work [10] the morphology of nanozeolite grown is poorer when more than one layer of seed applied.

SEM images of ZGC1-20, ZGC3-20, ZGC1-40 and ZGC3-40 are shown in Figure 3. It can be seen in Figure 3 that size and morphology of zeolite crystals are influenced by the amount of seeds immobilized on the modified glassy carbon, in which 3 mL of seeds gave more cuboid shape crystals with size about 1 μm. On the other hand, immersion for 40 hours in colloidal nanozeolite at 100 °C has caused cracks on the thin films which do not appear when the immersion time is 20 hours. Therefore the best prepared sample is ZGC3-20, which was used further for iron deposition.

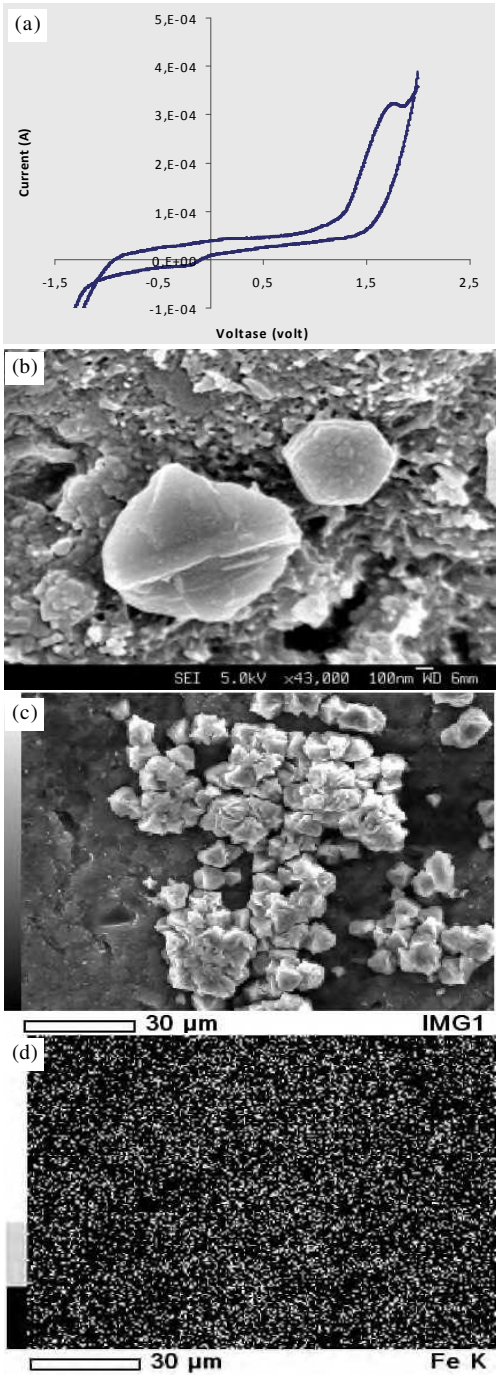

Figure 4. (a). Cyclic voltamogram of Fe(III) solution on ZGC3-20 plate, SEM image of plate Fe-ZGC3-20 (b). 43 kx, (c). 1 kx magnification and (d). EDS mapping for Fe in 1 kx image

Iron Electrochemical-Deposition in Thin Film Nanozeolite Grown on Modified Glassy Carbon

The containing Fe(III) ZGC3-20 plate that treated electrochemically then was labelled Fe-ZGC3-20. Figure 4 a shows the cyclic voltamogram of the electrochemistry experiment. It can be seen the appearance of potential reduction at -0.3 V, indicative of the reduction of $Fe^{2+} \rightarrow Fe^{0}$. Hence, it could be assumed that the reduction process of $Fe^{3+} \rightarrow Fe^{(0)}$ has occured. At +1.5 V, another peak was also observed, that could be assigned to the oxidation of $Fe^{2+} \rightarrow Fe^{3+}$ or/and the oxidation of oxygen ($O^{2-} \rightarrow O_2$).

However, it needs further investigation to understand this process. After electrochemical reduction of Fe(III) → Fe(0), the thin nanozeolite film was covered by white thin layer, which also can be observed by SEM (Figure 4(b)). It can be seen that the shape and size of nanocrystalline zeolite are unchanged after the electrochemical treatment, but some of the crystals combined to become larger aggregates, due to the weakening of the bonding between polyelectrolyte with the nanozeolite.

The EDS mapping of the surface of Fe-ZGC3-20 (Figure 4(d)) indicates that after electrochemical treatment, the surface thin film consists of about 0.30% (w/w) iron that spread evently both on the surface covered by nanozeolite thin film and that from modified glassy carbon.

CONCLUSION

Preparation of iron nanoparticle by electrochemical method has been attempted. The success of this preparation greatly depends on the success of the synthesis of thin film of FAU type nanozeolite grown on modified glassy carbon electrode. There is indication that nanozeolite obtained has particle size < 100 nm. The amount of seed added and the immersion time in FAU colloid influence the overall quality of the thin film. Cyclic voltamogram indicates successful Fe(0) formation, while SEM image shows the formation mostly occur outside the zeolite. It needs further investigation to observe iron nanoparticle formation inside the pores of nanozeolite.

ACKNOWLEDGMENT

The RUUI 2009 grant from The University of Indonesia is greatly acknowledged.

REFERENCES

[1]. Y. ZHANG, F.CHEN, J. ZHUANG, Y. TANG, D. WANG, A. DONG and N. REN, *Chem. Commun.,* (2002) 2814-2815

[2]. H. BONNEMAN and R. M.RICHARDS, *Eur. J. Inorg. Chem*., (2001) 2455-2480

[3]. N. R. JANNA, L. GEARHEART and C. J. MURPHY, *Chem. Commun.,* (2001) 617

[4]. D.L. HUBER, *Small* , **1** (2005) 482-501

[5]. I.T. ANGGRANINGRUM, *Laporan RUUI 2008*, (2008)

[6]. M. LASSINANTTI, J. HEDLUND, *J. Sterte, Micro. Meso. Mater.,* **38** (2000) 25-34

[7]. H. TOVINA, *Skripsi S1 Departemen Kimia FMIPA UI*, (2009)

[8]. E. DUBOIS, J. CHEVALET, *Langmuir*, **19** (2003) 10892-10900.

[9]. B. A. HOLMBERG, H.T. WANG, J.M. NORBECK and Y.S.YAN, *Micro. Meso. Mater*., **59** (2003) 13-28

[10]. H. TOVINA, Y. K. KRISNANDI, I. T. ANGGRANINGRUM, AMINAH, *J. Makara Sains*, Submitted July (2010)

Jurnal Sains Materi Indonesia
Indonesian Journal of Materials Science

Vol. 12, No. 2,Februari 2011, hal : 134 - 136
ISSN : 1411-1098

Akreditasi LIPI Nomor : 452/D/2010
Tanggal 6 Mei 2010

STUDY OF THERMOMECHANICAL EFFECTS OF MAIN CHAIN LIQUID CRYSTAL ELASTOMER AS FUNCTION OF CROSSLINKER CONCENTRATION

Irna Farikhah[1,2] and Yusril Yusuf[1]

[1]*Department of Physics, Faculty of Mathematics and Natural Sciences-Gadjah Mada University*
Sekip Utara, BLS 21, Bulaksumur, Yogyakarta 55281, Indonesia
[2]*Department of Physics, Faculty of Mathematics and Natural Sciences-IKIP PGRI Semarang*
Sidodadi Timur 24, Semarang 55125, Indonesia
e-mail : irnafarikhah@yahoo.co.id

ABSTRACT

STUDY OF THERMOMECHANICAL EFFECTS OF MAIN CHAIN LIQUID CRYSTAL ELASTOMER AS FUNCTION OF CROSSLINKER CONCENTRATION. Thermomechanical effects of dry Main Chain Liquid Crystal Elastomer (MCLCE) with the different concentration of crosslinker 8 %, 12 %, 14% and 16% have been studied. Length of MCLCE monotonically shrinks parallel to the director, while it expands perpendicularly to the director, with a somewhat faster change at nematic isotropic transition phase, $T_{ni.}$ The result of the investigation showed that the value of maximum contraction is greater and faster than maximum expansion.

Key words : Main Chain Liquid Crystal Elastomers (MCLCE), Thermomechanical effects, Function of crosslinker concentration

ABSTRAK

STUDI EFEK TERMOMEKANIK RANTAI UTAMA DARI ELASTOMER KRISTAL CAIR SEBAGAI FUNGSI KONSENTRASI *CROSSLINKER*. Efek termomekanik dari rantai utama pada elastomer kristal cair kering (*MCLCE*) dengan konsentrasi *crosslinker* yang berbeda pada 8 %, 12 %, 14 % dan 16 % telah dipelajari. Panjang dari *MCLCE* secara monoton memendek paralel terhadap *director*, namun memanjang secara tegak lurus terhadap *director*, dengan perubahan yang cepat pada fasa transisi *nematic isotropic* (T_{ni}). Hasil dari penelitian ini menunjukkan bahwa nilai kontraksi maksimal lebih besar dan lebih cepat dari ekspansi maksimal.

Kata kunci : *Main Chain Liquid Crystal Elastomers* (*MCLCE*), Efek termomekanik, Fungsi konsentrasi *crosslinker*

INTRODUCTION

The invention of Liquid Crystal (LC) by Friedrich Reinitzer in 1888 had improved the research of its properties. Some properties of LC had been investigated especially in molecular structure and electrical response of LC. It was not until the early 1970s that the successful commercialization of a pocket calculator with a display of device that utilized liquid crystals sparked an intense interest in the field [1].

In the last twenty years, the interest of LC has blossomed and incorporated with varied material. In this point, Liquid Crystal Elastomers (LCE) was developed and improved, which LC is a unique material with special properties combination LC and rubber properties. The elastic properties of LCE made it very potential to be developed as artificial muscles [1 ,2].

LCE was synthesized first by Finkelmann at 1981 and had been improved until the invention of Main Chain Liquid Crystal Elastomer (MCLCE) [2,3]. Polydomain Side Chain Liquid Crystal Elastomer (SCLCE) was the first LCE which was invented and then developed to be monodomain SCLCE. After the invention of SCLCE, the research of LCE was growing until the discovery of monodomain MCLCE [4].

As early as 1975, De Gennes predicted qualitatively the extraordinary mechanical and optical properties that should be expected from nematic MCLCE, where the mesogenic units are connected

within the polymer backbone to build up the polymer network [5].

One of the most outstanding features of nematic elastomers is a reversible change in length at the nematic to isotropic phase transformation for monodomain samples that are macroscopically ordered with respect to the director. This charge in shape is due to the coupling of the liquid crystalline order with the polymer chain conformation of the network. The coupling has been investigated in detail for SCLCE [6,7], where the mesogenic moieties are attached as side groups to the monomer units of the network. However, only few investigations have been performed on main 56 chain elastomers [8].

There had been substantial research on the SCLCE. Based on result, the effects of SCLCE was still relatively small so that we need another type of LCE in order to obtain the larger effects to be applied on artificial muscle. MC LCE is one of the LCE type that has been predicted to be more appropriate to be applied as artificial muscle.

EXPERIMENTAL METHOD

The polydomain MCLCE was synthesized in a one-step reaction, by dissolving the monomer 2-ethyl-1,4-phenylen bis [4-[4-(vinyloxil) buboxy] benzoate] ($C_{34}H_{38}O_6$) and 8 %, 12 %, 14 % and 16 %, the chain extender 1,1,3,3,-tetramethyldisiloxane ($C_{14}H_{14}OSi_2$). Monodomain MCLCE was prepared in three types crosslinking concentration, 8 %mol, 12 %mol, 14 %mol and 16 %mol of the crosslinking agent pentamethylcyclopentasiloxane ($C_5H_{20}O_5Si_5$) in toluene. The monodomain MCLCE was obtained by mechanical stretching in order to obtain the uniform director orientation, $\hat{n}$, parallel to the stretching direction.

To measure the length changes of LSCE during the variation of temperature, we prepared type of rectangular LSCE sample that is slicing parallel to $\hat{n}$ (planar sample). The sample is observed by a microscope (Nikon) equipped with a temperature controller. The image of each temperature photographed during the heating and cooling processes with a range between 30 ^oC until 120 ^oC for 8 %mol, 12 %mol, 14 %mol and 16 %mol of the crosslinking agent.

MCLCE samples were placed in glass. Samples are monodomain MCLCE. Monodomain planar MCLCE was obtained from cutting sample parallel with the director, **n**. A polarizing microscope was used to observe the thermo-mechanical effects which linked to a CCD camera and a PC (Personal Computer). CCD camera was used to take the picture of thermomechanical effects and the picture was saved in the PC.

RESULTS AND DISCUSSION

Figure 1 shows the observation of thermomechanical effects of MCLCE with 8 %, 12 %, 14 % and 16 % cross linking concentrations, through heating and cooling.

The anisotropic thermomechanical effects for MCLCE samples during the heating and the cooling

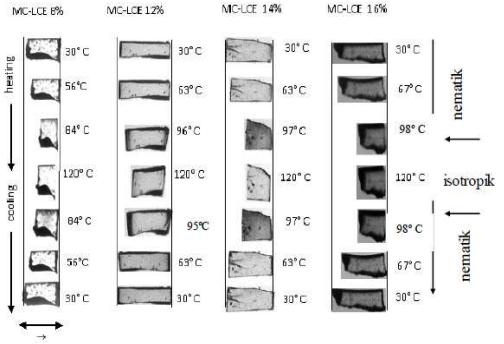

Figure 1. Thermo-mechanical effect induced shape changes of MCLCE for planar samples. MCLCEs shrink on heating and expand on cooling (parallel the director), $\|$**n.** In contrast, MCLCEs expand $\perp$n on heating and shrink on cooling

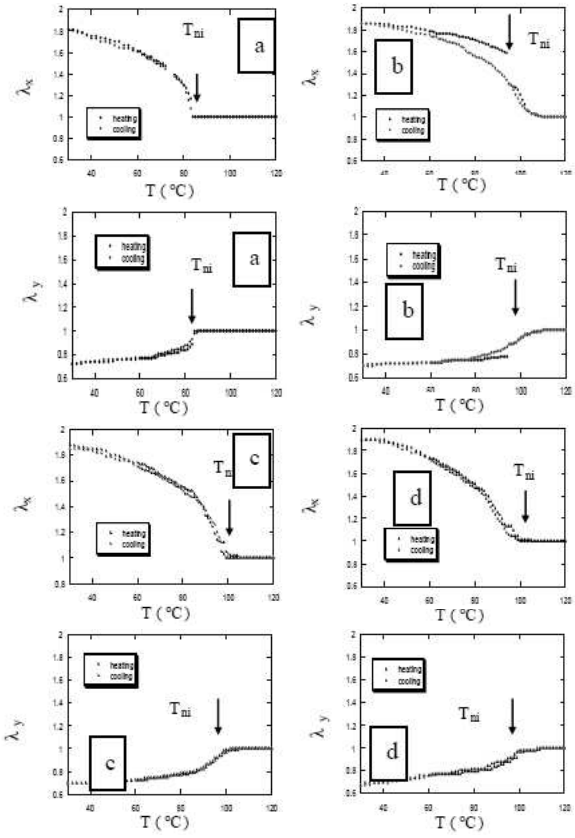

Figure 2. Temperature dependence of the relative length changes, $\lambda_x \| n$ and $\lambda_y \perp n$ for dry MCLCE-8, MCLCE-12, MCLCE-14 and MCLCE-16 samples during the heating and the cooling processes. The drastic length changes are observed at Tc ($T_{ni}^{MCLCE-8}$ ~84^oC, $T_{ni}^{MCLCE-12}$ ~95^oC, $T_{ni}^{MCLCE-14}$ ~97^oC and $T_{ni}^{MCLCE-16}$ ~98^oC), the apparent nematic-isotropic phase transition temperature of the dry MCLCE.

Vol. 12, No. 2,Februari 2011, hal : 134 - 136
ISSN : 1411-1098

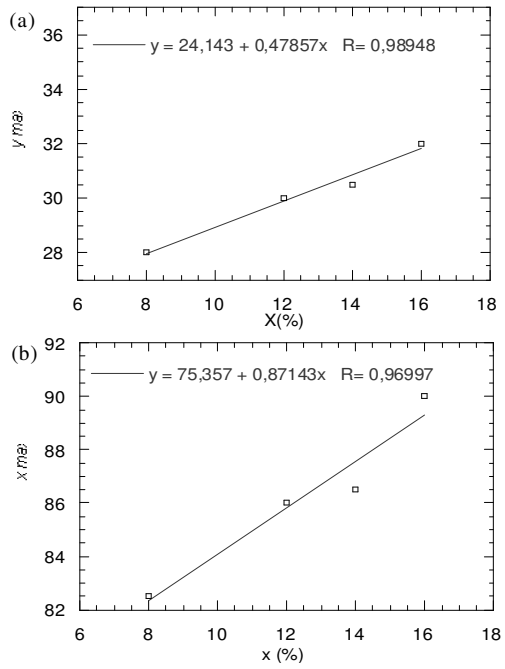

Figure 3. The dependence of the maximum length change, λ_{max}, on the concentration of crosslinking, X%, of MCLCEs in the isotropic is plotted. (a)maximum expantion, $\lambda_{y\ max}$ and (b). maximum contraction, $\lambda_{x\ max}$

processes are shown in this figure. When increasing the temperature, the planar samples shrink parallel to $\hat{n}$ ($\hat{x}$) and expand perpendicular to $\hat{n}(\hat{y})$. After cooling, all samples returned to their original shape.

Figure 2 shows the relative length changes of MCLCEs parallel to $\hat{n}(\hat{x})$ and as a function of temperature. Upon increasing temperature, all samples monotonically shrank parallel to $\hat{n}(\hat{x})$ with a somewhat faster decrease in the vicinity of T_c ($T_c^{MCLCE-8}$ ~ 84°C, $T_c^{MCLCE-12}$ ~ 95°C $T_c^{MCLCE-14}$ ~97°C and $T_c^{MCLCE-16}$ ~98°C).

The relative length changes of planar samples as a function of temperature, $\lambda_i(T)$ is defined as the ratio of expansion/shrinkage length to the initial length in the isotropic phase (T = 120 °C). Length measurements were made in the middle of each edge far from the other edges. The relative error was ~± 1 % due to the pixel size of the photo micrograph.

The maximum expansion was in the direction perpendicular to $\hat{n}(\hat{y})$ (Figure 3(a)). The maximum expansion is about 28 % for MCLCE 8 %, 30 % for MCLCE 12 %, 30.5 % for MCLCE 14 % and 32 % for MCLCE 16 %. In contrast, MCLCE monotonically shrink (parallel to $\hat{n}$ ($\hat{x}$)) is about 82.5 % for MCLCE 8 %, 86 % for MCLCE 12 %, and 86.5 % for MCLCE 14 % and 90 % for MCLCE 16 % (Figure 3(b)).

CONCLUSION

This work has shown that thermo-mechanical effects of MCLCE is a function of cross linker concentration of MCLCE. The effects showed in the changes of length. There are maximum expansion and contraction. Result of the investigation showed that the value of maximum contraction is greater and faster than the maximum expantion.

ACKNOWLEDGMENT

We wish to thank Simon Krause and Heino Finkelmann for sending us some of the samples used in these measurements. This work is partially supported by Hibah Bersaing DIKTI 2009 and Hibah Kompetensi DIKTI 2009.

REFERENCES

[1]. H. KAWAMOTO, *Proc. IEEE*, **90** (4) (2002) 460-500

[2]. P. G. DE GENNES, *The Physics of Liquid Crystals*, Clarendon Press, Oxford, 2nd Edition, (1993)

[3]. M. WARNER and E.M. TERENTJEV, *Liquid Crystal Elastomers*, Clarendon Press, Oxford, (2003)

[4]. H. FINKELMANN, H.J. KOCK and G. REHAGE, *Macromol. Chem.*, **2** (1981) 317

[5]. Y. YUSUF, Y.ONO, Y. SUMISAKI, P.E. CLADIS, H.R. BRAND, H. FINKELMANN and S. KAI, *Phys. Rev. E*, **69** (2004) 021710

[6]. Y. YUSUF, Y. SUMISAKI and S. KAI, *Chemical Physics Letters*, **382** (2003) 198

[7]. Y. YUSUF, Swelling Dynamics and Electromechanical Effects of Liquid Crystal Elastomers as An Artificial Muscle, *Ph.D. Thesis Kyushu University Jepang*, (2005)

[8]. M. A. ROLANDO, *Adsorption and Diffusion in Nanoporous Materials*, CRC Press Taylor and Francis Group, NW Suite 300, (2007)

Akreditasi LIPI Nomor : 452/D/2010
Tanggal 6 Mei 2010

PHASE IDENTIFICATION OF SYNTHESIZED HYDROXYAPATITE IN DIFFERENT CALCINATION TEMPERATURE

Decky J. Indrani[1] and Bambang Soegijono[2]
[1]Dept of Dental Materials Science, Faculty of Dentistry-University of Indonesia
Kampus Baru UI, Depok 16424, Indonesia
[2]Dept of Physics, Faculty of Mathematics and Natural Sciences-University of Indonesia
Kampus Baru UI, Depok 16424, Indonesia
e-mail : decky@ui.ac.id

ABSTRA CT

PHASE IDENTIFICATION OF SYNTHESIZED HYDROXYAPATITE IN DIFFERENT CALCINATION TEMPERATURE. For bone tissue engineering, hydroxyapatite scaffolds for cell growth are attracting due to their bioactivity and similarity to human bone component. The sol-gel route used in previous studies provided high crystalline hydroxyapatite and second phase occurred at higher calcination temperature. The aim of the present research was to synthesize and characterize HA prepared using the wet precipitation method in different calcinations temperature. The synthesis of hydroxyapatite was prepared using calcium and phosphorous precursor. The synthesized hydroxyapatite were then calcined at temperatures up to 900 °C. Rietveld refinement was used to examine the entire XRD patterns and FT-IR measurement was employed to observe the functional group of the synthesized HA. Results showed that HA material with the apatite structure were produced as was analyzed by XRD and Rietveld refinements. Chemical analysis indicated the existence of P-O vibrational modes from phosphate group and O-H from absorbed water confirming the formation of HA. Rietveld analysis revealed the existance of CaO phase at 300 °C, however, it was not observed at higher calcination temperature. The present study indicated that the wet precipitation method has induced the formation of HA without CaO phase at temperature above 300 °C. HA with increased crystallinity were produced in line with the raise in temperature.

Key words : Hydroxyapatite, Calcination, XRD, FT-IR, Sol gel

ABSTRAK

IDENTIFIKASI FASA HIDROKSIAPATIT HASIL SINTESIS PADA BERBAGAI SUHU KALSINASI. Dalam rekayasa jaringan tulang, *scaffolds* hidroksiapatit (HA) untuk pertumbuhan sel merupakan hal yang menarik untuk dikembangkan karena sifat bioaktifitasnya serta kemiripannya dengan komponen tulang manusia. Jalur *Sol Gel* telah dipergunakan dalam penelitian sebelumnya dan menghasilkan tingkat kristalinitas HA yang tinggi serta fasa kedua yang muncul pada suhu yang tinggi. Tujuan dari penelitian ini adalah untuk mensintesis dan mengkarakterisasi HA yang dihasilkan melalui proses presipitasi basah pada berbagai suhu kalsinasi. Sintesis dari HA dilakukan dengan menggunakan kalsium dan fosfor sebagai prekursor. HA yang disintesis kemudian dikalsinasi pada suhu hingga 900 °C. Penghalusan *Rietveld* digunakan untuk mengkaji seluruh data *XRD*. Pengukuran *FT-IR* dipergunakan untuk melihat gugus fungsi dari HA yang dihasilkan. Data menunjukkan bahwa material HA dengan struktur apatit telah dihasilkan dan telah dianalisis dengan *XRD* serta penghalusan *Rietveld*. Analisis kimia mengindikasikan adanya moda vibrasi gugus P-O dari grup fosfat dan gugus O-H dari molekul air yang diserap. Analisis *Rietveld* menunjukkan keberadaan fasa CaO pada 300 °C, namun fasa ini tidak terlihat pada suhu kalsinasi yang lebih tinggi. Penelitian ini telah menunjukkan bahwa metode presipitasi basah telah memungkinkan terbentuknya HA tanpa fasa CaO pada suhu diatas 300 °C. HA dengan tingkat kristalinitas yang lebih tinggi dihasilkan sejalan dengan meningkatnya suhu.

Kata kunci : Hidroksiapatit, Kalsinasi, *XRD*, *FT-IR*, *Sol gel*

INTRODUCTION

In the field of dentistry, bone defects frequently result from high energy trauma, infections or from physiological bone resorption which may pose problems when not treated. Being the main mineral component in

Vol. 12, No. 2, Februari 2011, hal : 137 - 140
ISSN : 1411-1098

human bone [1], calcium phosphate has been an attracting material for bone replacement [2] or for scaffold in bone tissue engineering [3]. For bone tissue engineering, HA scaffold should degrade that match with the cell growth, whereas the degree of degradation is dependent with the crystallinity of the material.

The most resembling calcium phosphate based bioceramics has been hydroxyapatite. Studies on synthesize of HA include solid state reaction, hydrothermal methods, sol gel route or wet chemical synthesis. The sol gel route have produced HA with high crystallinity and is often associated with CaO phase which was noticed at calcination temperature above 600°C [4]. Synthesis of HA via the wet chemical precipitation route based on the reaction of calcium nitrate and diammonium hydrogen phosphate revealed with $Ca_3(PO4)_2$ at 600 °C [5]. The route based on the reaction of calcium hydroxide and phosphoric acid under slow stirring and with pH 9.5 has produced HA with CaO and $CaCO_3$ phases after heat treatment [6]. The aim of the present study, therefore, was to synthesis HA using the wet chemical precipitation, with vigorous stirring and pH 7 and to identify phases developed during calcination.

EXPERIMENTAL METHOD

The synthesis were carried out by a reaction between $Ca(OH)_2$ (Merck) and H_3PO_4 (85 %, Merck). H_3PO_4 suspension was added in a dropwise manner and in a controlled rate to the $Ca(OH)_2$ suspension, while vigorous stirring being maintained for 24 hours using a magnetic stirrer (Heidolph MR 3001, Germany). At the end of the stirring process, the pH was adjusted until a final natural pH 7 was obtained. The supernatant was then decanted and wet cakes of HA obtained from the precipitant were subjected to filtering. Air drying and repeatedly washing were done, and further drying was conducted at 100 °C. Heat treatment was finally applied at the synthesized HA powder varying from 300 °C to 900 °C at 200 °C intervals with a heating rate of 5 °C/minute.

X-Ray Diffraction (XRD) measurement was performed using Phillips PW-1170 Diffractometer (Cu-Kα = 1.5404Å). Disc samples of different calcination temperature were scanned between 20° and 80° with a stepwise of 0.02°/0.6 Sec. The diffraction data was analysed using RIETAN (Rietveld Analysis) for phase identification for each diffraction pattern obtained at each calcination temperature.

Fourrier Transformed Infra Red (FT-IR) measurement was employed to support the existance of the synthesized HA by observing the functional groups in the chemical state of the materials. FT-IR spectroscopy (Spectrum One, Perkin Elmer, Germany) using KBr pellete technique was conducted in the range of 4000-450 cm^{-1} .

RESULTS AND DISCUSSION

The diffraction patterns from the synthesized HA powder samples are demonstrated in Figure 1. Correspondence with the view, the diffraction patterns are characterized by an intense background that displayed peaks which are typically HA, as expected, and in general are similar with those published in several literatures.

At low temperature, the diffraction peaks are not having good resolution and intensity showing amorphous HA. Broad peaks indicating the amorphous of the natural mateiral. A gradual increase in the intensity with enhanced resolution are observed as the calcination temperature rose. At 900 °C, an abrupt change of the pattern is noticeably with narrow and sharp peaks than others. To achieve satisfactory fits of the difraction patterns, a close inspection at the diffraction pattern is necessary.

Based on the refinements at 300 °C (Figure 2), Rietveld refinements showed good fitting quality with minimum values. The diffraction data observed two phases from the synthesized HA. Minor CaO phase (JCPDS 43-1001) was noticed at around 2θ = 36°-38°. The existance of the second phase was probably because of implying H_3PO_4 solutions with concentration of 85 %. The OH^- ions present in $Ca(OH)_2$ suspension were reacted by the 85 % H_3PO_4 solutions; consequently, remaining calsium stayed in the precipitated HA forming a new phase of calcium oxide (CaO). Previous research

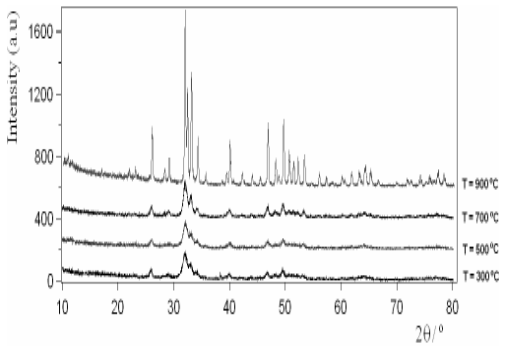

Figure 1. XRD pattern of HA samples calcined at 300-900 °C

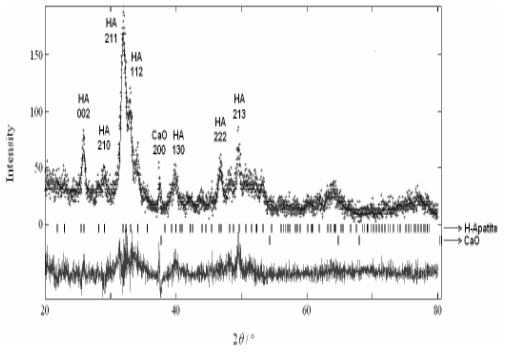

Figure 2. Refinements of the of the synthesized HA calcined at 300 °C

Table 1. Lattice parameters and crystallinity of the synthesized HA with calcinations temperature ranging from 300 °C to 900 °C

Suhu (°C)	300°C	500°C	700°C	900°C
a (Å)	9.4030(2)	9.3976(1)	9.4068(2)	9.4183(2)
b (Å)	9.4030(2)	9.3976(1)	9.4068(2)	9.4183(2)
c (Å)	5.8785(1)	6.8826(9)	6.8768(1)	6.8798(1)
γ	120°	120°	120°	120°
Crystallinity (%)	19.971	22.050	26.641	41.642

reported the existence of second phases, such as CaO, $CaCO_3$ or $Ca_3(PO4)_2$. In the present study, however, CaO phase was noticed only at 300 °C and was not observed at higher calcination temperatures.

Major HA phase, $Ca_{10}(PO_4)_6(OH)_2$, identical to the standard JCPDS 09-0432 for HA, owing a hexagonal crystal structure and described in the space group P 6_3/m (176) with the number of atom per unit cell as $Ca_1 = 4$, $Ca_2 = 6$, P = 6, $O_1 = 6$, $O_2 = 6$, $O_3 = 12$ and H = 2. At further calcination temperatures up to 900 °C, Rietveld refinements also proved the formation of HA with lattice parameters and crystallinity as in Table1.

With respect ro the calcination temperatures, the four lattice parameters displayed evident similarities that point out the analogy between the synthesized HA and the standard HA, having lattice parameters of a = b = 9.432Å , c = 6.881 Å and γ = 120° [7,8]. It seemed that transition of the atoms in the crystals of the synthesized HA approach a perfection of the standard HA unit cell dimension. In addition, this indication can be seen by increased crystallinity (Table 1) and viewed by a better resolution and higher intensities of the crystal planes (Figure 4).

The formation of HA is supported by the FT-IR analysis. The transmittance spectra (Figure 4) showed a characteristic of bio-apatites. Signature bands for HA arise from P-O and O-H bonds for phosphate (PO_4) and OH (hydroxyl) groups respectively.

P-O bonds for PO_4^{3-} ions from PO_4, groups occurred as vibrational modes around 1100 cm^{-1} to 1000 cm^{-1}, 962 cm^{-1} and 473 cm^{-1} due to stretching, and regions at 602 cm^{-1} and 569 cm^{-1} are assigned to stretching and bending. Whereas 633 cm^{-1} region from O-H showed

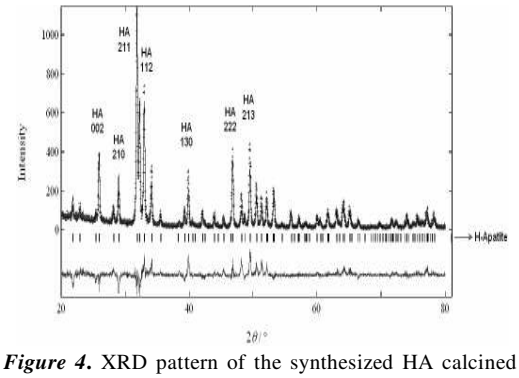

Figure 4. XRD pattern of the synthesized HA calcined at 900 °C

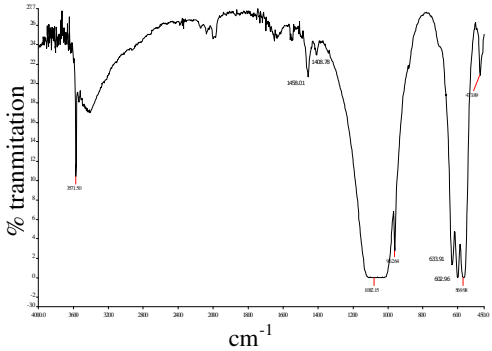

Figure 6. FT-IR spectra of the synthesized HA

absorbed water in HA. Carbonates (CO_3^{2-}) are detected around 1408 cm^{-1} and 1458 cm^{-1}. This was may be due to replacing of some hydroxyl molecules by the carbonates [9]. This situation similarly existed in [10] which is explained as an effect of atmospheric CO_2 uptake by utilizing a reactor without a cover in the experiments. The occurance of carbonates would be an advantage for the use of HA as scaffold for tissue engineering since biological apatites in human bone contain carbonate ions and bonded water. As an addition, these amorphous components in HA would improve the biodegradation of the scaffold [11].

Furthermore, the wet chemical precipitation is a favourable method to some reasons. It produces high percentage of pure product, low working temperature, large amount of HA can be produced at a time, ease in its experiment procedure, and also produce at reasonable cost.

CONCLUSSION

In the present study, HA phase synthesized using the wet chemical precipitation based on the reaction of $Ca(OH)_2$ with H_3PO_4 was identified by XRD measurement, Rietveld refinements and confirmed by the FT-IR analysis. The second phase, CaO, occurred only at 300 °C. The crystal structure is found to be strongly dependent on the calcination temperatures. Further study will be exploring the degradation of the synthesized HA at each calcination temperature that match with the cell growth.

REFERENCES

[1]. E.L. SMITH, R.L. HILL, I.R. LEHMAN, R.J. LEHKOWITZ, P. HANDLER, A. WHITE, *Principles of Biochemistry Mamalian Biochemistry*, 7th Ed., Mc Graw Hill Book Company, New York, (1983)

[2]. S-H. OH, R.R. FINONES, C. DARAIO, S-H. CHEN, S. JIN, *Biomaterials*, **26** (2005) 4938-4943

[3]. I.O. SMITH, L.R. MCCABE, *Journal of Nanomedicine*, **2** (2006) 189-184

Vol. 12, No. 2, Februari 2011, hal : 137 - 140
ISSN : 1411-1098

[4]. K.P. SANOSH, M-C. CHU, BALAKRISHNANA, T.N. KIM, S-J. CHO, *Bull Mater. Sci.*, **32** (5) (2008) 465-460

[5]. D.K. PATTANAYAK, P. DIVYA, UPADHYAY, R.C. PRASAD, B.T. RAO, T.R.R. MOHAN, *Trends Biomater Artif Organ*, **8** (2) (2005)

[6]. M.H. SANTOS, M. OLIVEIRA, L.P. SOUZA, H.S. MANSUR, W.L. VASCONCELOS, *Material Research*, **7** (4) (2004)

[7]. D. MCCONNELL, D.W. FOREMAN, *Canad. Mineral.*, **8** (1966) 431-436

[8]. K. SUDARASNAN, R.A. YOUNG, *Acta Crystallogr.*, **B25** (1969) 1534-1543

[9]. M. VIGNOLES, G. BONES, D.W. HOLCOMB, R.A. YOUNG, *Calcif. Tissue Int.*, **41** (1988) 33-40

[10]. L. WANG, Y. LI, C. LI, *J Nanopart Res*, **11** (2009) 691-699

[11]. J. GOMES-MORALES, J. TORRENT-BURGUES, T. BOIX, J. FRAILE, R. RODRIGUES-CLEMENTE, *Cryst. Res. Technol*, **36** (1) (2001) 15-26

Akreditasi LIPI Nomor : 452/D/2010
Tanggal 6 Mei 2010

INFLUENCE OF HIDROXYPROPYL METHYLCELULLOSE AND PECTIN MATRIX ON THE SOLUBILITY PROFILE AND CRYSTAL STABILITY OF THEOPHYLLINE

Yoga W. Wardhana and Mulyadi G. Tedjasaputra
Faculty of Pharmacy-Universitas Padjadjaran
Jl. Raya Bandung-Sumedang Km. 21 Jatinangor 45363, Sumedang, Indonesia
e-mail : ayodhna@gmail.com or ayodhna@yahoo.co.id

ABSTRACT

INFLUENCE OF HYDROXYPROPIL METHYLCELULLOSE AND PECTIN MATRIX ON THE SOLUBILITY PROFILE AND CRYSTAL STABILITY OF THEOPHYLLINE. Humidity is one of a factor affecting drug stability. Theophylline is a good sample which easily modified by humidity. In this study, we investigate the effect of polymer matrix of hidroxypropyl methylcelullose (HPMC) and pectin to inhibit the humidity-caused crystal stability changes of theophylline. Theophylline anhydrous (Ta) and mixture of Ta and matrix (80 : 20, 70 : 30 and 60 : 40) were used as the object of the study. The mixture was pressed to tablets using a Single Punch 12 mm flat E. Korsch machine. Humidity exposure was performed using a desiccator in room temperature (27 °C), with 94 % of relative humidity for 3 weeks of storage. The ability of matrix in inhibiting the change of Ta to theophylline monohydrate (Tm) was determined by comparing the result of dissolution test and X-Ray diffraction patterns from material test before and after humidity exposure. The results suggest that both polymers inhibited the changes of Ta to Tm. However, pectin was more superior than HPMC in inhibiting the hydration.

Key words : Humidity, HPMC, Pectin, Solubility, Crystal stability, Theophylline

ABSTRAK

PENGARUH MATRIKS *HYRDROXYPROPYL MEHTYLCELLULOSE* DAN *PECTIN* TERHADAP PROFIL KELARUTAN DAN STABILITAS KRISTAL DARI *THEOPHYLLINE*. Kelembaban merupakan salah satu faktor yang mempengaruhi stabilitas obat. *Theophyline* merupakan contoh yang menarik karena mudah terpengaruh oleh kelembaban. Studi ini mempelajari pengaruh dari matriks polimer *hidroxypropyl methylcelullose* (*HPMC*) dan *pectin* dalam menghambat perubahan stabilitas kristal *theophyline* yang diakibatkan oleh kadar air. *Theophylline anhydrous* (Ta) dan campuran dari Ta dan matriks (80 : 20, 70 : 30, 60 : 40) menjadi obyek dalam penelitian ini. Campuran ini dicetak hingga membentuk tablet dengan mempergunakan *punch* tunggal 12 mm *flat* E (*korsch machine*). Pemaparan terhadap kelembaban dilakukan dengan menggunakan desikator pada suhu ruang (27 °C), dengan tingkat kelembaban relatif (*RH*) 94 % selama 3 minggu. Kemampuan matriks untuk menghambat perubahan pada Ta menjadi *theophyline* monohidrat (Tm) ditentukan dengan membandingkan hasil pada tes dissolusi dan pola *XRD* dari material sebelum dan sesudah pemaparan kepada kelembaban. Hasil menunjukkan bahwa kedua polimer yang diuji mampu menghambat perubahan dari Ta menjadi Tm. Meskipun demikian, *pectin* cenderung lebih unggul dari pada *HPMC* dalam menghambat proses hidrasi.

Kata kunci : Kelembaban, *HPMC*, *Pectin*, Kelarutan, Stabilitas kristal, *Theophylline*

INTRODUCTION

Theophylline is known as the drug of choice for asthma. Theophylline has three crystalline forms, including one monohydrated and two anhydrous crystalline. Two anhydrous forms are obtained by different crystallization process, one is obtained by cooling a solution with a higher melting point than the crystals, the other is obtained by vacuum dehydration of the monohydrate. All forms have a different physical and chemical properties. Regard to their solubility, the anhydrous form dissolves in water faster than the monohydrate form. Furthermore, anhydrous form can transform to the monohydrate form in humid environment through recrystallization following the dissolution of anhydrous form in sorbed water [1].

In pharmaceutical dosage forms, solubility play an important role for their efficacy. Drug with higher

Vol. 12, No. 2,Februari 2011, hal : 141 - 144
ISSN : 1411-1098

solubility will easily absorbed on gastrointestinal tract, and therefore will give a faster pharmacological effect. One of the method to study the drug solubility is by a dissolution test, where the drug with high solubility will reach a high concentration faster [2].

As the drug of choice for asthma, theophylline has to be used with caution due to its toxicity to central nervous system. For many drugs and therapeutic indications, conventional multiple dosing of immediate release formulations provides satisfactory clinical performance with an appropriate balance of efficacy and safety. Use of hydrophilic matrices for oral controlled release of drugs is a common practice in the pharmaceutical industry [3].

In this study, we examined the changes in hydration and release profiles of a direct compression anhydrous tablets with two hydrophilic matrices in some variation, which has differing in water binding characteristic. The hydrophilic matrices we used were pectin and cellulose derivative (Hidroxypropylmethyl cellulose/ HPMC).

Pectin is a complex polysaccharide comprising mainly esterified D-galacturonic acid residues in an α-(1-4) chain. The acid groups along the chain are largely esterified with methoxy groups in the natural product. It has been used in a colon biodegradable pectin matrix with a pH sensitive polymeric coating, which retards the onset of drug release, overcoming the problems of pectin solubility in the upper GI tract [4]. Pectin has hygroscopic characteristic to make a viscous gelation forming with sweetly taste [5].

HPMC or hypromellose as The PhEur 2005 describes is a partly *O*-methylated and *O*-(2-hydroxypropylated) cellulose. Hypromellose defined in the USP 28 specifies the substitution type by appending a four digit number to the nonproprietary name: e.g., hypromellose 1828. The first two digits refer to the approximate percentage content of the methoxy group (OCH_3). The second two digits refer to the approximate percentage content of the hydroxypropoxy group ($OCH_2CH(OH)CH_3$), calculated on a dried basis. In oral products, hypromellose is primarily used as a tablet binder, in film coating, and as a matrix for use in extended-release tablet formulations.

Pectin has been used in film coating formulations containing chitosan and hydroxypropyl methylcellulose in the investigation of the biphasic drug release properties of film-coated paracetamol tablets [4].

In this work, we put theophylline anhydrous and those matrices as tablets under extremely relative humidities for 3 weeks. The high capacity of those matrices for water uptake, gelling and for the formation of hydrogen bonds can crucially affect the hydration and solubility of the drug during storage.

EXPERIMENTAL METHOD

Materials

The following materials were used, theophylline anhydrous (ex china, batch J0450/09(200805015), expiry april 2012), pectin (ex Shin Etsu) and Hypromellose 2910 (ex Shin Etsu).

Methods

All materials were dried for 24 hours at 70 °C, and mixed at the composition of Ta and matrices (HPMC or Pectin) 100 : 0; 80 : 20; 70 : 30 and 60 : 40. The materials were then compressed to tablets with a nominal weight of 125 mg using 12 mm flat punches at Single Punch E. Korsch tablet machine. Ten tablets of all formulation were individually tested for weight, diameters, hardnesses and thicknesses homogenity.

Tablets from each formulation were then taken as samples for dissolution test and recorded for the X-Ray diffraction patterns using Multi-Purpose X-Ray Diffractometer (X'Pert Pro MRD Type PW 3050/60 PANalytica, BATAN Bandung). The rest of the tablets were then stored at desiccator in a room temperature (27 °C) and 94 % relative humidity for 3 weeks. After 3 weeks, each tablets from all formulation were checked for its release profile and X-Ray diffraction patterns. The results were then compared to those of before 3 weeks of storage.

RESULT AND DISCUSSION

Pectin and HPMC gave different tablet characteristics (Table 1). Tablets made from pectin gave brown-white colour, while those made from HPMC gave clear white colour.

All Ta were changed to Tm under 3 weeks extreme relative humidity (27 °C, 94% RH). Polymer matrices were proved to inhibit the hydration during humidity exposure (Figure 1 and Figure 2).

Table 1. Tablet Characteristics

Evaluation	Ta 100 %	Ta 80 %		Ta 70 %		Ta 60 %	
		Pectin	HPMC	Pectin	HPMC	Pectin	HPMC
Weight (mg)	124 ± 0,562	124,95 ± 0,825	125,05 ± 0,605	125,3 ± 0,657	125,2 ± 0,617	126 ± 0,725	125,3 ± 0,733
Thickness (mm)	3,454 ± 0,014	3,363 ± 0,012	3,684 ± 0,014	3,484 ± 0,017	3,942 ± 0,015	3,628 ± 0,019	3,996 ± 0,018
Diameter (mm)	6,075 ± 0,009	6,094 ± 0,008	6,096 ± 0	6,095 ± 0,005	6,096 ± 0	6,096 ± 0	6,096 ± 0
Hardness (N)	40,75 ± 4,064	39 ± 3,84	41,05 ± 3,471	41,75 ± 3,72	40,75 ± 3,726	43 ± 2,51	40,5 ± 3,348

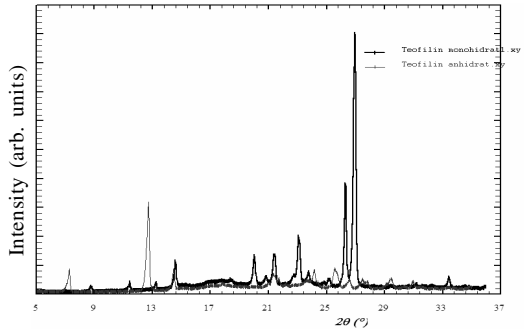

Figure 1. X-Ray diffraction patterns of Ta and Tm

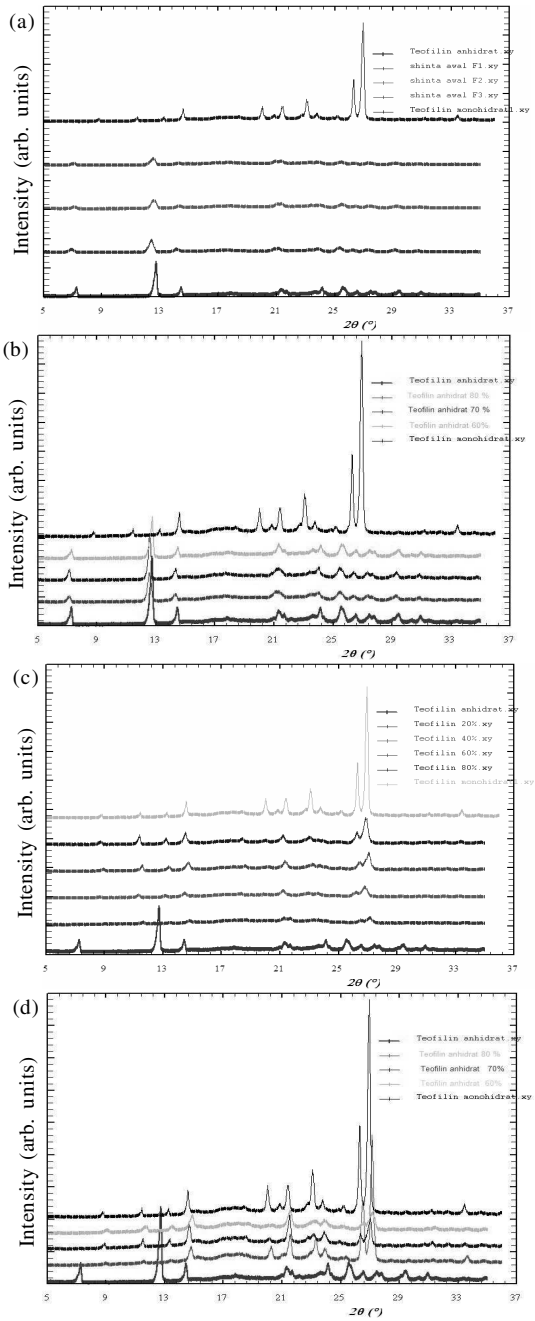

Figure 2. X-Ray diffraction patterns : Ta before storage and Ta with matrices before and after 3 weeks humidity exposure (a). Pectin matrix before storage, (b). HPMC matrix before storage, (c). Pectin matrix after storage and (d). HPMC matrix after storage

Table 2. Hydration rate percentages for each formula

Ta	Hydration at 2θ : 26,925° Before		Hydration at 2θ : 26,925° After		Differences	
	Pectin (%)	HPMC (%)	Pectin (%)	HPMC (%)	Pectin (%)	HPMC (%)
100 %	1.89	1.89	100.7	100.7	98.81	98.81
80 %	1.81	1.86	34.84	17.6	33.03	15.74
70 %	1.71	1.75	14.63	16.27	12.92	14.52
60 %	1.33	1.71	7.64	14.10	6.31	12.39

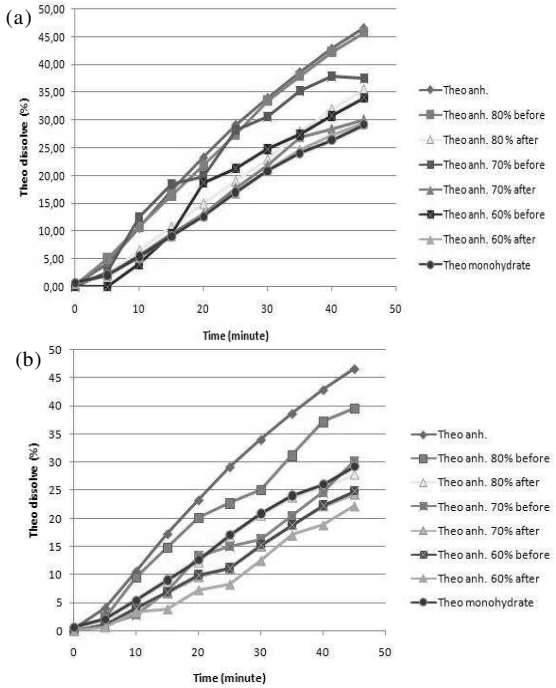

Figure 3. Dissolution profile (a). Pectin matrix and (b). HPMC matrix

The diffraction patterns showed that pectin matrix patterns on 2θ degrees was not as displaced as those of HPMC matrix. It suggest that pectin was more superior than HPMC in inhibiting the hydration of theophylline. When we calculated the 2θ intensity between materials tested before and after storage, the result show that on the ratio of Ta and matrix at 60 : 40 the hydration at pectin was 6,31 % whereas HPMC was 12,39%. It suggest that pectin has ability to detain hydration 2 folds stronger than HPMC. This calculation result were given on Table 2.

Result of the dissolution test showed that pectin matrix has ability to mantain stability of Ta from hydration during dissolution process more superior than HPMC matrix. Figure 3 showed that the profile of HPMC matrix release before and after humidity exposure, except on 20 % HPMC matrix, were below those of Tm. The results of pectin, however, were on the contrary.

CONCLUSION

Ta under humidity exposure will be degraded to Tm that have a lower solubility. This changes can be

Vol. 12, No. 2,Februari 2011, hal : 141 - 144
ISSN : 1411-1098

inhibited by highly hydrophilic polymer matrix such as pectin. The overall effect of hydration on drug release is the result of conflict between the tendency of theophylline hydration to slow drug release and the tendency of tablet swelling to accelerate drug release. The later tendency can cancel the initial tendency with hygroscopic polymer matrices and reducing particle size that favors gelling of the polymer.

ACKNOWLEDGMENT

The authors would like to thanks to Indonesian Atomic Agency (BATAN) Bandung for their collaboration, and to Shinta R. P. and Ria P. for the data collection.

REFERENCES

[1]. C. ALVAREZ-LORENZO, J.L. GÓMEZ-AMOZA, R. MARTINEZ-PACHECO, C. SOUTO and A. CONCHEIRO, *Drug Development of Industrial Pharmaceutical*, **26** (1) (2000) 13 - 20

[2]. A.A. DESPHANDE and C.T. RHODES, *Drug Development of Industrial Pharmaceutics,* **22** (1996) 531-539

[3]. JAIN and K. KEWAL, *Drug Delivery Systems*, Humana Press, Switzerland, (2008) 217

[4]. R.C. ROWE, SHESKEY, J. PAUL, QUINN and E. MARIAN, *Handbook of Pharmaceutical Excipients*, 6th Ed. RPS Publishing, London, (2009) 478-479

[5]. D. MUHIDIN, *Agroindustri Papain dan Pektin*, Penebar Swadaya, Jakarta, (2001)1-34

Akreditasi LIPI Nomor : 452/D/2010
Tanggal 6 Mei 2010

TARGETING DESIGN TO THE LUNG AND PULMONARY INTRACELLULAR STRUCTURE OF ENDOGENOUS GENE BY IRQ MODIFIED NANO CARRIER

Diky Mudhakir[1], Hidetaka Akita[2] and Hideyoshi Harashima[2]
[1]School of Pharmacy-Bandung Institute of Technology (ITB)
Jl. Ganesha No. 10, Bandung 40132, Indonesia
[2]Faculty of Pharmaceutical Sciences, Hokkaido University
Kita-ku, Kita-12, Nishi-6, Sapporo 060-0812 Japan
e-mail : mudhakir@fa.itb.ac.id

ABSTRACT

TARGETING DESIGN TO THE LUNG AND PULMONARY INTRACELLULAR STRUCTURE OF ENDOGENOUS GENE BY IRQ MODIFIED NANO CARRIER. Inhibition of angiogenesis is a novel strategy for the treatment of lung cancer. For efficient therapy, vectors must firstly reach the target tissue and subsequently demonstrate an efficient intracellular targeting. In this study, we attempted to design a vector for in vivo pulmonary targeting which was able to deliver small interfering Ribonucleic Acid (siRNA) for endogenous gene of angiogenesis in pulmonary endothelial cells. siRNA was condensed with polycation agent and encapsulated in lipidous nano carrier. To obtain high level of lung accumulation, we controlled the surface of nano-carrier by changing the length of Polyethylene glycol (PEG) moiety. These nano carriers showed prominent Ribonucleic acid interference (RNAi) effect, when luciferase gene was used as a target. In addition, an efficient transgene knockdown of Vascular Endothelial Growth Factor Receptor 1 (VEGFR1), a responsible gene of angiogenesis, can be obtained by the Instantaneous Respiratory Exchange Ratio (IRQ) modified nano carrier with the use of Stearyl-R8 (STR-R8) peptide, known as an endosomal membrane inducer. In conclusion, pulmonary targeting of nano carrier by encapsulating siRNA can be developed by controlling the PEG length and the structure of nano carrier for efficient intracellular targeting.

Key words : Pulmonary, PEG moiety, Intracellular trafficking, Endogenous gene, Endosomal membrane inducer

ABSTRAK

DESAIN NANO *IRQ* YANG DIMODIFIKASI SEBAGAI PEMBAWA *AGENT* ENDOGEN DENGAN TARGET KE PARU-PARU DAN INTRASELULERNYA. Penghambatan angiogenesis adalah strategi baru dalam pengobatan kanker paru-paru. Untuk memberikan terapi yang efisien, vektor harus mencapai target organ dan berinternalisasi secara efisien ke dalam organ tersebut. Pada penelitian ini, telah dikembangkan vektor yang target pada paru-paru secara in vivo dan sekaligus menghantarkan *small interfering Ribonucleic Acid* (*siRNA*) gen endogen pada sel endotel paru-paru. *siRNA* dikondensasi dengan senyawa polikation dan dienkapsulasi dalam vektor lipid berukuran nano. Untuk memperoleh tingginya akumulasi di paru-paru, permukaan dari vektor nano tersebut dikontrol dengan mengubah panjang rantai dari *Polyethylene glycol* (*PEG*). Vektor nano yang dikembangkan menunjukkan efek *Ribonucleic acid interference* (*RNAi*) yang menonjol, saat gen *lusiferase* digunakan sebagai target. Selain itu, penghambatan translasi *Vascular Endothelial Growth Factor Receptor 1* (*VEGFR1*), gen penentu pada angiogenesis, dapat dicapai dengan memodifikasi permukaan vektor *Instantaneous Respiratory Exchange Ratio* (*IRQ*) dengan peptide *Stearyl-R8* (*STR-R8*) yang dikenal sebagai penginduksi fusi membran endosom. Kesimpulannya, vektor nano yang mengenkapsulasi *siRNA* target ke paru-paru dapat dikembangkan dengan mengontrol panjang rantai *PEG* dan struktur vektor nano untuk target intraselular secara efisien.

Kata kunci : *Pulmonary*, *PEG moiety*, *Intracellular trafficking*, Gen Endogen, *Endosomal membrane inducer*

INTRODUCTION

Lung cancer remains a major health problem as the leading cause of cancer-related death worldwide [1]. Non Small Cell Lung Cancer (NSCLC) includes squamous cell carcinoma, adenocarcinoma and large cell carcinoma and represents approximately 80 % of all lung cancers. Unfortunately, the majority of

Vol. 12, No. 2,Februari 2011, hal : 145 - 152
ISSN : 1411-1098

patients present with advanced NSCLC at the time of iagnosis and die from the disease. First line therapy with cisplatin-based chemotherapy showed modest benefit with an extension in survival of approximately 2 months [1,2]. The need for more effective treatments has led to the development of new therapeutic approaches targeting tumor biology.

Investigators in non viral vector development have introduced a variety of strategies to overcome barriers for macromolecules such as small interfering Ribonucleic Acid (siRNA) delivery. These includes cellular internalization, intracellular trafficking in terms of endosomal escape and decoating process to release siRNA to the cytoplasm. In addition, for systemic in vivo applications, an important factors should be considered, including physicochemical properties that affect stability in the blood (i.e. particle size and zeta potential of the vector) and the immune system (i.e. reticuloendothelial system capture of the vector) [3].

PEGylated nanoparticles with multiple components are the most promising non viral vector for systemic delivery. It was reported that nanoparticles containing Polyethylene glycol (PEG), Solid Nucleic Acid Lipid Particles (SNALPs), targeted to specific tissue and showed Ribonucleic acid interference (RNAi) mediated gene silencing in hepatitis B [4]. Thus, it is expected that the use of PEG moiety would promote to pulmonary targeting. Additionally, the multiple components used in the vector design would induce an efficient cytosolic delivery of siRNA particularly an escape from the endocytic vesicles and decoating process.

Angiogenesis, i.e. the formation of new blood vessels, plays a central role in tumor growth, invasion, metastasis, and thus represents an attractive therapeutic target [1]. To date, a number of molecules regulating angiogenesis have been described. Of these, Vascular Endothelial Growth Factor (VEGF) is the most important growth factor controlling angiogenesis in normal and tumor cells [1,5]. The Vascular Endothelial Growth Factor Receptor (VEGFR) family consists of six growth factors including VEGF-A, VEGF-B, VEGF-C, VEGF-D, VEGF-E and placental growth factor (PIGF) which mediate their angiogenic effects via three receptors, VEGFR1-3. Binding of VEGF ligand to the receptor triggers downstream signaling pathways involved in enhancing vascular permeability, endothelial proliferation, invasion, migration and survival. VEGFR-1 and VEGFR-2 are important mediators of angiogenesis and VEGFR-3 is involved in lymphangiogenesis [1].

In the present study, nanoparticles designed for sophisticated lung targeting which addressed to knock down endothelial VEGFR1 gene expressed in the pulmonary endothelial cells were developed. In addition, to induce prominent gene silencing of the nanoparticles, the use of octaarginine (R8) as a fusogenic peptide enhancer was demonstrated.

EXPERIMENTAL METHOD

Preparation of IRQ Modified Liposomes

Three types of [^{3}H]CHE labeled liposomes, conventional liposomes (Conv-Lip), IRQ-modified liposomes (IRQ-Lip) 5% and IRQ-Lip 10% were prepared by the hydration method. Those liposomes were labeled with 0.03% of [^{3}H]CHE. Conv-Lip were composed of cholesteryl (Cho), Phosphatidylcoline (EPC) in a molar ratio of 3 : 7. To prepare the IRQ-Lip, two concentrations of Stearyl (STR)-IRQ were included (5 and 10 % of the total lipid in the [^{3}H]-Cho/EPC liposomes). These lipids were dissolved in 125 μL of chloroform and the solvent was then removed by nitrogen gas under reduced pressure in a glass tube to give a thin film. The lipid film was hydrated with Phosphate Buffer Saline (PBS) (pH 7.4), vortexed for 5 sec and sonicated within 1 minute by probe-type sonicator.

Synthesis of IRQ-PEG$_{900}$-DOPE and IRQ-PEG$_{2000}$-DSPE

Synthesis of IRQ-PEG$_{900}$-DOPE was performed following the procedure used for the synthesis of Cl31-PEG$_{450}$-DOPE [6]. While IRQ-PEG$_{2000}$-DSPE was synthesized as described previously [6]. To attach the IRQ to the surface of liposomes, the IRQ peptide was modified by adding cysteine residues, so that peptide can be readily conjugated to Mal-PEG-lipid to form the IRQ-PEG-lipid. In this study, two types of PEG were used, these were Mal-PEG$_{900}$-NHS and Mal-PEG$_{2000}$-DSPE. The IRQ-PEG$_{900}$-DOPE was synthesized by a two steps reaction of NHS groups of Mal-PEG$_{900}$-NHS and NH_3 primer of DOPE resulted in Mal-PEG$_{900}$-DOPE, followed by reaction between moiety of Mal-PEG$_{900}$-DOPE and cystein of IRQ peptide. The former reaction was carried out at room temperature for 2 hours in DMSO and the molar ratio of Mal-PEG$_{900}$-NHS, DOPE and triethylamine were 0.4, 0.4 and 0.8 μmol, respectively.

The latter synthesis was performed by coupling of the thiol group of IRQ peptide and the maleimide of Mal-PEG$_{900}$-DOPE. IRQ peptide and Mal-PEG-lipid were dissolved in H_2O at concentrations of 10 mM and mixed with equal ratios of 1 : 1. The reaction was carried out at room temperature overnight. The product was then identified by a Matrix-Assisted Laser Desorption/ Ionization Time-Of-Flight (MALDI-TOF) mass spectrometry.

The IRQ-PEG$_{2000}$-DSPE (distearoylphosphatidyl ethanolamine) was synthesized by a single step reaction of maleimide moiety of Mal-PEG$_{2000}$-DSPE with thiol groups of the IRQ as described in the latter synthesis step of IRQ-PEG$_{900}$-DOPE above. The coupling between thiol group of peptide and the maleimide of Mal-PEG$_{2000}$-DSPE was performed as described in the previous study [7].

The product of IRQ-PEG_{2000}-DSPE was structurally confirmed by a MALDI-TOF mass spectrometry. Sinapic acid was used as a matrix for mass spectrometric analysis of the peptide product. Sample solution was 5 μL product in 100 μL aqueous solution of 30% acetonitrile containing 0.1% Trifluoroacetic acid (TFA). Two μL of aliquots were spotted onto a MALDI-TOF target plate and analyzed by a Voyager-DE PRO Mass Spectrometer (Applied Biosystems, Foster City, CA).

Preparation of PEGylated Liposomes

(PEG-Lip) [^{3}H]CHE labeled PEG-Lip was prepared by hydration method. The liposomes were labeled with [^{3}H]CHE of around 0.03 %. Liposomes were basically composed of EPC and Cho in a molar ratio of 7 : 3. To prepare PEG-Lip, 10 % of Mal-PEG_{2000}-DSPE was incorporated into the liposomes.

Briefly, total lipids (1 mM) were dissolved in ethanol solution in a glass tube. The maleimide-PEG-lipid was added to the ethanol solution, followed by addition of 125 μL chloroform. The organic solvent was evaporated by nitrogen gas. To obtain a transparent and homogenous thin lipid film, 125 μL chloroform was added and evaporated. Aqueous phase of PBS was added into a dried lipid film. The vesicles were vortexed and sonicated in one minute by probe-type sonicator. Liposome were stored at 4 ^{o}C for a maximum of one week.

Preparation of IRQ-Modified PEGylated Liposomes (IRQ-PEG-Lip)

Liposomes were basically composed of EPC and Cho (7 : 3 molar ratio) and reaction mixture between Mal-PEG_{2000}-DSPE and IRQ (1 : 1) was incorporated at 5 % of the total lipid. Liposomes were prepared by hydration method. Briefly, total lipid (1 mM) was dissolved in ethanol solution. The reaction mixture was added to the ethanol solution. To increase evaporation, 125 μL of chloroform was added. The organic solvent was evaporated by nitrogen gas in a glass tube. To the obtained film, aqueous PBS 0.6 mL was added and the glass tube was sonicated for 15 sec in a bath type sonicator. The liposomes were then purified by gel filtration on Sephadex G-100 column. Liposomes were stored at 4 ^{o}C for a maximum of one week.

Biodistribution of the Liposomes

In the preliminary study, five types of liposomes, Conv-Lip, IRQ-Lip 5%, IRQ-Lip 10%, PEG_{2000}-Lip, IRQ-PEG_{2000}-Lip 5%, were individually injected into a 8 weeks Balb/c mice via the tail vein. The liposomes were fixed at 10 nmol lipid/g BW. After 6 hours, the mice were sacrificed and their lung and liver were collected. To obtain an actual uptake of liposomes in tissues, the portion of liposomes in the vascular space was removed by heart perfusion. After weighing, the samples were solubilized in Soluene-350 for 5 hours at 50 ^{o}C. To confirm lung accumulation, two types of liposomes, IRQ-PEG_{900}-Lip and IRQ-PEG_{2000}-Lip, were independently injected to each mouse.

Handling of the samples were the same as described above. Radioactivities were then determined by liquid scintillation counter, with Hionic Fluor.

Preparation of IRQ-Modified Liposomes Encapsulating siRNA

For transgene expression study, siRNA was encapsulated in IRQ-Lip, IRQ-PEG_{900}-Lip, IRQ-PEG_{2000}-Lip. These nanoparticles were prepared using a hydration method. In this study, two types of siRNA were used, each for luciferase gene and endogenous VEGFR1 gene, respectively. siRNA for luciferase gene was used in the preliminary study to screen the potential formula and it was encapsulated in all types of liposomes used. An anti-luciferase siRNA was 21 mer and it sequences were 5'-GCGCUGCUGGUGCCAACCCTT-3', 5'-GGGUUGGCACCAGCAGCAGCGCTT-3'. In the latter study, siRNA for VEGFR1 was encapsulated in the IRQ-PEG_{900}-Lip.

Firstly, siRNA and STR-R8, as a polycation agents, were firstly dissolved in RNase-free water. To condense the siRNA, the siRNA solution was added to the polycation solution while vortexing at room temperature.

The concentrations of both solutions were fixed at 0.1 mg/mL. The siRNA/STR-R8 complexes were prepared at a nitrogen/phosphate (N/P) ratio of 2.9. A volume of 0.25 mL aliquot of condensed siRNA suspension was added to the lipid film, which was formed by evaporation of a chloroform solution of 137.5 nm lipids, on the bottom of a glass tube followed by a 10-min incubation at room temperature to hydrate the lipids. In this experiment, the lipid composition used was DOPE/PA/IRQ-PEG-lipid/Cho-GALA in a molar ratios of 7 : 2 : 1 : 0.1.

In the case of IRQ-PEG_{900}-Lip encapsulating siRNA for VEGFR1, STR-R8 of 5, 10 and 15 % of the total lipids was incorporated to make a final concentration of 0.55 mM. To coat condensed siRNA with lipids, the glass tube was sonicated approximately 1 min in a bath-type sonicator (125 W, Branson Ultrasonics, Danbury, CT). Liposomes were stored at 4 ^{o}C for a maximum of one week. The size distribution and zeta potential of each sample was determined using a Zetasizer Nano ZS ZEN3600 (MALVERN Instrument, Worchestershire, UK).

Vol. 12, No. 2,Februari 2011, hal : 145 - 152
ISSN : 1411-1098

Transgene Expression of IRQ-Modified Liposomes Encapsulating siRNA

For transgene expression study of IRQ-PEG-Lips coated anti-luciferase siRNA, 5 x 10^4 HeLa cells stably expressing luciferase (~10^8 RLU/mg protein) were seeded onto a 24-well plate in 0.6 mL of Dulbecco`s Modified Eagle`s Medium (DMEM) containing 10 % Fetal Calf Serum (FCS) and were incubated for 24 hours.

Before transfection, cells were washed with 0.5 mL PBS. IRQ-PEG-Lips corresponding to 0.4 μg siRNA were suspended in 0.25 mL OPTI-MEM containing serum and then were incubated with cells for 3 hours at 37 °C. Next, 1 mL medium supplemented with serum was added to the cells, followed by incubation for an additional 21 hours. After 24 hours, cells were washed with 0.5 mL PBS and then were solubilized with reporter lysis buffer (Promega, Madison, WI).

Luciferase activity was initiated by addition of 50 μL of luciferase assay reagent (Promega, Madison, WI) to 20 μL of cell lysate and measured by means of a luminometer (Luminescencer-PSN, ATTO, Japan). The amount of protein in the cell lysate was measured usig a BCA protein assay kit (PIERCE, Rockford, IL). Results were expressed in relative light units (RLU)/mg protein.

For transgene expression study of IRQ-PEG-Lips coated anti-VEGFR1 siRNA, two days before infection, 2 x 10^5 Mouse fetal lung mesenchyme-4 (MFLM-4) cells were seeded onto a 6-well plate in 2 mL of DMEM containing 10 % FCS. Before transfection, cells were washed with 1 mL DMEM. IRQ-PEG-Lips coated siRNA corresponding to 6.4 μg siRNA were suspended in 1 mL DMEM containing 10 % FCS and were incubated with cells for 3 hours at 37 °C. Two mL medium supplemented serum was added to the cells, followed by incubation for an additional 21 hours.

Cells were solubilized with 1 mL reporter lysis buffer. mRNA was extracted from the samples and converted to complementary DNA (cDNA) by reverse transcriptase. The amount of cDNA was determined by Real Time Polymerase Chain Reaction (PCR). Results were expressed in percentage of RNAi effect.

Table 1. The size and zeta-potential of prepared liposomes for pharmacokinetics and transgene expression studies in HeLa cells

Types of liposomes	Size (nm)	Zeta-potential (mV)
Conv-Lip	81 ± 3.5	2 ± 2.6
IRQ-Lip 5%	85 ± 2.7	37 ± 3.6
IRQ-Lip 10%	83 ± 4.1	49 ± 4.4
IRQ-PEG_{900}-Lip	111 ± 2.8	30 ± 3.2
IRQ-PEG_{2000}-Lip	107 ± 3.1	7 ± 1.8
Luciferase siRNA-IRQ-PEG_{900}-Lip	117 ± 4.6	24 ± 4.1
Luciferase siRNA-IRQ-PEG_{2000}-Lip	110 ± 3.8	6 ± 2.9

RESULTS AND DISCUSSION

The present studies aimed to develop an intelligent delivery system which is able to selectively target the lung and subsequently its endothelial cells. In addition, the function of the developed nanoparticles was examined by evaluating the delivery of macromolecules siRNA to the cytosol of lung endothelial cells.

Characterization of Prepared siRNA-Coated IRQ-PEG-Lips

During preparation of the liposomes or coated particles for the use of pharmacokinetics and transgene expression studies in HeLa cells, the STR and the maleimide moeity acted as an anchor to the lipid bilayer leaving IRQ peptide freely attached to surface (IRQ-Lip) or freely attached to the terminal of PEGylated liposomal surface (IRQ-PEG-Lip). The size and ζ potential of prepared nanoparticles are summarized in Table 1. Particles for pharmacokinetics study had a size of around 80 nm. Incorporation of STR-IRQ to the Conv-Lip shifted its charges from neutral to positive one. In addition, the higher insertion density of the IRQ, the more positive their charges since the IRQ peptide is rich in arginine residues. When PEG moiety was inserted to the lipid bilayer, the size was slightly increased.

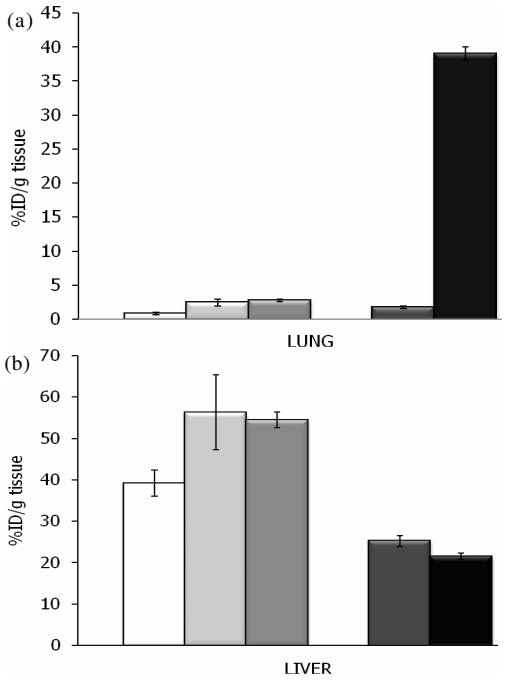

Figure 1. The tissue uptake of Conv-Lip, IRQ-Lip 5 %, IRQ-Lip 10 %, mPEG-Lip and IRQ-PEG2000-Lip 5 % in the lung and liver. The distribution was expressed as the percentage injection dose per tissue (%ID/tissue) in the lung (a) and liver (b). Open bars, light gray bars, gray bars, dark gray bars and closed bars indicate the tissue uptake at 6 hours after an i.v. injection of Conv-Lip, IRQ-Lip 5 % and IRQ-Lip 10 %

Furthermore, the use of long PEG moiety reduced its charges. These results are in line with the fact that the attachment of PEG moiety on the surface of liposomes neutralizes the effect of any charged component [7]. In general, IRQ-PEG_{900}-Lip and IRQ-PEG_{2000}-Lip had comparable sizes. Similar tendencies were observed for other coated particles between PEG_{900} and PEG_{2000} moeity, indicating that there were no significant differences in the physicochemical properties between PEG_{900}- and PEG_{2000}-modified nanoparticles.

Pharmacokinetics of IRQ-Lips and IRQ-PEG_{2000}-Lips

To determine *in vivo* distribution of IRQ-Lip, the accumulation of IRQ-Lip with the density of 5 % and 10 % in the lung were evaluated 6 hours after i.v administration (Figure 1A) and then compared to Conv-Lip as a control. The result showed that a small amount of Conv-Lip was recovered in the lung with the level of less than 1 % Injected Dose/g tissue (ID/g tissue). Incorporation of STR-R8 at 5 and 10 % to liposomal surface did not improve the uptake to the lung (Figure 1(a)). In addition, hepatic distribution was drastically increased as the result of modification with R8 (Figure 1(b)). IRQ-Lips were accumulated in the liver reaching approximately 80 %.

These results are in line with the previous study showing that the liver was the major clearance uptake of positively cationic liposomes [8]. It is possible that IRQ-Lip could be recognized by various opsonins or macrophages in the liver. When PEG_{2000} moiety was incorporated into the liposomes and the terminal of PEG moeity was conjugated with the IRQ, lung accumulation was drastically enhanced to approximately 39 % ID/g tissue at 6 hours post i.v. administration (Figure 1(a)). It is likely that the use of PEG_{2000} moiety reduced the recognition by opsonin so that liver accumulation was lower compare to that of IRQ-Lips. These results revealed that lung targeting of IRQ-modified nanoparticles could be improved by the incorporation of PEG moiety.

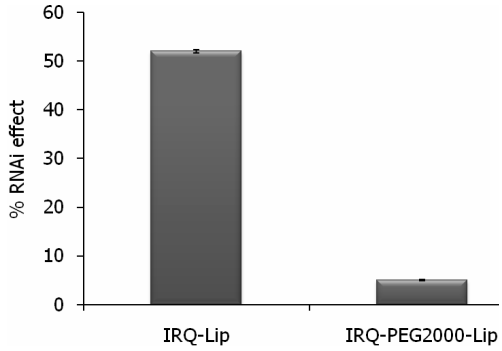

Figure 2. The effects of PEG moiety on the in vitro gene silencing of luciferase gene expression using siRNA. HeLa cells stably expressing luciferase were independently transfected with IRQ-Lip or IRQ-PEG2000-Lip containing luciferase or GFP. Luciferase activities were measured 24 hours after transfection and were expressed as percentage of silencing effect. The data represent as the mean of three data.

Silencing Activity of IRQ-Lips and IRQ-PEG_{2000}-Lip

For examining the efficiency of the delivery of macromolecules such as siRNA, we then compared the two liposomes, IRQ-Lip and IRQ-PEG_{2000}-Lip. When siRNA for reporter luciferase gene was encapsulated in IRQ-Lip, the transgene expression was knocked down by approximately 50% (Figure 2). This result is consistent with the previous study showing that gene silencing of IRQ-Lip was occurred. IRQ-Lip was internalized into cells via clathrin-mediated endocytosis and caveolar endocytosis. Additionally, the IRQ peptide was demonstrated to facilitate the escape from the endocytic vesicles [9].

Although, it was internalized via two cellular uptake pathways, it has been demonstrated that Clathrin-Mediated Endocytosis (CME) is a responsible pathway to induce RNA interference (RNAi) effect [10]. Therefore, after IRQ-Lip internalized through CME and entrapped in the endosomes, the IRQ peptide mediates endosomal escape. Thus, siRNA is released into the cytosol after decoating process occurred. However, when PEG moiety was inserted into the liposomes,

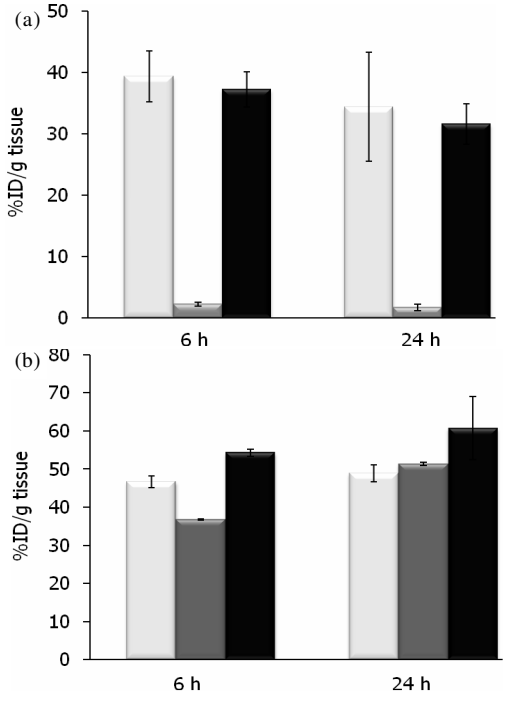

Figure 3. The tissue uptake of IRQ-PEG2000-Lip 5 %, unmodified PEG900-Lip and IRQ-PEG900-Lip in the lung and liver. The distribution was expressed as the percentage injection dose per tissue (%ID/tissue) in the lung (a) and liver (a). Light gray bars, gray bars and closed bars indicate the tissue uptake at 6 hours after an i.v. injection of IRQ-PEG2000-Lip 5 %, unmodified PEG900-Lip and IRQ-PEG900-Lip, respectively. The data represent mean SE (n = 3).

Vol. 12, No. 2,Februari 2011, hal : 145 - 152
ISSN : 1411-1098

transgene expression was severely inhibited (Figure 2). It was reported that the PEG moiety does not inhibit the endosomal escape, but it impaired the decoating process [6]. Decoating process is occurred subsequently during fusion step between liposomal membranes and endosomal membrane. It is presumable that length of PEG interrupts the interaction between the two membranes so that siRNA is still encapsulated in the lipid vesicles. Based on the results of pharmacokinetics and in vitro gene silencing studies, the use of PEG has advantages and disadvantageous that is termed as PEG dilemma.

Pharmacokinetics of IRQ-PEG$_{900}$-Lip and IRQ-PEG$_{2000}$-Lip

An alternative strategy to solve these hurdles is by modifying length of PEG moiety. The hypothesized that shorter PEG length would not only facilitate lung targeting of IRQ-Lip, but also compromise with the fusion process of the membranes to induce cytosolic release of siRNA. To confirm lung targeting by utilizing shorter PEG moiety, we first individually injected [^{3}H]-IRQ-PEG$_{900}$-Lip and [^{3}H]-IRQ-PEG$_{2000}$-Lip and specific the lung accumulation was observed at 6 hours and 24 hours post i.v. administration. The use of short PEG$_{900}$ moeity exhibited comparable results compared to that of PEG$_{2000}$ moeity. At the same indicated time, the IRQ-PEG$_{900}$-Lip was taken up by the lung of approximately 37 % ID/g tissue. Moreover, the lung accumulation of the IRQ-PEG$_{900}$-Lip and IRQ-PEG$_{2000}$-Lip were 34 % and 31 % ID/g tissue at 24 hours post i.v. administration (Figure 3(a)).

These results exhibited that the uptake of the IRQ-PEG-Lips in the lung remained after 24 hours and its accumulation was enhanced by 18.5 fold compared to that of unmodified PEG$_{900}$-Lip. This observation depicted their actual uptake in the lung because an impurity of the nanoparticles in the vascular space was removed by heart perfusion technique. These results indicated that lung accumulation of IRQ-modified liposomes can be achieved by shortening the PEG moiety approximately PEG$_{900}$. As to the accumulation of the nanoparticles in the liver, it is likely that modification of PEG moiety did not affect in liver uptake. The nanoparticles were taken up by the liver in a range of approximately 50-60 % ID/g tissue (Figure 3(b)). High liver accumulation can not be avoided since the positive charges of IRQ-nanoparticles were also responsible for the uptake.

Thus, it is hypothesized that flexibility of the IRQ to interact with its receptor was enhanced by modifying the PEG moiety. It is probable that an interaction between the IRQ with its receptor on the surface of lung endothelial cells is more prominent when the IRQ was attached to the tip of PEG moiety rather than attachment to liposomal surfaces.

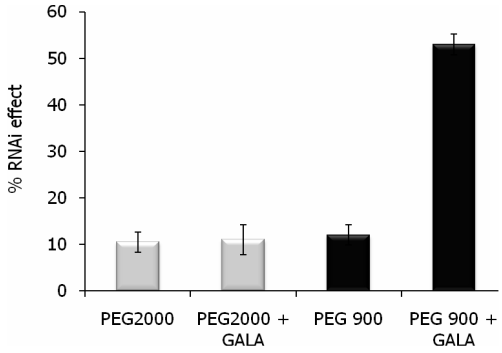

Figure 4. The effects of different PEG length on the in vitro gene silencing of luciferase gene expression using siRNA. HeLa cells stably expressing luciferase were independently transfected with IRQ-PEG-Lips containing luciferase or GFP. The cells were treated with IRQ-PEG2000-Lip, IRQ-PEG2000-Lip containing GALA, IRQ-PEG900-Lip and IRQ-PEG900-Lip containing GALA. Luciferase activities were measured 24 hours after transfection and were expressed as percentage of silencing effect. The data are represented as the mean of three data.

Therefore, the IRQ peptide would more freely reach the receptor compared to that of direct attachment to surface of the liposomes.

Transgene Expression of IRQ-PEG-Lips Coated Anti Luciferase siRNA

To investigate the function of IRQ-PEG-Lips, firstly siRNA for luciferase gene was encapsulated in the nanoparticles. After 24 hours post transfection to the HeLa stably expressing luciferase, the RNAi effect was determined. When siRNA was encapsulated in IRQ-PEG$_{2000}$-Lip, transgene knocked down was limited approximately to 11 % (Figure 4). This result was consistent with the previous study whose results showed that the use of PEG moiety inhibited the decoating of lipid vesicles [6]. When PEG$_{2000}$ moeity attached was replaced with the shorter PEG$_{900}$ moiety, RNAi effect was also inhibited in the absence of fusogenic peptide GALA. However, with incorporation of GALA to the surface of liposomes, transgene expression was drastically enhanced to approximately 53 % (Figure 4). GALA is a pH sensitive fusogenic peptide (WEAALAEALAEALAEHLAEALAEALE- ALAA) in the form of Cholesteryl-GALA (Cho-GALA) to modify the lipid vesicles. It was reported that it improved

Table 2. The size and zeta-potential of IRQ-PEG900-Lips coated anti-VEGFR1 siRNA for transgene expression studies in MFLM-4 cells.

Types of liposomes	Size (nm)	Zeta-potential (mV)
IRQ-PEG$_{900}$-Lip	84 ± 4.8	19 ± 5.3
IRQ-PEG$_{900}$-Lip + STR-R8 5%	116 ± 3.9	43 ± 2.6
IRQ-PEG$_{900}$-Lip + STR-R8 10%	122 ± 3.2	51 ± 3.4
IRQ-PEG$_{900}$-Lip + STR-R8 15%	117 ± 4.3	44 ± 4.9

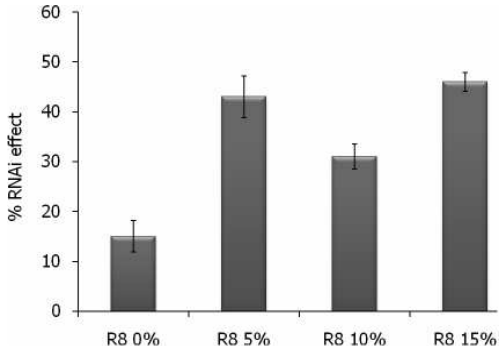

Figure 5. The effects of incorporation of STR-R8 on the in vitro silencing of VEGFR1 gene expression using siRNA. MFLM-4 cells were independently transfected by IRQ-PEG900-Lips containing VEGFR1 or GFP. The cells were treated with IRQ-PEG900-Lips without incorporation of R8 (R8 0 %), incorporation of R8 5 %, 10 % and 15 %.VEGFR1 activities were measured 24 hours after transfection and were expressed as percentage of silencing effect. The bars represent the mean of three data.

transfection activity of encapsulating plasmid DNA due to an enhanced endosomal release [11]. It is presumably that during the IRQ mediates escape nanoparticles from the endosomes, this synthetic pH-responsive pore-forming peptide at the N-terminus of the vectors assisted the escape of the cargo into cytosol by effectively fused with the endosomal membranes and disrupted their integrity [12].

Transgene Expression of IRQ-PEG-Lips Coated AntiVEGFR1 siRNA

Since the IRQ-PEG_{900}-Lip exhibited high lung accumulation and prominent gene silencing in vitro, it is then addressed to deliver its content of siRNA to the primary barrier of the lung endothelial cells. Thus, siRNA for marker luciferase gene was replaced by siRNA for specific endothelial gene marker. In this study, expression of several endothelial gene markers in the lung endothelial MFLM4 cells, such as CD31, Tie-2, VEGFR-1 and VEGFR-2, were examined.

The results showed that VEGFR-1 and VEGFR-2 were expressed in high level in MFLM4 cells (unpublished data). We then focused on the VEGFR-1 gene since it plays an important role in angiogenesis. To examine silencing activity in the endothelial cells, nanoparticles encapsulating synthetic double-stranded anti-VEGFR-1 siRNA (21 base pairs) were tested for their ability to deliver siRNA to the cytosol and to elicit an RNA interference effect. Physical characteristics of prepared nanoparticles was shown in Table 2. Inclusion of STR-R8 to the liposomes resulted in increasing size and charge of nanoparticles. However, similar tendencies in size and charge of coated particles modified R8 indicating that there were no significant changes in their physicochemical properties. As a result, siRNA-IRQ-PEG_{900}-Lips equivalent to 6.4 μg of siRNA resulted in 15% silencing of VEGFR1 activity (Figure 5). However, when stearyl-R8 was incorporated to the liposomal surfaces, RNAi effects was improved. Particularly, inclusion of

STR-R8 15 % to the total lipid vesicles resulted in drastically enhancement in transgene knocked down to approximately 46%. The enhancement of RNAi effect by the use of STR-R8 15 % was 3-fold compared to that without STR-R8. It was very clear the effects of STR-R8 on gene silencing of IRQ-PEG_{900}-Lip in the MFLM4 cells. Principally, the nanoparticles have designed to overcome hurdles in intracellular targeting. They were equipped with fusogenic lipid 1,2-dioleoyl-sn-glycero-3-phosphoethanolamine (DOPE), the IRQ peptide and the Cho-GALA. The presence of the DOPE affects an acidification in the endocytic vesicles so that fusion occurs between the liposomal membrane and endosome during escape [13].

Secondly, the use of IRQ promotes the endosomal escape by fusion-independent mechanism. Lastly, the Cho-GALA is expected to induce pore-formation of endocytic vesicles at low pH compartment so that decoating process is induced. Collectively, siRNA would be released in high extent to the cytoplasm. However, novel strategy should be implemented to improve the cytosolic release due to the low RNAi effect.

In the present study, we utilized the R8 which is incorporated to the surface of liposomes by the use of stearyl moiety as an anchor. Fusion to endosome was postulated as the main mechanism of escape. For fusion to take place between different membranes, three steps are required specific recognition of the site of fusion, close apposition of membranes and fusion or coalescence of membranes [13,14].

At decreasing endosomal pH, the total positive charge on IRQ-PEG-Lips containing R8 remains high due to full protonation of all arginine moieties [13,15]. In addition, R8 interact efficiently with amphoteric components embedded in the endosomal membrane even at acidic pH, not only through electrostatic interactions, but more importantly through bidentate hydrogen bonding. R8 seems to play an additional role in enhancing fusion through insertion into the endosomal membrane after being neutralized by negatively charged membrane components.

The formed ion pair may insert into the membrane and move inwards, driven by the transmembrane potential. This is expected to bring the lipid film of the liposome into intimate contact with the endosomal membrane, resulting in their fusion. This action is thought to increase at acidic pH when the potential across the endosomal membrane is high [13,16]. Oligo and polyarginines were reported to bind to anionic membrane-bound fatty acid salts, cholesterol derivatives, or phosphatidyl glycerol to form hydrophobic ion pairs that are soluble in chloroform or octanol [13,15,17].

Vol. 12, No. 2,Februari 2011, hal : 145 - 152
ISSN : 1411-1098

CONCLUSION

The use of long PEG_{2000} moiety drastically improved lung accumulation. However, it provided poor transgene expression. The use of short PEG_{900} moiety exhibited a high pulmonary uptake, comparable to long PEG_{2000} moiety. In addition, the use of IRQ-PEG_{900}-Lip containing siRNA for VEGFR1 in combination with the R8 showed prominent gene silencing in pulmonary endothelial cells. Collectively, the use of PEG_{900} moiety and its incorporation along with the R8 into the IRQ-modified nanoparticles is promising vector design for efficient pulmonary targeting as well as the subsequent pulmonary endothelial cells targeting.

ACKNOWLEDGMENT

This work was supported by the Core Research for Evolution of Science and Technology (CREST), Japan Science and Technology (JST). The authors also wish to thank Dr. Kusnandar Anggadiredja for his helpful advice in writing the English manuscript.

REFERENCES

[1]. S. SUN and J.H. SCHILLER, *Crit. Rev. Onc. Hem.*, **62** (2007) 93-104
[2]. J.H. SCHILLER, D. HARRINGTON and C.P. BELANI, *N. Engl. J. Med.*, **346** (2002) 92-98
[3]. S.D. LI and L. HUANG, *Gene Ther.*, **13** (2006) 1313-1319
[4]. D.V. MORISSEY, J.A. LOCKRIDGE, L. SHAW, K. BLANCHARD, K. JENSEN and W. BREEN et al., *Nat. Biotechnol.*, **23** (2005) 1002-1007
[5]. N. FERRARA, *J. Mol. Med.*, 77 (1999) 527-543
[6]. D. MUDHAKIR, E. TAN, H. AKITA and H. HARASHIMA, *Design of Smart-Nano Device for Intracellular Targeting, Gruber-Soedigdo Lecture 3rd*, Paper, Bandung Institute of Technology, (2010)
[7]. T.S. LEVCHENKO, R. RAMMOHAN, A.N. LUKYANOV, K.R. WHITEMAN and V.P. TORCHILIN, *Int. J. Pharm.*, **240** (2002) 95-102
[8]. D. MUDHAKIR, H. AKITA, I.A. KHALIL, S. FUTAKI and H. HARASHIMA, *Drug Metab. Pharmacokinet.*, **20** (2005) 275-281
[9]. D. MUDHAKIR, E. TAN, H. AKITA and H. HARASHIMA, *J. Control Release*, **125** (2008) 164-173
[10]. D. MUDHAKIR, E. TAN, H. AKITA and H. HARASHIMA, *Proceedings American Institute of Physics*, (2010) in press.
[11]. Y. SAKURAI, H. HATAKEYAMA, H. AKITA, M. OISHI, Y. NAGASAKI, S. FUTAKI and H. HARASHIMA, *Biol. Pharm. Bull.*, **32** (2009) 928-932
[12]. Y. WANG, S.S. MANGIPUDI, B.F. CANINE and A. HATEFI, *J. Control Release*, **137** (2009) 46-53
[13]. A. SAYED, I.A. KHALIL, K. KOGURE, S. FUTAKI and H. HARASHIMA, *J. Biol. Chem.*, **283** (2008) 23450-23461
[14]. P. MEERS, J. BENTZ, D. ALFORD, S. NIR, D. PAPAHADJOPOULOS and K. HONG, *Biochemistry*, **27** (1998) 4430-4439
[15]. N. SAKAI and S. MATILE, *J. Am. Chem. Soc.*, **125** (2003) 14348-14356
[16]. J. MALECKI, A. WIEDLOCHA, J. WESCHE and S. OLSNES, *EMBO J.*, **21** (2002) 4480-4490
[17]. J.B. ROTHBARD, T.C. JESSOP and P.A. WENDER, *Adv. Drug Deliv. Rev.*, **57** (2005) 495-504

ISSN 1411-1098
Akreditasi LIPI Nomor : 263/AU1/P2MBI/05/2010

JURNAL SAINS MATERI INDONESIA
Indonesian Journal of Materials Science
Vol. 12, No. 2, February 2011

EDITORIAL PREFACE

The editorial board of Indonesian Journal of Materials Science (JUSAMI) is very grateful to receive many articles from research institutes and universities. In order to improve the communication quality between the stake holders, step by step JUSAMI will appear online. Communications with editorial board will be done by e-mail, jusami@batan.go.id, while the website can be accessed in http://jusami.batan.go.id.

This Indonesian Journal of Material Science, Vol. 12, No. 2, February 2011, is the regular edition, but it is special since all of the articles are written in English. After considering the contents accompanied by further selection process, the editorial board accepted 15 articles to be published in this regular edition. Contents of the 15 articles are distributed in 5 articles covering natural based materials such as natural rubber, palm oil and celluloses, 3 articles are talking about properties improvement of commercial polymer such as poly(vinyl chloride) and polypropylene, 3 articles are concerned with the development of nanomaterials, and 4 articles are covering materials for medical application.

Abu Hasan et. al. reported about curing characteristics of vulcanized natural rubber, while Indra Gunawan et. al. reported their attempts to improve the properties of irradiated natural rubber by adding silica particles. Tutun Nugraha et. al. reported results of their attempt to modify and utilize bentonite for the bleaching of crude palm oil to be utilized as vegetable oil, while the utilization of polyol from palm oil as raw material of polyurethane was reported by Evi Triwulandari et. al. Asep Riswoko et. al. has modified cellulose by grafting technique using electron beam irradiation method. These reports will contribute in the development of natural based materials especially in Indonesia.

Properties improvement such as processability, toughness, flexural modulus and tensile strength of commercial polymer materials are still presenting challenges in their application. Nutt Lumpikanond et. al. have attempted to answer the problems of poly(vinyl chloride) processability for doors and windows profiles by adding fillers. Ariadne L. Juwono et. al. have tried to improve the flexural modulus of polypropylene by adding bentonite in the form of nanocomposite while A. Zainal Abidin et. al. have grafted bentonite into acrylic polymer to make superabsorbent with high water absorbing and water storing characteristics.

Technology development for the synthesis and the treatment of nanomaterials to fulfill their applications are still becoming the point of interest. Akhmad Hermawan Yuwono et. al. studied the major factor causing the low nanocrystalinity of TiO_2 obtained from Sol Gel process, followed by annealing and hydrothermal treatment, while Yuni K. Krisnandi et.al. and Muhammad Ghufron et.al. focused their attention to iron based nanomaterials to be used as electrodes and magnetic materials.

Articles about material for medical application in this edition are represented by 4 articles. Irna Farikhah et. al. reported their studies on liquid crystal elastomers which have potential applications for artificial muscles. Decky J. Indrani et. al. reported their results of the study on hydroxy-apatite for bone tissue engineering. Yoga W. Wardhana et. al. described their attempts to improve drugs stability due to humidity, utilizing theophylline, known as medication for the asthmatics, as the example. Finally, Diky Mudhakir et. al. reported their attempts to improve the efficiency of lung cancer therapy by designing a vector to help the drug to reach the target tissue most efficiently.

It is hoped that the wide scope of theme being discussed in this edition can commence an interdisciplinary communication between the various stakeholders of material research and development whether they within research institution, university, government or the industries.

Editor

JURNAL SAINS MATERI INDONESIA
Indonesian Journal of Materials Science
Vol. 12, No. 2, Februari 2011

DAFTAR ISI